INFORMATION TO USERS

This manuscript has been reproduced from the microfilm master. UMI films the text directly from the original or copy submitted. Thus, some thesis and dissertation copies are in typewriter face, while others may be from any type of computer printer.

The quality of this reproduction is dependent upon the quality of the copy submitted. Broken or indistinct print, colored or poor quality illustrations and photographs, print bleedthrough, substandard margins, and improper alignment can adversely affect reproduction.

In the unlikely event that the author did not send UMI a complete manuscript and there are missing pages, these will be noted. Also, if unauthorized copyright material had to be removed, a note will indicate the deletion.

Oversize materials (e.g., maps, drawings, charts) are reproduced by sectioning the original, beginning at the upper left-hand corner and continuing from left to right in equal sections with small overlaps.

UMI®

University of Alberta

LOGNORMAL SUM APPROXIMATIONS FOR ULTRA-WIDE BANDWIDTH APPLICATIONS

by

Faruq Rajwani ©

A thesis submitted to the Faculty of Graduate Studies and Research in partial fulfillment of the requirements for the degree of **Master of Science.**

Department of Electrical and Computer Engineering

Edmonton, Alberta

Spring 2005

Canada

Abstract

The problem of determining the distribution and probability density function of a sum of lognormal random variables occurs in the design and study of ultra-wide bandwidth wireless systems. Many approximations have been proposed assuming that the sum distribution can be represented by another lognormal random variable. None of these approximations are valid for a wide range of parameters. A new method to calculate an approximation to the lognormal sum distribution, based on curve fitting is introduced in this thesis.

Expressions for the performance of a pulse amplitude and position modulation (PAPM) ultra-wideband (UWB) system in lognormal fading channels with maximal ratio combining (MRC) have been derived using Wilkinson's approximation. Simple expressions for the error rate performance of a diversity PAPM UWB system based on using the new approximation are derived, calculated, and compared to results obtained by using Wilkinson's approximation for the performance of MRC and equal gain combining.

Acknowledgements

Contents

List of Tables

List of Figures

Acronyms

Acronym	Definition
1G	first generation
2G	second generation
AWGN	additive white Gaussian noise
BER	bit error rate
BPSK	binary phase shift keying
CDF	cumulative distribution function
CF	characteristic function
EGC	equal gain combining
EM	electromagnetic
GSL	GNU Scientific Library
iid	independent, identically distributed
ISI	intersymbol interference
LOS	line of sight
MRC	maximal ratio combining
niid	non-independent, identically distributed
PAPM	pulse amplitude and position modulation
PDF	probability density function
PSK	phase shift keying
RF	radio frequency
RMS	root mean square

RV	random variable
SC	selection combining
SNR	signal-to-noise ratio
SSC	switch and stay combining
UWB	ultra-wideband

List of Symbols

Symbol	Definition
a	path loss exponent
$b_n^{0,1}$	bit of the n-th transmitted symbol
E_{av}	average symbol energy of digital constellation
E_s	symbol energy
$E[X]$	expectation of X
$f_o(\cdot)$	PDF of lognormal RV $\Lambda(0, \sigma^2)$
$f_X(\cdot)$	PDF of RV X
$h(t)$	impulse response of channel
$I_0(\cdot)$	modified Bessel function of the first kind and zeroth order
L	lognormal RV
L_i	i-th summand in lognormal sum RV
$\bar{L}$	vector of lognormal RVs
m_X	mean of RV X
$n_l(t)$	Gaussian noise signal on l-th branch
$\bar{n}_l$	vector notation of $n_l(t)$
N	number of diversity branches or numbers of summands in a lognormal sum distribution
$\Pr(\cdot)$	probability of the argument
$p(t)$	pulse shape
P_{ei}	error rate for bit b_n^i

$P_{ei|\beta}$	conditional error rate for bit b_n^i assuming RV β is fixed
$Q(\cdot)$	complementary CDF of zero-mean, unit variance Gaussian distribution
$r_l(t)$	received baseband signal on l-th branch
$r_{RF_l}(t)$	received RF signal at l-th branch
$\mathscr{R}$	radius of a cell
$R(x)$	autocorrelation of pulse shape $p(t)$
$\tilde{R}_i(\cdot)$	correlation of template waveform $\phi_i(t)$ and $p(t)$
$s(t)$	transmitted signal
T_f	time duration of frame
$\hat{X}$	approximation to the RV X
Y_i	corresponding Gaussian RV to i-th summand in a lognormal sum RV
α_l	complex fading gain for the l-th branch
β_l	magnitude of complex fading gain for the l-th branch
β_{EGC}	lognormal sum distribution in EGC combining
β_{MRC}	lognormal sum distribution in MRC combining
δ	time shift in PAPM modulation
$\delta_D(\cdot)$	Dirac delta function
γ	average symbol SNR
γ_s	instantaneous symbol SNR
$\Gamma(\cdot)$	Gamma function
λ_i	decision variable for bit b_0^i
$\Lambda(m, \sigma^2)$	lognormal distribution with corresponding normal distribution $N(m, \sigma^2)$
$\Phi_Z(\omega)$	characteristic function of RV Z
ρ_{ij}	correlation coefficient between i-th and j-th RVs
ψ	exponentially decaying multipath intensity profile parameter
$\phi_i(t)$	template waveforms in correlator
σ_X^2	variance of RV X
θ	phase of received signal
θ_l	phase of complex fading gain for the l-th branch

Chapter 1

Introduction

1.1 Overview

Wireless communications is a fundamental part of our daily lives. We use many wireless applications on a daily basis such as cellular phones, wireless networks, satellite television and broadcast radio. There are also many new products being developed based on ultra-wideband (UWB), radio frequency identification tags, and Wi-Max. The trend is leading toward wireless devices overtaking the use of traditional devices. In fact, in 2000, the total number of cellular phone subscribers in Japan overtook the number of fixed line subscribers [1].

This trend will continue around the world as new technologies are introduced and quality of service is improved. First generation (1G) cellular phone systems were deployed in the early 1980's based on analog frequency modulation and frequency division multiple access. In the early 1990's, the second generation (2G) of cellular systems were introduced. One of the new standards, called Global System Mobile (GSM) was introduced to alleviate the inability to roam throughout Europe caused by many incompatible 1G systems. In North America, the limited capacity in the 1G system led to the development of two digital cellular standards, IS-54/136 and IS-95. These 2G standards made a switch from analog to digital modulation to increase the system capacity. Currently third generation cellular

1

phone technology is being deployed. It allows for voice and data traffic with applications such as mobile internet, picture messaging and video conferencing. Researchers are also working on fourth generation standards that will allow for very high data rates through mobile devices.

As these new technologies are developed, a portion of the radio frequency (RF) spectrum must be assigned to the users. With a finite amount of spectrum available to each technology, users are required to share the spectrum. The sharing of frequencies between users leads to co-channel interference, and as a result, all users will experience a degradation in the quality of service. To determine the performance of systems in these environments it is necessary to determine accurate and simple channel models.

1.2   Wireless Channels

Developing devices, standards, and understanding current technology requires a model of the channel in which these devices will operate. The wireless channel is a hostile environment, that is, it changes with time and location. In this section we will describe in detail different types of fading and interference present in a cellular system.

1.2.1   Small-Scale Fading

In a propagation environment that is filled with buildings, generally there is no line-of-sight (LOS) path from the transmitter to the receiver. The signal, in the form of an electromagnetic (EM) wave, reaches it destination by scattering and reflecting from the surfaces of buildings, and diffracting around buildings. Scattering is the result of the wave passing through a medium that consists of many objects that are small compared to the wavelength. In a practical setting, rough surfaces, street signs, leaves, and lamp posts will cause scattering. Reflection occurs when the wave reaches an object that is much larger in dimension than its wavelength. This could be the wall of a building or the surface of the earth. Since the reflecting surfaces have different electrical properties, the wave can either

2

be completely reflected for a perfect conductor, or be partially reflected and partially transmitted for a perfect dielectric. Waves can also bend around an obstruction, this is called diffraction. The bending is explained by Huygen's principle that states for every point on a wavefront, there is a point source that produces a secondary wave that combine to produce the new wavefront. The secondary wavefront is the source of the wave bending around the obstacle.

As a result of the scattering, reflecting and diffracting, the waves will arrive at the receiver from different directions and with different propagation delays. This phenomenon known as multipath propagation, is constructed by plane waves with randomly distributed amplitudes, phases, and angles of arrival. The waves add up constructively or destructively to cause small-scale fading, or fading for short. Fading is defined as changes in amplitude, phase, and multipath delay of the signal over a small distance or time.

Multipath propagation also results in frequency modulation due to Doppler shift. In the channel, either the mobile or the surrounding objects can be moving relative to the base station. When the mobile is moving, there is a shift in the carrier frequency, which is known as Doppler shift. Depending on whether the mobile is moving toward or away from the base station, the Doppler shift can be positive or negative. If the surrounding objects are moving, a time varying Doppler shift is introduced onto the multipath components. This shift will dominate the fading when the surrounding objects are moving at a faster rate than the mobile. The Doppler spread will largely determine how long the channel can be considered to be a constant, otherwise known as the coherence time.

When the coherence time is greater than a symbol period we call this slow fading. This is because the fading parameters change slower than the rate of the transmitted signal allowing us to assume that the channel is constant over several symbol periods. A channel is said to undergo fast fading if the coherence time is smaller than symbol period. This means that the channel characteristics will change during a symbol period and cause signal distortion.

Another result of multipath propagation is time dispersion, which causes flat or frequency selective fading. Flat fading is when the channel gain is flat and has a linear phase

3

response over the bandwidth of the signal. The channel gain changes in time but the spectrum of the transmitted signal is maintained. A measure by which we can determine if a channel is flat or frequency selective is the coherence bandwidth, which is defined as the frequency range where we can assume the channel spectrum to be flat. The coherence bandwidth is inversely proportional to the root mean square (RMS) delay spread. For a flat fading channel, the bandwidth of the transmitted signal must be smaller than the coherence bandwidth, and the symbol period must be much larger than the RMS delay spread of the channel. If the channel gain is flat and has a linear phase response over a range smaller than the bandwidth of the signal, it is said to undergo frequency selective fading. This results in multiple faded copies of the transmitted signal arriving at the receiver delayed in time. This can result in intersymbol interference (ISI) if the symbol period is larger than the difference in arrival times of adjacent copies. For frequency selective fading the coherence bandwidth of the channel is smaller than the signal bandwidth and the symbol period is smaller than the RMS delay spread.

When the received signal undergoes fading, the envelope is a statistical quantity. A Rayleigh distribution is commonly used to model the amplitude of the received envelope R in a flat fading channel. The probability density function (PDF) of this distribution is

$$f_R(r) = \frac{r}{\sigma_R^2} \exp(-\frac{r^2}{2\sigma_R^2}) \tag{1.1}$$

where σ_R^2 is the mean power of the received signal. The phase of the distribution is uniform and is expressed as

$$f_\theta(\theta) = \frac{1}{2\pi}. \tag{1.2}$$

The Rayleigh distribution is also used to express the sum of zero mean Gaussian noise on quadrature carriers. When the channel has a LOS component, the Rayleigh distribution is no longer a valid model. A better model is the Ricean distribution which can be derived from the sum of non-zero mean, Gaussian noise on quadrature carriers. The Ricean distribution is expressed as

$$f_R(r) = \frac{2r(K+1)}{\sigma_R^2} \exp\left(-K - \frac{(K+1)r^2}{\sigma_R^2}\right) I_0 \left(2r\sqrt{\frac{K(K+1)}{\sigma_R^2}}\right) \tag{1.3}$$

4

where $E[R^2] = \sigma_R^2$, $I_0(\cdot)$ is the modified Bessel function of the first kind and zeroth order, and K is the Rice factor, defined as the ratio of the specular component power to the scattered component power. When $K = 0$, the Ricean distribution simplifies to a Rayleigh distribution and when $K = \infty$ it models a channel with no fading. Being able to model different fading environments by changing K makes the Ricean distribution more versatile than the Rayleigh distribution.

Another important distribution is the Nakagami distribution that was developed based on empirical data [2]. The distribution is given by

$$f_R(r) = \frac{2m^m r^{2m-1}}{\Gamma(m)} \sigma_R^{2m} \exp\left(-\frac{mr^2}{\sigma_R^2}\right) \tag{1.4}$$

where $m \geq \frac{1}{2}$ and $\Gamma(\cdot)$ is the Gamma function. The Nakagami distribution degenerates to a Rayleigh distribution when $m = 1$ and a one-side Gaussian distribution when $m = 1/2$. The special case of $m = \infty$ models a no fading environment. The Nakagami distribution can sometimes be used to approximate a Ricean distribution by carefully selecting the parameter m. While small-scale fading in a wireless system will in large part determine the performance of the system, other factors such as path loss and shadowing will also affect the performance.

1.2.2 Large-Scale Path Loss and Shadowing

While it is important to know the model of the channel over small distances and times, it is also important to model the system over larger distances. As the receiver moves farther away from the transmitter, the local average received signal will decrease. This is known as large-scale path loss.

The basic path loss model is the free space propagation model which predicts that the received power decays as a square of the transmitter-receiver separation distance. The model can be used when there are no obstructions such as the ground, foliage, buildings and hills. In built up areas, using the free space propagation model will result in large errors due to reflection, scattering, and diffraction of the transmitted signal. In such an environment the path loss is a function of the separation distance to a power α. The path

5

loss exponent must be determined experimentally. It can take values of 2 for free space, 2.7 to 3.5 for an urban environment, and 4 to 6 inside a building with obstructions [3]. While this model is simple, it is not always the best method by which to predict the path loss. Many empirical models have been proposed by collecting experimental data. These more complex models take into account transmission frequency, base station height, mobile height, and degree of urbanization [4].

Propagation models only consider the transmitter-receiver separation distance. Another factor that must be taken into consideration is that the surrounding buildings and hills can differ between two locations having the same separation distance. This leads to a variation in the received signal power that has an average signal power predicted by the path loss calculation. This variation is known as shadowing. Experimental results have shown that the variation can be accurately represented by a lognormal distribution. The received signal in units of decibels (dB) is then a Gaussian distribution. The mean is obtained by averaging the received signal over 20 to 30 wavelengths to average out the multipath fading.

1.2.3 Interference

A major factor in the performance of cellular phone systems is interference. There are many sources for interference but the primary sources are mobiles in the same cell, mobiles in other cells, base stations using the same frequencies, or other systems that leak energy in the cellular frequency band. Interference leads to disruptions, cross-talk, missed calls and dropped calls due to a larger number of errors in transmission.

In a mobile phone system there is a limited number of available frequencies or channels. Assigning all these channels to one high power transmitter would result in the mobile receiving high power, undesired signals from other base stations. This type of interference when the received signal consists of undesired signals on the same transmission frequency is known as co-channel interference. It is possible to mitigate the co-channel interference by employing a cellular concept where the area is serviced by a number of low power transmitters, or cells, as opposed to one large transmitter. All the available channels are

6
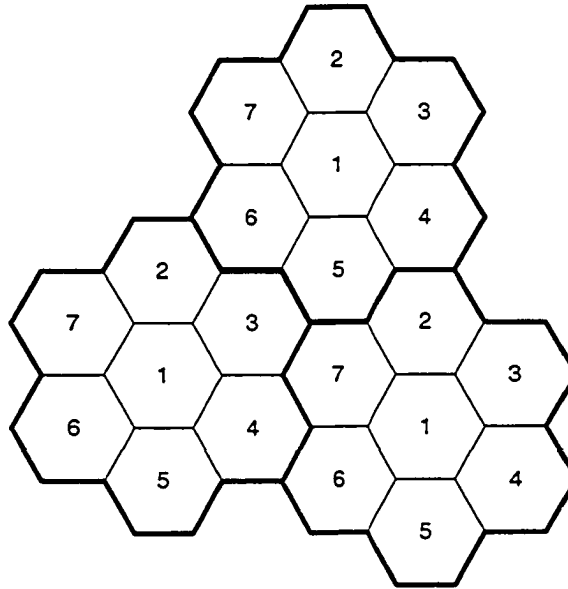
Figure 1.1. Illustration of frequency reuse with 7 sets of channels.

split into frequency sets and assigned to base stations so that neighboring base stations use different frequency sets. If the channels are assigned in a systematic way to maximize the distance between cells using the same frequencies, it is possible to reduce the co-channel interference. The process of assigning cells with a small set of the available frequencies is known as frequency reuse. This concept is illustrated in Figure 1.1 where the number in each hexagonal cell corresponds to a particular set of channels.

Reducing co-channel interference is not as simple as increasing the transmitter power. Thermal noise can be overcome by increasing the transmit power, which raises the signal-to-noise ratio (SNR), but increasing the transmit power will increase the co-channel interference at neighboring co-channel cells. Co-channel interference can be reduced by increasing the distance D between the center of co-channel cells and reducing the radius of each cell $\mathscr{R}$. This will allow the path loss between co-channel cells to provide isolation from the co-channel cells, which will reduce the co-channel interference. For hexagonal cells, as in Figure 1.1, the $D/\mathscr{R}$ ratio is given by

$$\frac{D}{\mathscr{R}} = \sqrt{3\mathscr{N}} \qquad (1.5)$$

where $\mathscr{N}$ is the number of sets of channels. The co-channel interference is reduced by

7

increasing $\mathcal{N}$, but this results in a smaller capacity per cell. This means there is a trade-off between capacity and co-channel interference.

Given that we know a shadowed signal is well modeled by a lognormal distribution it is possible to model the co-channel interference in a shadowed environment using the same distribution. The difference being that we require the distribution of a sum of lognormal random variables to account for numerous co-channel interferers. Having a model for the co-channel interference makes it possible to determine the performance of the system.

1.3   Ultra-Wide Bandwidth Channels

Major advances are occurring in wireless communications with the introduction by the Federal Communications Commission in the United States of "new spectrum" at the noise floor. The huge amount of spectrum is allowing the introduction of ultra-wide bandwidth radios that can overlay existing systems. The ultra-wideband (UWB) systems can be used for a number of applications such as localization with centimeter level accuracy, precision navigation, through-wall imaging, and short range high-speed network access [5].

Since UWB transmission is composed of very short pulses, the symbol period is smaller than the RMS delay spread of the channel resulting in frequency selective fading. This type of fading can be modeled by both frequency and time domain models, however, discrete time domain models are the industry accepted practice [6]. The channel impulse response of such a channel is

$$h(t) = \sum_{l=0}^{N-1} \alpha_l \delta_D(t - \tau_l) \tag{1.6}$$

where α_l is the amplitude of the fading, τ_l is a random delay, and $\delta_D(\cdot)$ is the Dirac delta function. Due to the short range nature of UWB, most commercial applications being developed are for indoor environments. Accordingly, we can no longer assume that Ricean or Nakagami distributions will model the fading amplitude. In fact, empirical studies have shown that a lognormal distribution is a better model to the fading amplitude distribution than a Rayleigh distribution [6]–[8]. The fading amplitude can also be assumed to be a real number since UWB is a carrier-less system. However, to account for random pulse

8

inversions, the fading amplitude is expressed as $\alpha_l = \theta_l \beta_l$ where $\theta_l \in \{\pm 1\}$ with equal probability and β_l is the lognormally distributed fading amplitude. A number of complex models that accurately model empirical results have been summarized by Foerster and Li [6]. In this thesis, to provide tractable expressions, a simplified channel model is used that limits the number of paths and sets discrete steps for the random delay. The details of the channel model used in this thesis can be found in Chapter 4.

1.4 Diversity Schemes

Diversity is a scheme whereby the properties of the radio propagation channel are exploited to improve the performance of the wireless link. In a fading environment, there may be numerous channels separated by space, frequency or time, that can be considered to be independent or nearly so. That is, it is highly unlikely that all the channels will experience a fade at the same time. By using independent signals it is possible to improve the SNR at the receiver. Diversity is also explained by looking at the probability $\mathcal{P}$ that the SNR of any of the channels is below some threshold. With independently faded channels, the probability that all N channels are below the threshold is $\mathcal{P}^N$.

It is possible to achieve diversity using space, angle, polarization, frequency, multipath and time. Space diversity is implemented by using multiple transmitter or receiver antennas. By separating the antennas by a large enough distance, the branches will experience independent fading. Direction or angle diversity is achieved by using directional antennas that receive signals from a small angle of the arrival spread. Polarization diversity exploits the fact that horizontal and vertical polarizations of an EM wave are uncorrelated [9] in typical cellular transmission environments. Frequency diversity is employed by using multiple carrier frequencies separated by the coherence bandwidth of the channel. Transmission using frequency diversity is not bandwidth efficient so spread spectrum systems implement frequency diversity using frequency hopping, where symbols are transmitted on a sequence of carrier frequencies. Multipath diversity collects the paths with different delays using a RAKE receiver. Time diversity transmits replicas of the signal separated by at least the co-

9
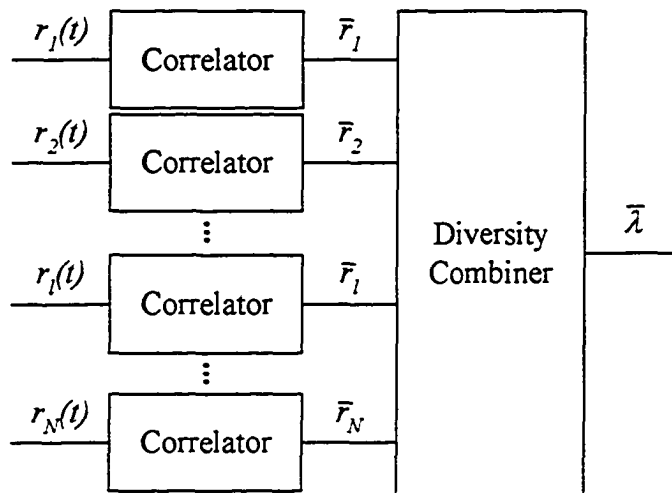
Figure 1.2. Postdetection diversity receiver.

herence time of the channel. In most cases the multiple received replicas can be considered to undergo independent fading. The limitation is that there could be an unacceptable delay introduced by transmitting multiple copies of the signal. It is also possible to combine a number of diversity techniques. One example of this is space-time coding that employs a combination of space and time diversity.

To implement the diversity techniques it is required to combine the different paths to increase the received SNR. The combining can take place at the modulation frequency which is called predetection combining or at baseband which is called postdetection combining. Theoretically the performance of the two is identical [4], but in this thesis we will only consider postdetection combining. A postdetection diversity scheme is shown in Figure 1.4. The received signal at RF $r_{RF_l}(t)$ is demodulated to baseband and then passed through a correlator detector. This baseband signal is applied to a diversity combiner as shown in Figure 1.4. Given that a signal $s(t)$ is transmitted, the received signal on the l-th diversity branch is

$$r_l(t) = \alpha_l s(t) + n_l(t) \tag{1.7}$$

where $\alpha_l = \beta_l e^{-j\theta_l}$ is the complex fading gain and $n_l(t)$ is the Gaussian noise on the l-th branch. For simplicity, (1.7) is expressed in vector notation as

$$\bar{r}_l = \alpha_l \bar{s} + \bar{n}_l. \tag{1.8}$$

10

Some of the combining techniques that can be used are maximal ratio combining (MRC) and equal gain combining (EGC). The following sections will explain the details of the combining techniques.

1.4.1 Maximal Ratio Combining

In MRC each diversity branch is co-phased and weighted by their respective fading gain and then combined. The resultant signal

$$\tilde{\lambda} = \sum_{l=1}^{N} \alpha_l^* \tilde{r}_l, \tag{1.9}$$

where α_l^* is the complex conjugate of the fading gain, is then sent through a detector to determine which symbol was transmitted. The variance of the noise at the detector can then be expressed as

$$\sigma_{\tilde{n}}^2 = \frac{N_0}{2} \sum_{l=1}^{N} \alpha_l^2 \tag{1.10}$$

assuming that the variance of the noise on each branch before co-phasing is $N_0/2$. The instantaneous symbol SNR is then obtained as

$$\gamma_s = \sum_{l=1}^{N} \frac{\alpha_l^2 E_{av}}{N_0} \tag{1.11}$$

where E_{av} is the average symbol energy of the digital constellation. Using (1.11) it is possible to express the average SNR as

$$E[\gamma_s] = \gamma = \frac{E_{av}}{N_0} \sum_{l=1}^{N} E[\alpha_l^2]. \tag{1.12}$$

The SNR produced by MRC is the largest when compared to all other linear combining diversity schemes. This is only true when the signal is independent of the noise, the fading is slow, and the noise components on different branches are uncorrelated [10]. It is shown in [10] that the optimal performance of MRC is independent of the fading distribution. While MRC provides the best performance the drawback is the increased complexity required to implement such a system. It is also important to note that MRC requires coherent signal combination so we are limited to coherent modulation schemes such as binary phase shift keying (BPSK) and quadrature amplitude modulation.

11

1.4.2 Equal Gain Combining

An EGC system will co-phase each diversity branch and then combine the signals to generate

$$\bar{\lambda} = \sum_{l=1}^{N} e^{-j\phi_l} \bar{r}_l. \tag{1.13}$$

This is similar to MRC but with the branch weights set to one. The variance of the noise after the combining is

$$\sigma_{\bar{n}}^2 = \frac{N_0}{2}N \tag{1.14}$$

and the envelope of the combining signal is

$$\alpha = \sum_{l=1}^{N} \alpha_k. \tag{1.15}$$

As a result, the instantaneous SNR is given by

$$\gamma_s = \frac{\alpha^2 E_{av}}{NN_0}. \tag{1.16}$$

Now the average SNR is

$$\gamma = \frac{E_{av}}{NN_0} E\left[\left(\sum_{l=0}^{N} \alpha_l\right)^2\right]$$

$$= \frac{E_{av}}{NN_0} \sum_{l=0}^{N} \sum_{k=0}^{N} E[\alpha_l \alpha_k], \tag{1.17}$$

which can be simplified further if the fading of the diversity branches are independent. While the performance of EGC is inferior to MRC, EGC is easier to implement as no channel gain estimation is required [11]. In a practical system, EGC is only used in coherent modulation schemes that have equal energy symbols such as M-ary PSK.

1.4.3 Other Combining Techniques

There are many other combining techniques that use different algorithms to improve the performance of a system. One of these systems is selection combining (SC). In this system, the branch with the highest SNR is always selected. This is impractical in systems

12

with continuous transmission because it requires monitoring of the all the branches which is similar in complexity to MRC. Another possible diversity scheme is switch and stay combing (SSC). An SSC system will cycle through the branches until it finds one that exceeds a pre-set threshold. The receiver will then stay with this branch until it drops below the threshold at which time it will look for another branch that exceeds the threshold. The performance of SSC is worse than SC except near the threshold where the performance is identical [4].

There are also other generalized diversity schemes based on either MRC or EGC that combine a fixed number of the strongest paths out of the N available paths [12]. These schemes are denoted as SC/MRC or SC/EGC. The performance of SC/MRC approaches that of MRC, while SC/EGC can perform better than EGC in some cases [11]. Another type of diversity scheme used in multicarrier CDMA is a combination of antenna arrays each with a RAKE receiver that can exploit diversity in frequency and multipath.

1.5   Lognormal Random Variables

As discussed previously, the large-scale fading in a cellular environment is well modeled by a lognormal distribution. A lognormal random variable (RV) is defined such that taking the logarithm of the RV results in a Gaussian distribution. Let L be a lognormal RV and then define the Gaussian RV as $X = 10\log_{10} L$. The PDF of X is

$$f_X(x) = \frac{1}{\sqrt{2\pi}\sigma_X} \exp\left[-\frac{(x - m_X)^2}{2\sigma_X^2} \right] \tag{1.18}$$

where m_X is the mean, and σ_X is the standard deviation of X in units of dB. The PDF of L is then given by

$$f_L(l) = \begin{cases} \frac{1}{\lambda\sqrt{2\pi}\sigma_X l} \exp\left[-\frac{(10\log_{10} l - m_X)^2}{2\sigma_X^2} \right], & l > 0 \\ 0, & l \leq 0 \end{cases} \tag{1.19}$$

where $\lambda = \ln(10)/10$. The standard deviation of X, σ_X, is referred to in wireless systems as the dB spread. For practical cellular systems it takes on values in the range of 6 to 12

13

dB [13]. The lower end of the range at 6 dB represents a lightly shadowed transmission environment, while the higher end of the range at 12 dB represents a heavily shadowed environment. In UWB transmission environments, the dB spread takes on values in the range of 3 to 5 dB [8].

Since working with the natural logarithm is more convenient, we define a Gaussian RV $Y = \ln L$. The PDF of Y is

$$f_Y(y) = \frac{1}{\sqrt{2\pi}\sigma_Y} \exp\left[-\frac{(y - m_Y)^2}{2\sigma_Y^2}\right] \tag{1.20}$$

where m_Y and σ_Y are the mean and standard deviation respectively. The RV X is related to the RV Y by the relation

$$Y = \lambda X. \tag{1.21}$$

As a result the mean and standard deviation of Y is

$$m_Y = \lambda m_X, \tag{1.22}$$

$$\sigma_Y = \lambda \sigma_X. \tag{1.23}$$

The PDF of L can then be rewritten in terms of the moments of Y which is given by

$$f_L(l) = \begin{cases} \frac{1}{\sqrt{2\pi}\sigma_Y l} \exp\left[-\frac{(\ln l - m_Y)^2}{2\sigma_Y^2}\right], & l > 0 \\ 0, & l \leq 0. \end{cases} \tag{1.24}$$

The n-th moment of the lognormal RV L can be calculated from the moments of the Gaussian RV as

$$\begin{aligned} E[L^n] &= E[e^{Yn}] \\ &= \int_{-\infty}^{\infty} e^{yn} \frac{1}{\sqrt{2\pi}\sigma_Y} \exp\left[-\frac{(y - m_Y)^2}{2\sigma_Y^2}\right] dy \\ &= e^{nm_Y + \frac{1}{2}n^2\sigma_Y^2}. \end{aligned} \tag{1.25}$$

From (1.25) the mean of L is given by

$$E[L] = m_L = e^{m_Y + \frac{1}{2}\sigma_Y^2} \tag{1.26}$$

14

and the variance is given by

$$
\begin{aligned}
\sigma_L^2 &= E[L^2] - E^2[L] \\
&= e^{2m_Y + 2\sigma_Y^2} - e^{2m_Y + \sigma_Y^2} \\
&= e^{2m_Y + \sigma_Y^2}(e^{\sigma_Y^2} - 1).
\end{aligned}
\tag{1.27}
$$

A lognormal distribution is generally given in terms of the two parameters m and σ^2, which is denoted by $\Lambda(m, \sigma^2)$. The corresponding Gaussian distribution can be denoted by $N(m, \sigma^2)$. Figure 1.3 shows the PDF of $\Lambda(0, \sigma^2)$ for $\sigma = 0.15, 0.5, 1.3816$ and 2.0723. In units of dB the standard deviations are calculated to be $0.6514, 2.1715, 6.0$ and 9.0 respectively.

Given a lognormal RV $\Lambda(m, \sigma^2)$ the PDF can be written as

$$
\begin{aligned}
f_L(l) &= \frac{1}{\sqrt{2\pi}\sigma l} \exp\left[-\frac{(\ln l - m)^2}{2\sigma^2}\right] \\
&= \frac{1}{\sqrt{2\pi}\sigma l} \exp\left[-\frac{\ln^2(l e^{-m})}{2\sigma^2}\right] \\
&= e^{-m} f_0(l e^{-m})
\end{aligned}
\tag{1.28}
$$

where $f_0(\cdot)$ is a the PDF of the lognormal RV $\Lambda(0, \sigma^2)$. From (1.28) it can be observed that a PDF of a lognormal RV with nonzero mean is the same as the the PDF of the zero-mean lognormal RV $\Lambda(0, \sigma^2)$ but with the abscissa scaled by e^{-m} and the ordinate scaled by the same amount. This is illustrated in Figure 1.4 for $m = 0, 0.5, 1.0$ and 2.0.

While the PDF is important in certain calculations such as the bit error rate (BER), the cumulative distribution function (CDF) is important in outage probability calculations. The CDF of a lognormal PDF $\Lambda(m_Y, \sigma_Y^2)$ is given by

$$
\begin{aligned}
F_L(x) &= \Pr(L \le x) = \Pr(e^Y \le x) \\
&= \Pr(Y \le \ln x) \\
&= 1 - Q\left(\frac{\ln x - m_Y}{\sigma_Y}\right)
\end{aligned}
\tag{1.29}
$$

where $\Pr(\cdot)$ is the probability of the argument and $Q(\cdot)$ is the complementary CDF of a

15
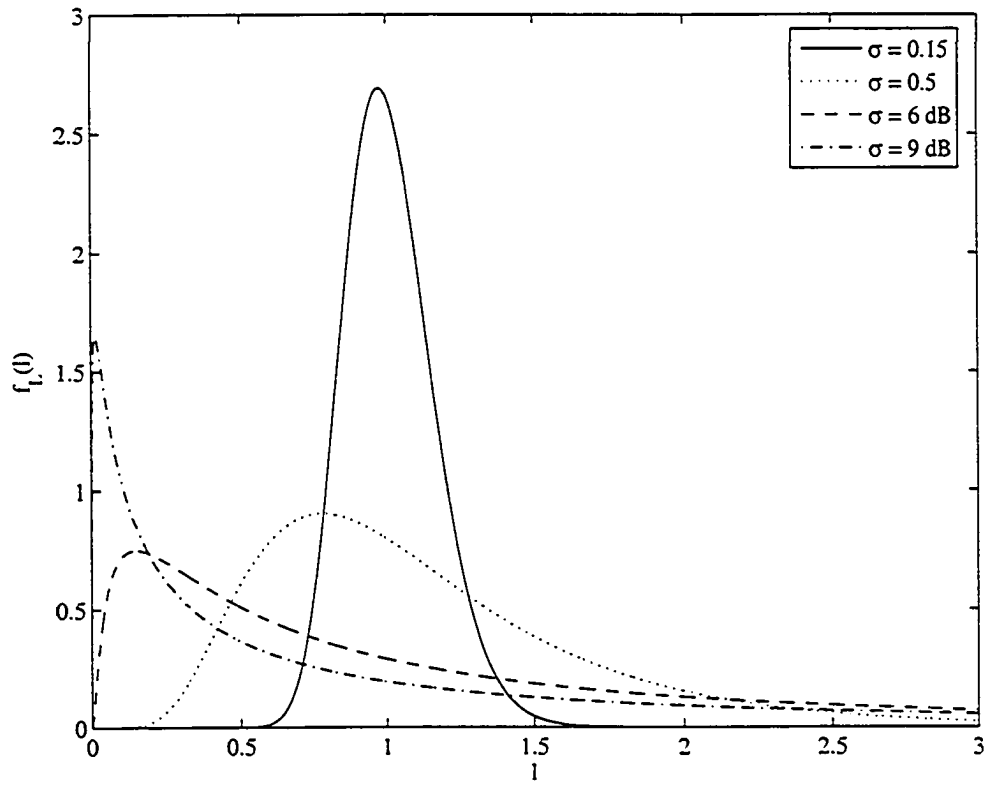
Figure 1.3. Lognormal PDF $\Lambda(0, \sigma^2)$ for $\sigma = 0.15, 0.5, 6$ dB and 9 dB.

16
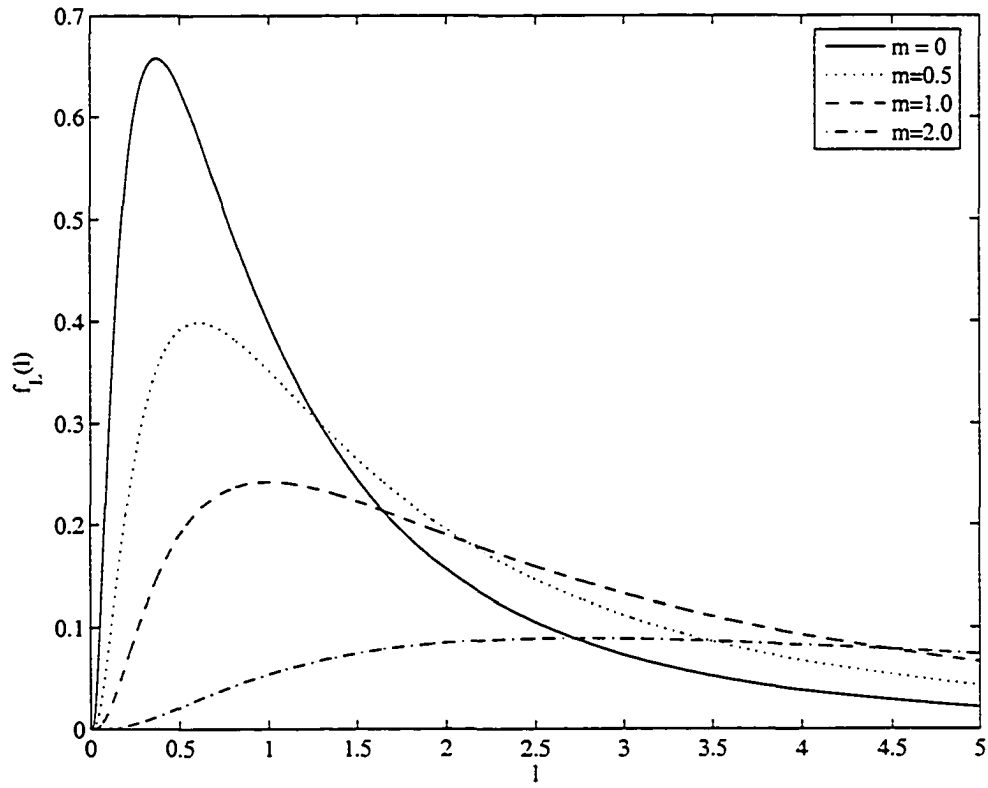
Figure 1.4. Lognormal PDF $\Lambda(m, 1)$ for $m = 0, 0.5, 1.0$ and 2.0.

17

zero-mean, unit-variance Gaussian distribution given by

$$Q(x) = \frac{1}{\sqrt{2\pi}} \int_x^\infty e^{-\frac{t^2}{2}} dt. \tag{1.30}$$

The CDF is plotted in Figure 1.5 for $\sigma = 0.15, 0.5, 6$ dB and 9 dB.

1.6 Sum of Lognormal Random Variables

Many problems in wireless communications such as outage probabilities in shadowing environments and detection of radar targets in lognormal clutter require the distribution and densities of a sum of lognormal RVs. Define a new RV Z, that is a sum of lognormal RVs, as given by

$$Z = \sum_{i=1}^N L_i = L_1 + L_2 + \cdots + L_N = e^{Y_1} + e^{Y_2} + \cdots + e^{Y_N} \tag{1.31}$$

where L_i and Y_i are defined in the same manner as L and Y in the previous section. It is also important to note that each summand can have a different mean and variance given by m_{Y_i} and $\sigma_{Y_i}^2$ respectively. When the mean and variance of each summand is different, we denote this as a sum of non-identically distributed lognormal RVs.

1.7 Literature Review

Numerous approaches have been proposed to compute the CDF and moments of a sum of independent lognormal RVs. Most of the methods are based on assuming that a sum of lognormal RVs is equivalent to another lognormal RV. This is expressed as

$$Z = L_1 + L_2 + \cdots + L_N = e^{Y_1} + e^{Y_2} + \cdots + e^{Y_N} \approx e^{\hat{Y}} = e^{\lambda \hat{X}} = \hat{Z} \tag{1.32}$$

where $\hat{Y}$ and $\hat{X}$ are Gaussian RVs, and $\hat{Z}$ is lognormally distributed. In this section, a brief description of these approximations is given along with a comparison of the different methods.

18
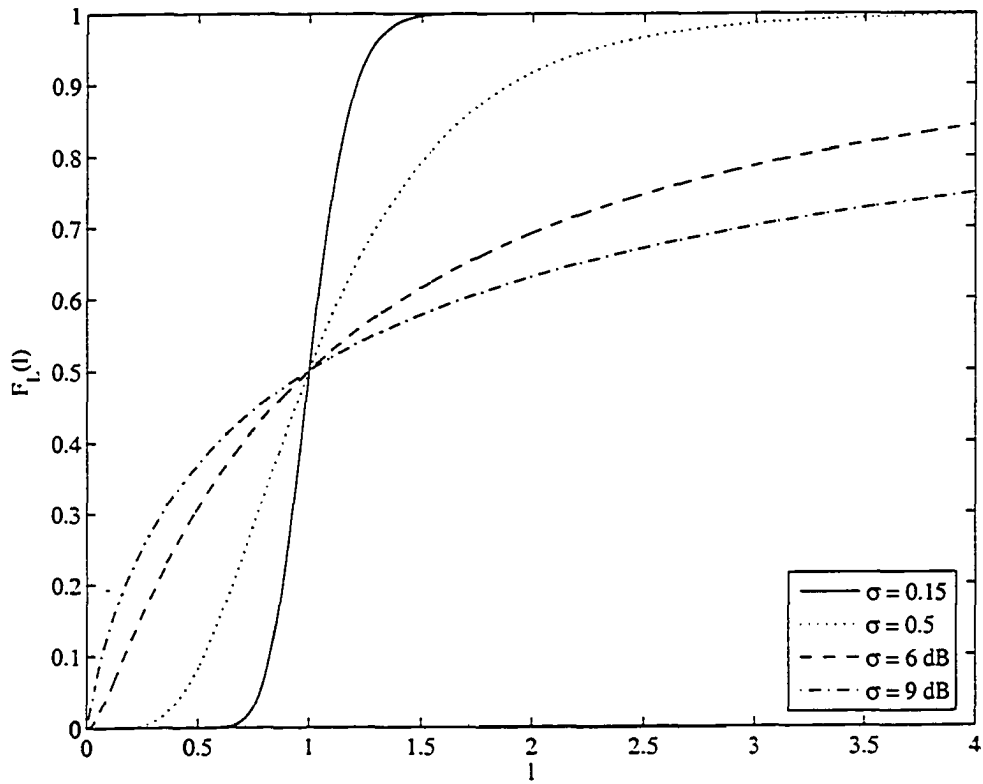
Figure 1.5. Lognormal CDF $\Lambda(0, \sigma^2)$ for $\sigma = 0.15, 0.5, 6$ dB and 9 dB.

19

1.7.1 Wilkinson's Method

Wilkinson's method is based on assuming that a sum of lognormal RVs can be approximated as another lognormal RV. To determine the mean and standard deviation of $\hat{Y}$, the first and second moments of Z and $\hat{Z}$ are matched. Using (1.25) the first moment of Z is given by

$$
\begin{aligned}
E[Z] &= E[L_1 + L_2 + \cdots + L_N] \\
&= E[L_1] + E[L_2] + \cdots + E[L_N] \\
&= \sum_{i=1}^{N} e^{m_{Y_i} + \frac{1}{2}\sigma_{Y_i}^2}.
\end{aligned}
\tag{1.33}
$$

Then equating (1.33) with the first moment of $\hat{Z}$ results in

$$
e^{m_{\hat{Y}} + \frac{1}{2}\sigma_{\hat{Y}}^2} = \sum_{i=1}^{N} e^{m_i + \frac{1}{2}\sigma_{Y_i}^2} = v_1.
\tag{1.34}
$$

Equating the second moments of Z and $\hat{Z}$ is expressed as

$$
\begin{aligned}
E[Z^2] &= E[(L_1 + L_2 + \cdots + L_N)^2] \\
&= \sum_{i=1}^{N} E[L_i^2] + 2\sum_{i=1}^{N-1}\sum_{j=i+1}^{N} E[L_i]E[L_j] \\
&= \sum_{i=1}^{N} e^{2m_{Y_i} + 2\sigma_{Y_i}^2} + \sum_{i=1}^{N-1}\sum_{j=i+1}^{N} e^{m_{Y_i} + m_{Y_j} + \frac{1}{2}\sigma_{Y_i}^2 + \frac{1}{2}\sigma_{Y_j}^2} \\
e^{2m_{\hat{Y}} + 2\sigma_{\hat{Y}}^2} &= \sum_{i=1}^{N} \sigma_{L_i}^2 + v_1^2 = v_2 + v_1^2
\end{aligned}
\tag{1.35}
$$

where

$$
\sigma_{L_i}^2 = E[L_i^2] - E^2[L_i],
\tag{1.36}
$$

$$
v_2 = \sum_{i=1}^{N} \sigma_{L_i}^2 = \sum_{i=1}^{N} e^{2m_{Y_i} + \sigma_{Y_i}^2}(e^{\sigma_{Y_i}^2} - 1).
\tag{1.37}
$$

Now it is possible to solve for $m_{\hat{Y}}$ and $\sigma_{\hat{Y}}^2$ by squaring both sides of (1.34) and dividing by (1.35), which yields

$$
m_{\hat{Y}} = \ln v_1 - \frac{\sigma_{\hat{Y}}^2}{2}
\tag{1.38}
$$

$$
\sigma_{\hat{Y}} = \ln\left(\frac{v_2}{v_1^2} + 1\right).
\tag{1.39}
$$

20

Given the moments $m_{\hat{Y}}$ and $\sigma_{\hat{Y}}$, the CDF of $\hat{Z}$ is

$$\Pr(\hat{Z} \leq x) = 1 - Q\left(\frac{\ln x - m_{\hat{Y}}}{\sigma_{\hat{Y}}}\right). \tag{1.40}$$

1.7.2 Schwartz and Yeh's Method

The method derived by Schwartz and Yeh is based on an exact expression for the first two moments of a sum of two lognormal RVs. Employing a recursive approach, the moments are calculated for a sum of more than 2 lognormal RVs by assuming that a sum of two lognormal RVs is also a lognormal RV. For example, suppose that $Z = L_1 + L_2 + L_3 + L_4$. The exact first two moments of $\ln(L_1 + L_2)$ are calculated. Then define a new Gaussian RV $Z_2 = \ln(L_1 + L_2)$, and let $Z = e^{Z_2} + L_3 + L_4$. Now compute the first two moments of $\ln(e^{Z_2} + L_3)$, and repeat the procedure for L_4. Since Schwartz-Yeh's method is recursive, we only need to consider the case of a sum of two lognormal RVs, i.e.

$$Z = L_1 + L_2 = e^{Y_1} + e^{Y_2} \approx e^{\hat{Y}} = \hat{Z} \tag{1.41}$$

where the Gaussian RVs Y_1 and Y_2 have means m_{Y_1} and m_{Y_2} and standard deviations σ_{Y_1} and σ_{Y_2} respectively. Define a new Gaussian RV, $Y_d = Y_2 - Y_1$ such that

$$m_{Y_d} = m_{Y_2} - m_{Y_1}, \tag{1.42}$$

$$\sigma_{Y_d}^2 = \sigma_{Y_1}^2 + \sigma_{Y_2}^2. \tag{1.43}$$

After a very long manipulation [14], the mean of $\hat{Y}$ is given by

$$m_{\hat{Y}} = m_{Y_1} + G_1 \tag{1.44}$$

where

$$G_1 = m_{Y_d}\Phi\left(\frac{m_{Y_d}}{\sigma_{Y_d}}\right) + \frac{\sigma_{Y_d}}{\sqrt{2\pi}}e^{-m_{Y_d}^2/(2\sigma_{Y_d}^2)}$$
$$+ \sum_{k=1}^{\infty} c_k e^{\frac{1}{2}k^2\sigma_{Y_d}^2}\left[e^{km_{Y_d}}\Phi\left(\frac{-m_{Y_d} - k\sigma_{Y_d}^2}{\sigma_{Y_d}}\right) + T_1\right], \tag{1.45}$$

21

$$T_1 = e^{-km_{Y_d}} \Phi \left(\frac{m_{Y_d} - k\sigma_{Y_d}^2}{\sigma_{Y_d}} \right), \tag{1.46}$$

and

$$c_k = \frac{(-1)^{k+1}}{k}. \tag{1.47}$$

The variance can also be computed similarly by

$$\sigma_Y^2 = \sigma_{Y_1}^2 - G_1^2 - 2\sigma_{Y_1}^2 G_3 + G_2 \tag{1.48}$$

where

$$\begin{aligned}
G_2 &= \sum_{k=1}^{\infty} b_k T_2 + \left[1 - \Phi \left(-\frac{m_{Y_d}}{\sigma_{Y_d}} \right) \right] (m_{Y_d}^2 + \sigma_{Y_d}^2) + \frac{m_{Y_d} \sigma_{Y_d}}{\sqrt{2\pi}} e^{-m_{Y_d}^2/(2\sigma_{Y_d}^2)} \\
&\quad + \sum_{k=1}^{\infty} b_k e^{-(k+1)m_{Y_d}+(k+1)^2 \sigma_{Y_d}^2/2} \Phi \left(\frac{m_{Y_d} - \sigma_{Y_d}^2(k+1)}{\sigma_{Y_d}} \right) \\
&\quad - 2 \sum_{k=1}^{\infty} c_k e^{-m_{Y_d}k + k^2 \sigma_{Y_d}^2/2} \left[m_{Y_k} \Phi \left(-\frac{m_{Y_k}}{\sigma_{Y_d}} \right) - \frac{\sigma_{Y_d}}{\sqrt{2\pi}} e^{-m_{Y_k}^2/(2\sigma_{Y_d}^2)} \right], \tag{1.49}
\end{aligned}$$

$$G_3 = \sum_{k=0}^{\infty} (-1)^k e^{k^2 \sigma_{Y_d}^2/2} T_1 + \sum_{k=0}^{\infty} (-1)^k T_2, \tag{1.50}$$

$$T_2 = e^{m_{Y_d}(k+1)+(k+1)^2 \sigma_{Y_d}^2/2} \Phi \left(\frac{-m_{Y_d} - (k+1)\sigma_{Y_d}^2}{\sigma_{Y_d}} \right), \tag{1.51}$$

$$b_k = \frac{2(-1)^{k+1}}{k+1} \sum_{j=1}^{k} \frac{1}{j}, \tag{1.52}$$

and

$$m_{Y_k} = -m_{Y_d} + k\sigma_{Y_d}^2. \tag{1.53}$$

It is obvious that this method is more computationally complex than Wilkinson's method. Approximately 40 terms are required in the infinite summations for accuracy to four significant digits [14]. With the moments derived using Schwartz and Yeh's method the CDF is then given by (1.40).

22

1.7.3 Farley's Method

The approach of Farley is based on assuming that the summands are N independent, identically distributed (iid) Gaussian RVs with mean m_Y and variance σ_Y^2. The complementary CDF of the lognormal sum

$$Z = \sum_{i=1}^{N} e^Y \tag{1.54}$$

is approximated as

$$\Pr(Z > l) \approx 1 - \left[1 - Q\left(\frac{\ln l - m_Y}{\sigma_Y}\right)\right]^N. \tag{1.55}$$

It was shown by Beaulieu and Abu-Dayya [15] that Farley's approximation is actually a strict lower bound on the complementary CDF of an iid lognormal sum. This can be shown by defining the two events

$$A = \{\text{at least one } L_i > l\},$$

$$B = \{\text{complement of event } A\}. \tag{1.56}$$

Since the two events, A and B, are mutually exclusive, the complementary CDF can be expressed as

$$\Pr(Z > l) = \Pr(Z > l, A) + \Pr(Z > l, B)$$

$$= \Pr(A) + \Pr(Z > l, B). \tag{1.57}$$

It can easily be shown that the second term in (1.57) is positive for continuous PDFs. As a result, a lower bound on the complementary CDF is given by

$$\Pr(Z > l) > \Pr(A) = 1 - \prod_{i=1}^{N} \Pr(L_i \leq l)$$

$$= 1 - \left[1 - Q\left(\frac{\ln l - m_Y}{\sigma_Y}\right)\right]^N. \tag{1.58}$$

Equivalently, the upper bound of CDF is given by

$$\Pr(Z \leq l) \leq \left[1 - Q\left(\frac{\ln l - m_Y}{\sigma_Y}\right)\right]^N. \tag{1.59}$$

23

Farley's method can also be extended to a sum of independent non-identical lognormal RVs. In this case the bounds on the CDF and its complement are

$$\Pr(Z \leq l) \leq \prod_{i=1}^{N} \left[1 - Q \left(\frac{\ln l - m_{Y_i}}{\sigma_{Y_i}} \right) \right], \tag{1.60}$$

$$\Pr(Z > l) > 1 - \prod_{i=1}^{N} \left[1 - Q \left(\frac{\ln l - m_{Y_i}}{\sigma_{Y_i}} \right) \right]. \tag{1.61}$$

1.7.4 Comparison of Methods

Numerous papers [13]–[19] have looked at the accuracy of the approximations to the lognormal sum distribution. Some of the works have looked at the accuracy of the moments while others have examined the accuracy of the CDF and complementary CDF. All the works are compared to simulation results to determine the accuracy of the approximation.

Schwartz and Yeh [14] compared the approximate CDF with one obtain through simulation and found that outside the range of 0.001 to 0.99, the approximate CDF did not match well to the simulated CDF for a sum of two lognormal RVs. As the number of summands was increased, the approximation to the CDF was found to deviate further from the simulated CDF. Schwartz and Yeh also studied how well the calculated moments approximated the actual moments of the sum distribution. It was found that for a sum of two lognormal RVs, the approximate mean and standard deviation were accurate. This is in contrast to Wilkinson's approximation [14] that does not accurately approximate the moments for a sum of two lognormal RVs. It was also shown that the estimated mean and standard deviation decreased in accuracy as the both the true variance and number of summands increased.

Beaulieu, Abu-Dayya and McLane [13],[15] compared the complementary CDF obtained using Wilkinson's, Schwartz and Yeh's, and Farley's approximations. It was reported in [14] that Wilkinson's approximation breaks down for $\sigma_X > 4$ dB but it is shown in [13] that this is only true when calculating the moments. In fact, Wilkinson's approximation is actually better than Schwartz and Yeh's for the complementary CDF. Farley's method was also compared and it was found that the approximation was almost an exact fit for the

24

values of the complementary CDF less than 10^{-2} and $\sigma_X = 6$ dB. However, for $\sigma_X = 12$ dB, Farley's approach was the best when compared to all the other approximations.

Cardieri and Rappaport [16] also compared the accuracy of Schwartz and Yeh's, and Wilkinson's method to simulation where the summands had different means and standard deviations. It was shown that Schwartz and Yeh's method is more accurate in calculating the moments of the sum distribution than Wilkinson's approximation. Also, it was shown that the error in Schwartz and Yeh's moment calculation is almost invariant with changing means and standard deviations.

By comparing the results of previous work it can be observed that when approximating the CDF, none of the approximations are valid over a large range of parameters such as the number of summands, the variance of the summands, and the range of the CDF. This thesis will look at determining a new approximation to the CDF that is valid over a large range of parameters.

1.8 Thesis Outline and Contributions

The ability to model the channel in a simple, yet accurate manner is required to be able to assess the performance of a wireless system. In particular, co-channel interference in a shadowing environment is an important problem that needs to be accurately modeled. Many previous works have looked at approximations to the lognormal sum distribution which can be used to model the co-channel interference. None of these works is widely accepted and accurate for a wide range of parameters. The work in this thesis will focus on determining a new approximation to the lognormal sum distribution that is accurate over a large range of parameters. The new approximation is well suited to UWB applications and is used to determine accurate expressions for the performance of a diversity pulse amplitude and position modulation (PAPM) UWB system with lognormal fading channels.

This thesis is organized as follows. Chapter 2 will investigate a new approximation to the lognormal sum CDF and PDF. Numerical results will be provided along with comparisons to Schwartz and Yeh's, Wilkinson's and Farley's approximations. Chapter 3 will

25

extend the result of Chapter 2 to a sum of correlated lognormal RVs. Again, numerical results and comparisons will be examined. Chapter 4 will examine the performance of a PAPM UWB system in lognormal fading with diversity reception. The approximation proposed in Chapter 2 will be used to find simple expressions for the performance of PAPM UWB with MRC and EGC combining. Finally, Chapter 5 will provide a conclusion and summary of contributions.

26

Chapter 2

Approximation to the Sum Distribution of Independent and Identically Distributed Lognormal Random Variables

The widely used approximations to lognormal sum distributions and densities by Wilkinson, and Schwartz and Yeh are based on the assumption that a lognormal sum distribution can be represented by another lognormal distribution. It is has been shown by many authors [13]–[18] that these approximations are only valid for a certain range of parameters. In this chapter, we will investigate a new approximation to the CDF and PDF for a sum of iid lognormal RVs that is more accurate over a larger range of parameters. Many numerical examples and results are provided to show the accuracy of the approximation.

27

2.1 CDF of the Lognormal Sum Distribution

A commonly used method for deriving a sum distribution is based on the characteristic function (CF). Given a sum of iid lognormal RVs

$$Z = \sum_{i=1}^{N} L_i,$$ (2.1)

the CF is given by [20]

$$\Phi_Z(\omega) = \prod_{i=1}^{N} \Phi_{L_i}(\omega)$$ (2.2)

where

$$\Phi_{L_i}(\omega) = E[e^{j\omega L_i}] = \int_{-\infty}^{\infty} f_{L_i}(x) e^{j\omega x} dx$$ (2.3)

is a Fourier transform of the PDF $f_{L_i}(x)$. Accordingly, the PDF of the sum distribution can be determined by taking the inverse Fourier transform of the CF which is given by

$$f_Z(x) = \frac{1}{2\pi} \int_{-\infty}^{\infty} \Phi_Z(\omega) e^{-j\omega x} d\omega$$ (2.4a)

$$= f_{L_1}(x) * f_{L_2}(x) * \cdots * f_{L_N}(x),$$ (2.4b)

where $*$ is the convolution operator. Using the results of [21] the CDF of Z is obtained as

$$F_Z(z) = \Pr(Z \le z) = \frac{1}{2} - \frac{1}{2\pi} \int_{-\infty}^{\infty} \frac{\Phi_Z(\omega)}{j\omega} e^{-j\omega z} d\omega$$ (2.5a)

$$= \frac{1}{2} - \frac{1}{\pi} \int_{0}^{\infty} \frac{\Im[\Phi_Z(\omega)] \cos(\omega z) - \Re[\Phi_Z(\omega)] \sin(\omega z)}{\omega} d\omega$$ (2.5b)

where $\Re[\cdot]$ and $\Im[\cdot]$ are the real and imaginary parts respectively. For most distributions it is possible to use this method to determine the sum distribution but it is not feasible with the lognormal distribution because there is no exact expression for the CF. Also it is difficult to numerically calculate the sum distribution using a N-fold convolution as in (2.4b) because the tail of the lognormal PDF decays very slowly as can be seen in Figure 1.3. A number of numerical methods including trapezoidal rule, Simpson's rule, adaptive

28

algorithms, fast Fourier transform, and a modified Clenshaw-Curtis method have been investigated by Beaulieu and Xie [17],[22] to evaluate (2.5b). It was determined that the modified Clenshaw-Curtis method was very accurate and highly efficient when compared to the other numerical methods.

While the above results are for iid RVs, the same method can be used for a sum of independent lognormal RVs with different means m_i and variances σ_i^2. From (1.28), it is possible to define a new RV as

$$L_i^* = e^{-m_i} L_i \tag{2.6}$$

where the PDF of L_i^* is

$$f_{L_i^*}(u) = f_{L_i}(u) e^{m_i}$$
$$= f_0(le^{-m_i}). \tag{2.7}$$

Now it can be seen that $L_i^* \sim \Lambda(0, \sigma_i^2)$, and m_i is a scaling parameter. The sum (1.31) can then be expressed in terms of a sum of lognormal RVs with zero mean as

$$Z = \sum_{i=1}^{N} c_i L_i^* \tag{2.8}$$

where $c_i = e^{m_i}$ is the weight to account for the scaling parameter. The characteristic function can then be written as

$$\Phi_Z(\omega) = \prod_{i=1}^{N} \Phi_{L_i}(\omega) = \prod_{i=1}^{N} \Phi_{L_i^*}(c_i \omega). \tag{2.9}$$

Due to the form of the CF it is possible to see that the parameter m_i is only a frequency scaling factor and there is no loss in generality in assuming it is equal to zero. This will allow us to focus on an approximation for a sum of zero-mean, independent lognormal RVs.

On a conventional plot of the CDF as seen in Figure 1.5, it is hard to see the characteristics of the CDF in the tails. Another way to visualize the CDF is to use a probability plot [23] that transforms a CDF of a RV into a straight line. For normal probability paper, the y-axis is transformed according to $\Phi^{-1}(\cdot)$, where

$$\Phi(x) = \frac{1}{\sqrt{2\pi}} \int_{-\infty}^{x} e^{-\frac{t^2}{2}} dt \tag{2.10}$$

29

is the zero-mean, unit-variance Gaussian CDF. This will result in a normal CDF being transformed into a straight line. For a lognormal probability paper, the abscissa must also be scaled by $10\log_{10}(\cdot)$ to obtain the x-axis in units of dB. Performing these two transforms, the lognormal CDF $F_L(l)$ is expressed as

$$\Phi^{-1}(F_L(\gamma)) = \frac{\lambda\gamma - m_Y}{\sigma_Y}$$

$$= \frac{\gamma - m_X}{\sigma_X} \qquad (2.11)$$

where $\gamma = 10\log_{10}l$. Notice that (2.11) is in the form of a straight line as is expected for the lognormal probability paper transform. The lognormal CDF plotted on lognormal probability paper is shown in Figure 2.1 for $\sigma = 0.15$, 0.5, 6 dB and 9 dB. Comparing Figures 1.5 and 2.1 you notice that it is easier to observe the behavior in the tails of the distributions using probability paper.

The CDF of a sum of independent lognormal RVs can be calculated using the modified Clenshaw-Curtis method described in [22]. The range being examined in this thesis is from 10^{-6} to $1 - 10^{-6}$, which is much larger than most previous works. For example, [14] only considered the range from 0.0005 to 0.9999. Also, Reference [13] simulated the CDF for values greater than 10^{-5}. Recently, Beaulieu and Xie [17] examined the accuracy of Farley's, Wilkinson's, and Schwartz and Yeh's method over the range 10^{-6} to $1 - 10^{-6}$. It was determined that none of the examined approximations were accurate over the entire range of interest, and the approximations deviated further from the actual values as the number of summands increased. They also proposed a minimax approximation based on lognormal probability paper that minimizes the maximum error [17]. While the minimax approximation reduces the maximum error when compared to other approximations, it is still not accurate over the entire range of interest because it approximates the sum distribution as another lognormal RV.

The sum of iid lognormal RVs for different numbers of summands is plotted on the same graph to compare their behavior in Figures 2.2 and 2.3. From the use of lognormal probability paper, it is possible to extract information about the behavior of the sum distribution. It is observed that the sum distributions are not lognormal (i.e. not straight lines)

30
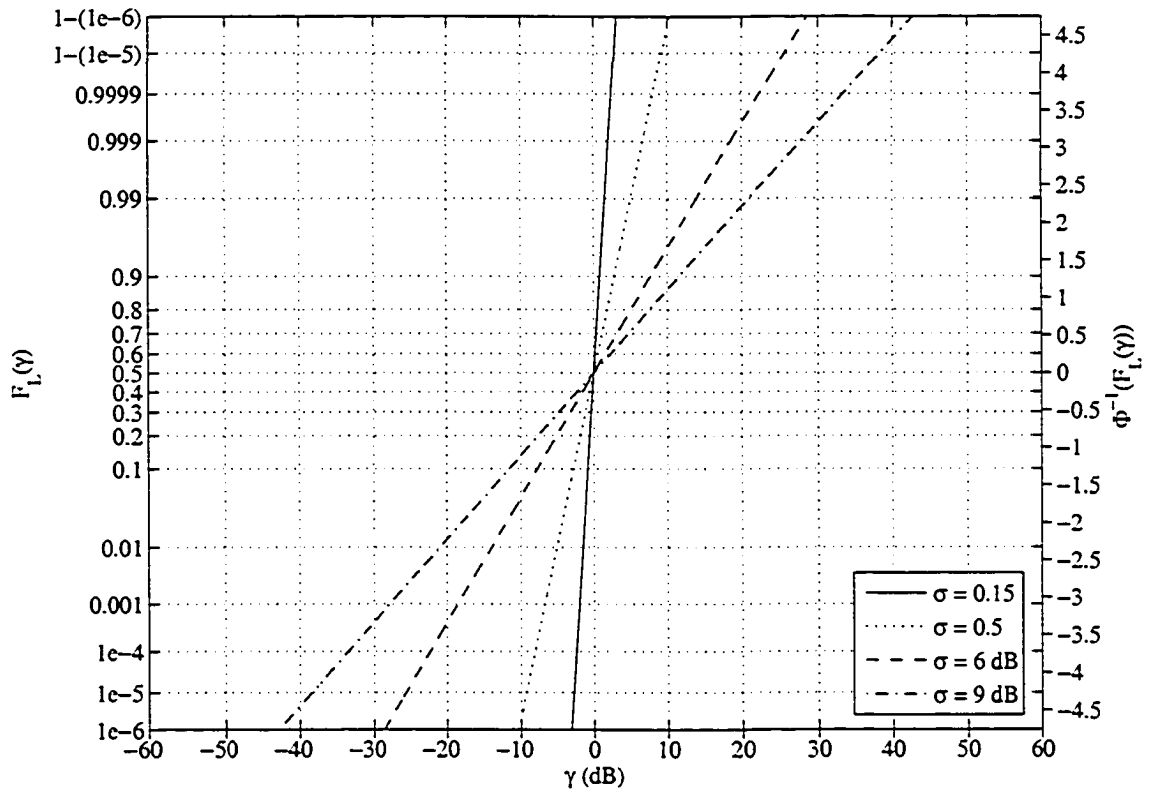
Figure 2.1. Lognormal CDF $\Lambda(0, \sigma^2)$ for $\sigma = 0.15$, 0.5, 6 dB, and 9 dB on lognormal probability paper.

31

but smooth curves, that are convex down, with increasing concavity as N increases. Only in the range [0.1, 0.9], are the CDFs close to a straight line. Outside this range, the curves deviate from a straight line. These observations are in contrast to many published examples that assume the sum distribution can be approximated as another lognormal distribution [14],[17].

It is also observed that while the tail of the complementary CDF is largely unaffected by the number of summands, the tail of the CDF is influenced by the number of summands. The complementary CDF tail asymptotically approaches that of of single lognormal RV. This is explained by Janos [24] who showed that the tail of a sum distribution approaches that of the summand in the distribution with the largest dB spread. However, in the iid case, the higher order moments of the sum distribution will approach N times the moments of a single lognormal RV.

2.2 CDF Approximation

It is clear from Figures 2.2 and 2.3 that a set of smooth functions could be used to approximate the CDF. Since the CDF has a nice shape on lognormal probability paper, it is easier to pick a function that will fit in this domain and then transform the function to obtain an approximation for the CDF. This corresponds to fitting a curve based on a plot of $\Phi^{-1}(F_L(\gamma))$ versus γ, which is the right hand axis of Figure 2.1.

Let $f(\gamma)$ be the approximating function defined on lognormal probability paper. Now it is possible to express the approximate CDF in units of dB as

$$F_Z(\gamma) = \Phi(f(\gamma)). \qquad (2.12)$$

The CDF can then also be written as

$$F_Z(z) = \Pr(Z \le z) = \Phi\left[f\left(\frac{\ln z}{\lambda}\right)\right]. \qquad (2.13)$$

It is necessary to empirically choose an approximating function. The requirements are that the function be simple, have few parameters, and provide an accurate approximation to the

32
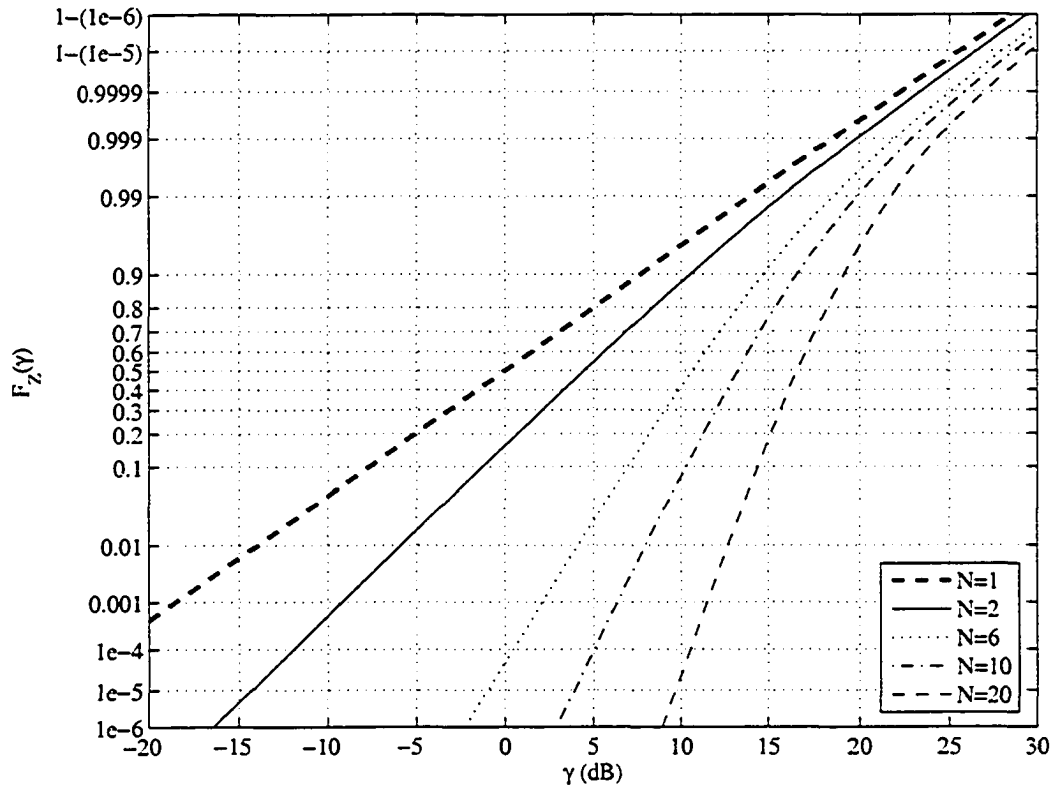
Figure 2.2. The CDF of a sum of N lognormal RVs ($\sigma_\chi = 6$ dB) for $N = 2, 6, 10$ and 20.

33
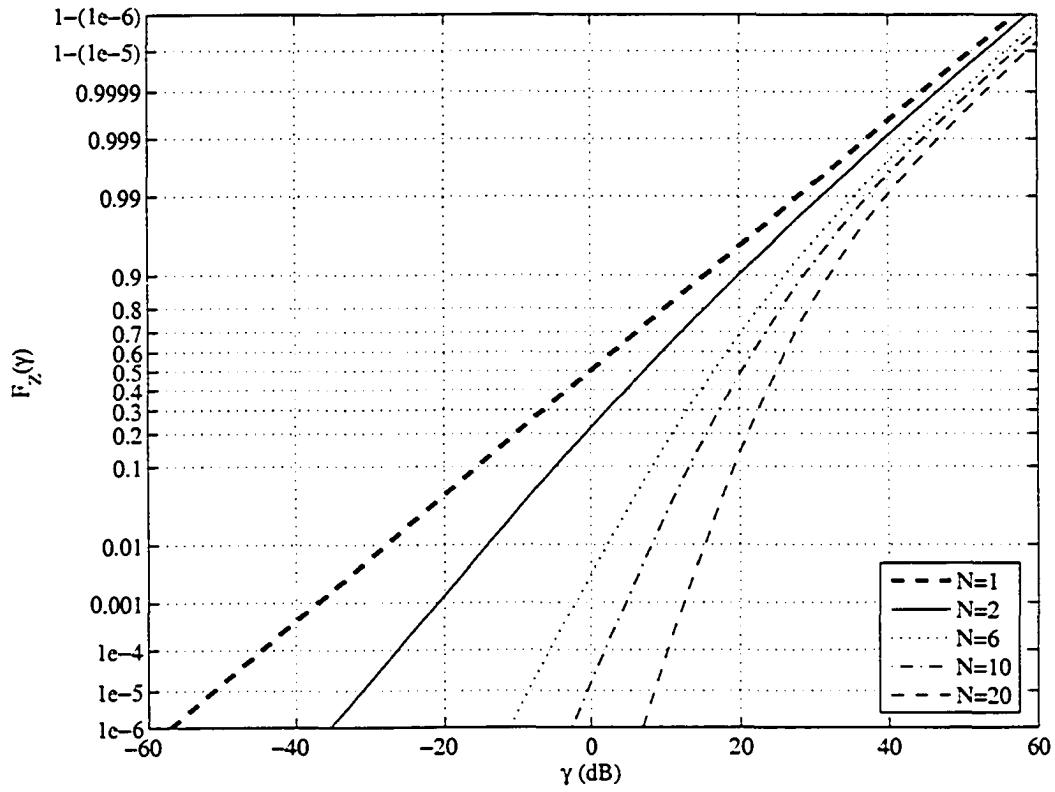
Figure 2.3. The CDF of a sum of N lognormal RVs ($\sigma_X = 12$ dB) for $N =2$, 6, 10 and 20.

34

distribution. From these criteria and the shape of the curves in Figures 2.2 and 2.3, it is evident that the quadratic function of the form

$$f(\gamma) = a_0 + a_1\gamma + a_2\gamma^2 \tag{2.14}$$

could be a possible choice for the approximating function, where a_0, a_1 and a_2 are parameters that need to be calculated. The parameters a_0, a_1 and a_2 are optimized using a non-linear least squares method [25],[26]. The results of the quadratic approximating function can be found in Figures 2.4 and 2.5, in which the markers are the exact CDFs and the solid lines are the approximations for each number of summands. While the approximate CDF obtained using the quadratic function is accurate over most of the range, it is less accurate for values of the CDF greater than 0.99 as the number of summands increases. As a result, the quadratic function does not provide the required accuracy needed for a good approximation.

Another possibility is using an exponential function with a negative exponent, which will have a shape very similar to the exact CDF. The form of such an approximating function is given by

$$f(\gamma) = a_0 - a_1 e^{-a_2\gamma} \tag{2.15}$$

where a_0, a_1 and a_2 are constants that need to be determined. The exponential approximation has an advantage that it is closed-form and very simple for a given number of summands. Given (2.15) the approximate CDF in units of dB is

$$F_Z(\gamma) = \Phi(a_0 - a_1 e^{-a_2\gamma}), \tag{2.16}$$

which can also written as

$$F_Z(z) = \Phi(a_0 - a_1 z^{-a_2/\lambda}). \tag{2.17}$$

The exponential approximating function is plotted in Figures 2.6 and 2.7 for $\sigma_X = 6$ dB and $\sigma_X = 12$ dB, respectively. It can be easily seen that the exponential approximating function is more accurate than the quadratic approximation over the entire range of the CDF and number of summands. To maintain this high accuracy, it is necessary to set the

35
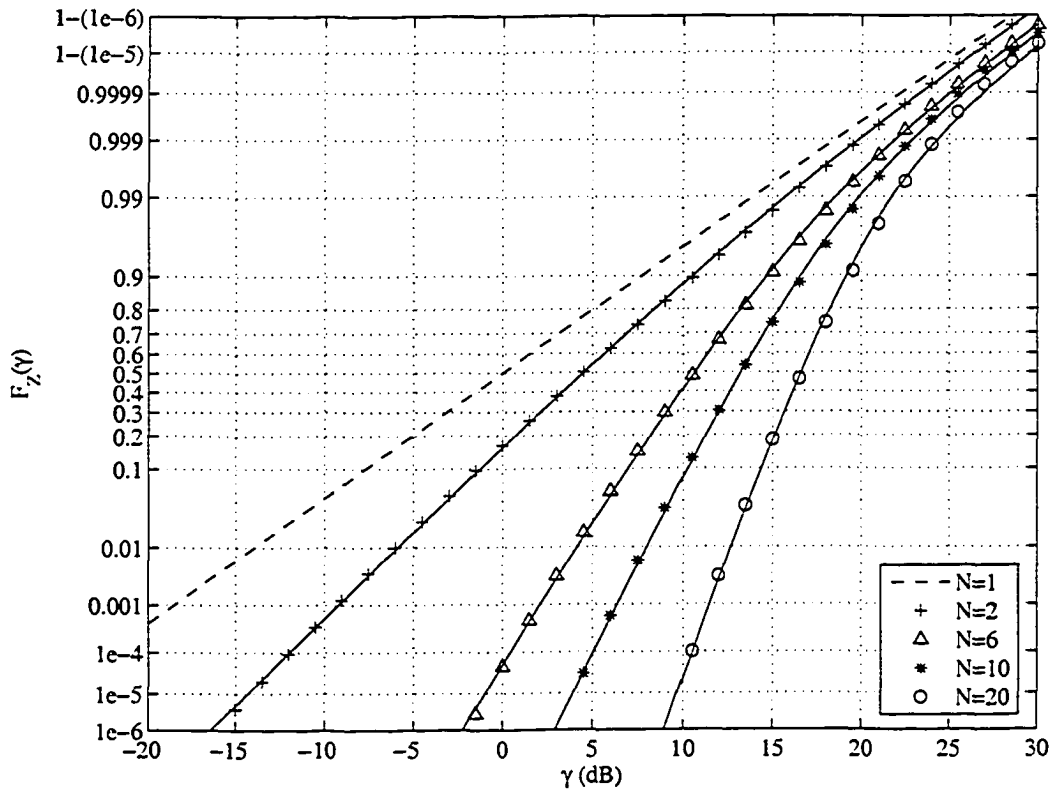
Figure 2.4. The CDF of a sum of N lognormal RVs ($\sigma_\chi = 6$ dB) and the quadratic approximating function $f(\gamma) = a_0 + a_1\gamma + a_2\gamma^2$ for $N = 2$, 6, 10 and 20 (line is exact and marker is approximate).

36

$F_z(\gamma)$

1–(1e–6)
1–(1e–5)
0.9999
0.999
0.99
0.9
0.8
0.7
0.6
0.5
0.4
0.3
0.2
0.1
0.01
0.001
1e–4
1e–5
1e–6

-60   -40   -20   0   20   40   60

γ (dB)

– – – N=1
+ N=2
△ N=6
∗ N=10
○ N=20
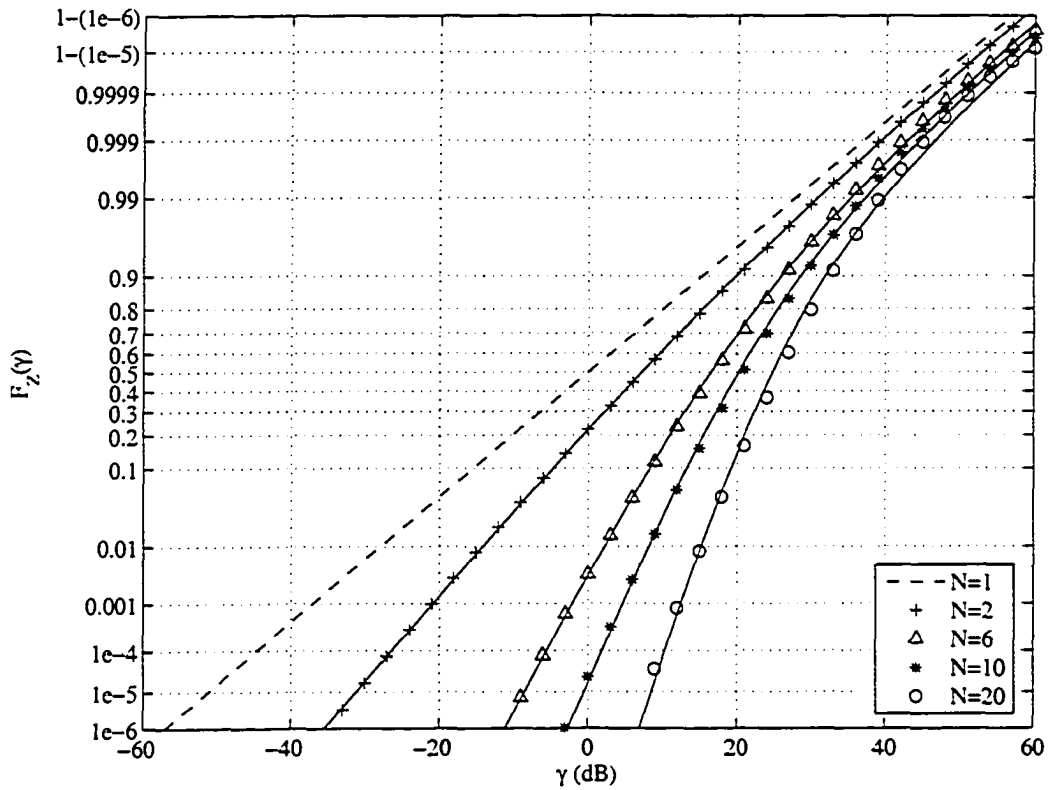
Figure 2.5. The CDF of a sum of N lognormal RVs ($\sigma_\chi = 12$ dB) and the quadratic approximating function $f(\gamma) = a_0 + a_1\gamma + a_2\gamma^2$ for $N = 2, 6, 10$ and 20 (line is exact and marker is approximate).

37
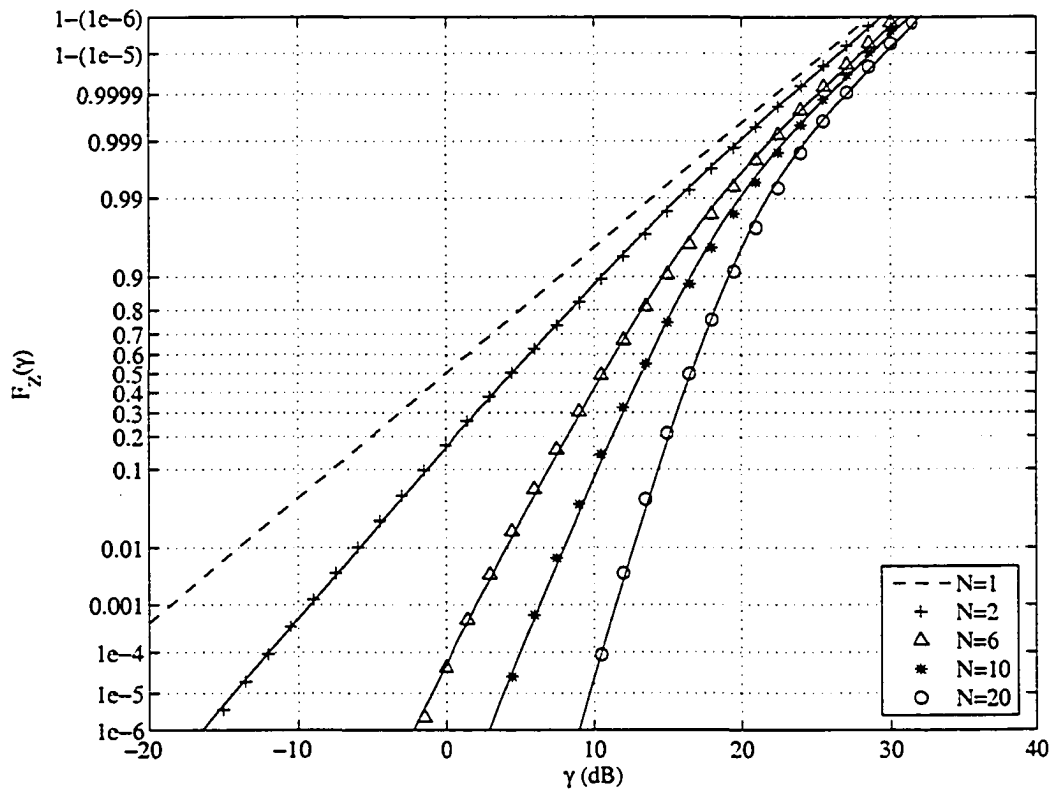
Figure 2.6. The CDF of a sum of N lognormal RVs ($\sigma_X = 6$ dB) and the approximating function $f(\gamma) = a_0 - a_1 e^{-a_2 \gamma}$ for $N = 2$, 6, 10 and 20 (line is exact and marker is approximate).

38
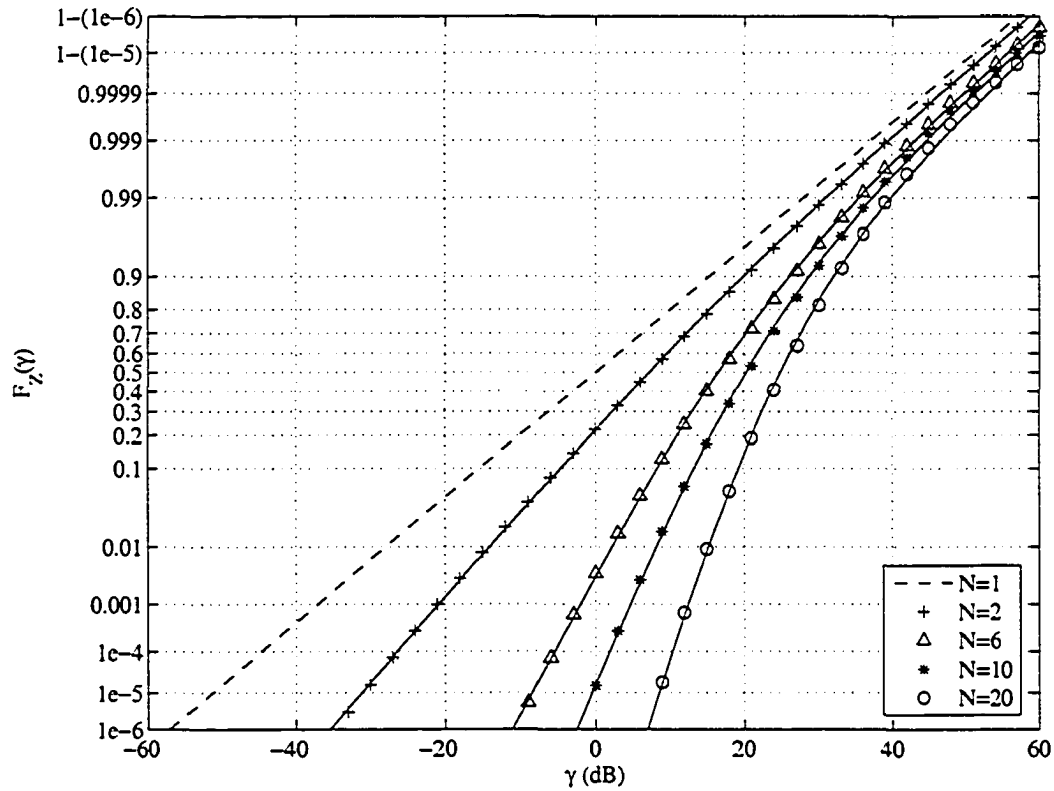
Figure 2.7. The CDF of a sum of N lognormal RVs ($\sigma_X = 12$ dB) and the approximating function $f(\gamma) = a_0 - a_1 e^{-a_2 \gamma}$ for $N = 2$, 6, 10 and 20 (line is exact and marker is approximate).

39

TABLE 2.1

The coefficients for the approximation $\Phi(a_0 - a_1 e^{-a_2 \gamma})$.

N	$\sigma_\chi = 6$ dB			$\sigma_\chi = 12$ dB		
	a_0	a_1	a_2	a_0	a_1	a_2
2	25.636	26.600	0.008282	23.911	24.670	0.004301
3	15.954	17.738	0.01553	16.333	17.674	0.007094
4	13.656	16.160	0.01993	12.688	14.512	0.009947
5	11.083	14.367	0.02702	11.217	13.483	0.01200
6	10.760	14.685	0.02938	10.132	12.809	0.01401
7	10.037	14.670	0.03335	9.465	12.531	0.01567
8	9.465	14.825	0.03723	8.942	12.382	0.01723
9	9.087	15.166	0.04051	8.523	12.326	0.01869
10	8.748	15.575	0.04381	8.205	12.373	0.02004
11	8.435	16.052	0.04720	8.027	12.532	0.02103
12	8.156	16.612	0.05061	7.772	12.624	0.02227
13	8.021	17.241	0.05297	7.615	12.788	0.02322
14	7.896	17.905	0.05529	7.423	12.937	0.02434
15	7.647	18.669	0.05897	7.290	13.120	0.02524
16	7.652	19.340	0.05999	7.144	13.311	0.02625
17	7.418	20.258	0.06385	7.033	13.515	0.02709
18	7.310	21.132	0.06632	6.942	13.731	0.02786
19	7.204	22.068	0.06883	6.826	13.952	0.02880
20	7.223	22.799	0.06961	6.745	14.181	0.02954

value of the parameters a_0, a_1 and a_2 for a particular sum, i.e. a particular set of values for N and σ_X. The calculated values of a_0, a_1 and a_2 for $\sigma_X = 6$ dB and $\sigma_X = 12$ dB can be found in Table 2.1.

Comparing the exponential approximation with the approximations discussed in Chapter 1 will provide an important measure that will determine if this exponential approximation is more accurate than Schwartz and Yeh's, Wilkinson's, and Farley's approximations. Figures 2.8 - 2.15 compares Wilkinson's, Schwartz and Yeh's, Farley's approximations with the exponential approximation for $N = 2, 6, 10$ and 20 for dB spreads of 6 and 12. As is illustrated in the figures, the exponential approximation is more accurate that Schwartz and Yeh's, Wilkinson's, and Farley's approximations for any number of summands and dB spread. For $N = 2$, all the approximations are relatively good because the distribution of two summands is almost a lognormal distribution.

Schwartz and Yeh's approximation is close to the exact distribution in the range 0.1 to 0.99 but deviates in the tails of the CDF and complementary CDF. In the tail of the CDF, Schwartz and Yeh's approximation deviates up to 3 orders of magnitude, and the deviation increases as the dB spread becomes larger. The same deviation is seen in the tail of the complementary CDF but it is much larger. For example, for $N = 20$ and $\sigma_X = 6$ dB, there is 7 orders of magnitude difference between Schwartz and Yeh's approximation and the exact CDF when the CDF equals $1 - 10^{-6}$. The performance of Schwartz and Yeh's approximation is much better in the tail of the CDF than in the tail of the complementary CDF.

The simpler Wilkinson's approximation is generally more accurate than Schwartz and Yeh's method for values of the CDF larger than 0.1. For 6 dB spread, Wilkinson's approximation is almost the same as Schwartz and Yeh's approximation, but slightly better in the tail of the complementary CDF and slightly worse in the tail of the CDF. This is in contrast to the case of 12 dB spread where Wilkinson's approximation is very close to the tail of the exact complementary CDF, but deviates more than Schwartz and Yeh's approximation in the tail of the CDF. For example, in the tail of the CDF, Wilkinson's approximation deviates 5 orders of magnitude for $N = 20$ and $\sigma_X = 12$ dB, while Schwartz and Yeh's method

41

only deviates by 3 orders of magnitude. In contrast to Schwartz and Yeh's method, Wilkinson's approximation for the tail of the complementary CDF improves as the dB spread increases. It is also observed that Wilkinson's method decreases in accuracy as the number of summands increases.

Farley's approximation is actually a strict upper bound for the CDF and a strict lower bound for the complementary CDF. It is observed that as the number of summands increases, the performance of Farley's approximation becomes worse. Also, the performance deteriorates as the dB spread becomes smaller. For example, Farley's approximation deviates in the tail of the CDF from the exact distribution by over 5 orders of magnitude for $N = 20$ and $\sigma_X = 6$ dB.

It is observed in Figures 2.8 - 2.15, that the exponential approximation is always better than any of the other approximations when considered over the entire range. In certain regions of the CDF, other approximations might be as accurate as the exponential approximation but if these approximations are good in one region, they are generally terrible in other regions. For example, Farley's approximation for $N = 20$ and $\sigma_X = 6$ dB is as accurate as the exponential approximation for values of the CDF greater than 0.999, but fails for values less than 0.99 and deviates by up to 3 orders of magnitude in the tail of the CDF. The areas of great interest are the tails of the CDF and complementary CDF. In these regions, the exponential approximation performs better than both Schwartz and Yeh's, and Wilkinson's approximation, and deviates very slightly from the exact distribution over the entire range of the CDF.

2.3 PDF Approximation

While the CDF of a sum of lognormal RVs is important in calculations such as outage probabilities, the PDF is equally important. For example, the PDF is required to be able to calculate the BER of certain communications systems. In general, given a CDF $F_Z(z)$, the

42
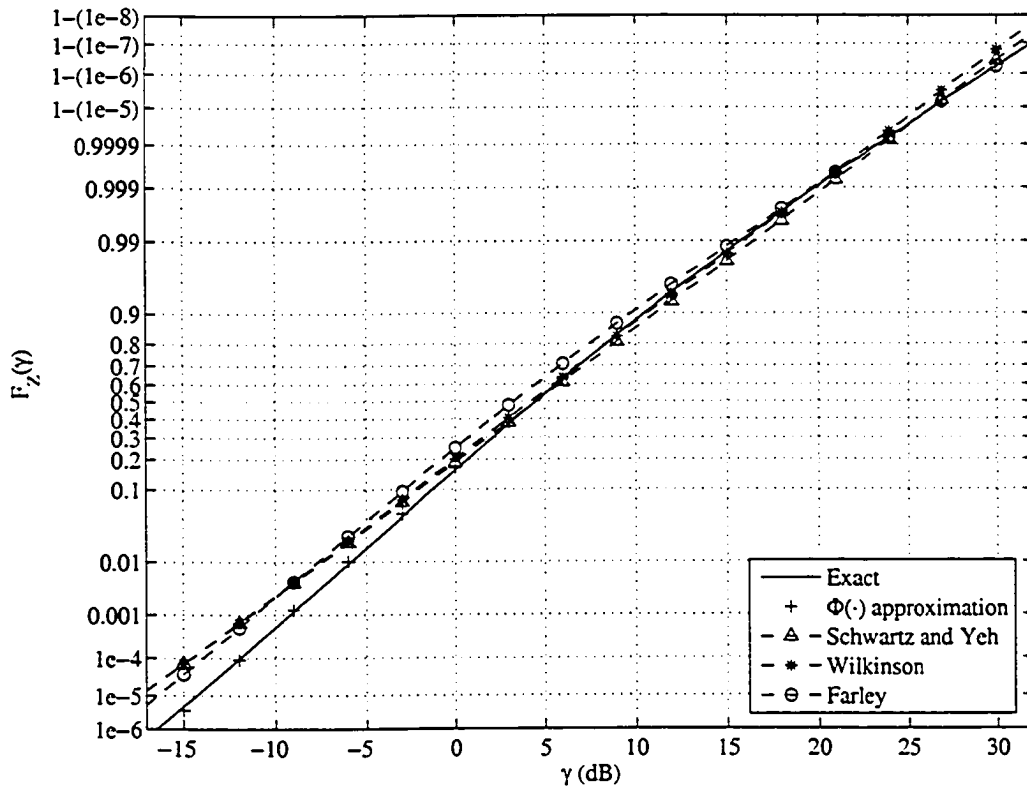
Figure 2.8. The CDF of a sum of $N = 2$ lognormal RVs ($\sigma_X = 6$ dB) and various CDF approximations.

43
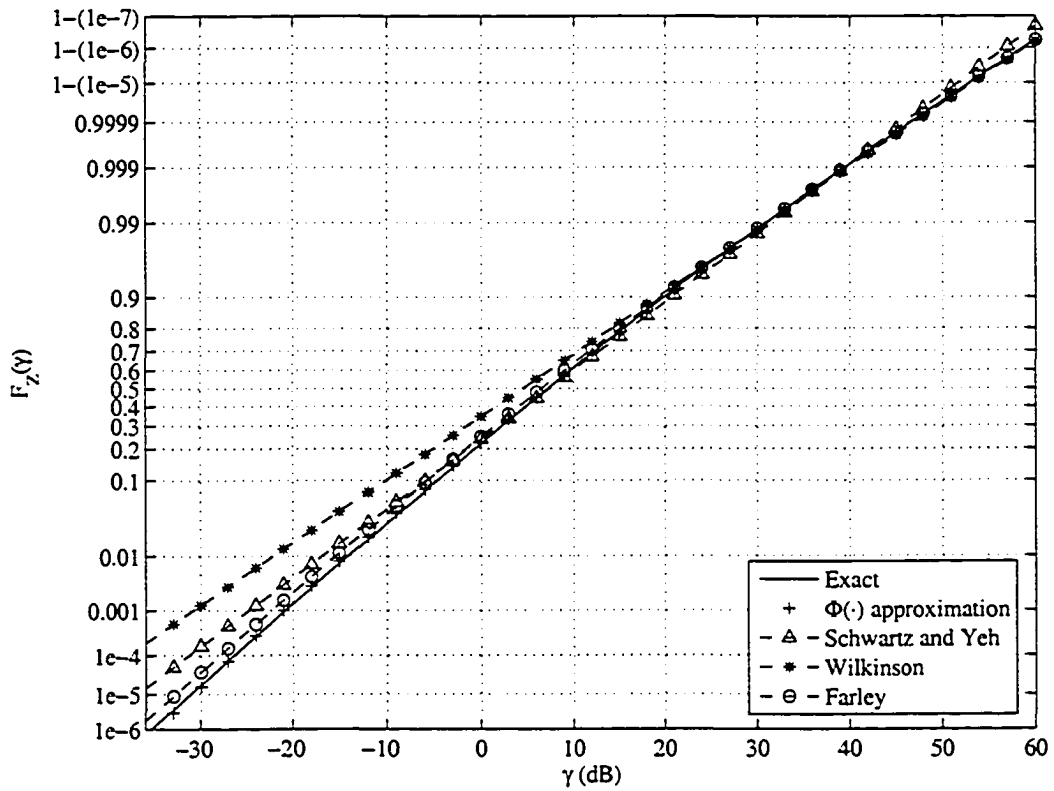
Figure 2.9. The CDF of a sum of $N = 2$ lognormal RVs ($\sigma_X = 12$ dB) and various CDF approximations.

44
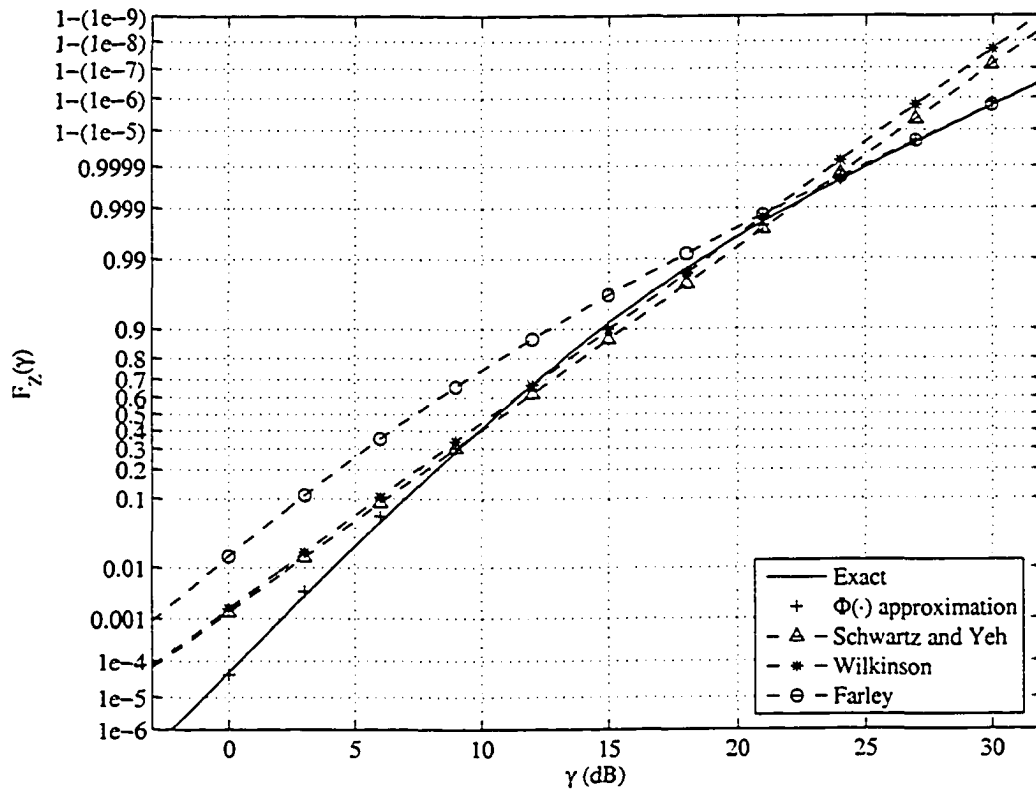
Figure 2.10. The CDF of a sum of $N = 6$ lognormal RVs ($\sigma_X = 6$ dB) and various CDF approximations.

45
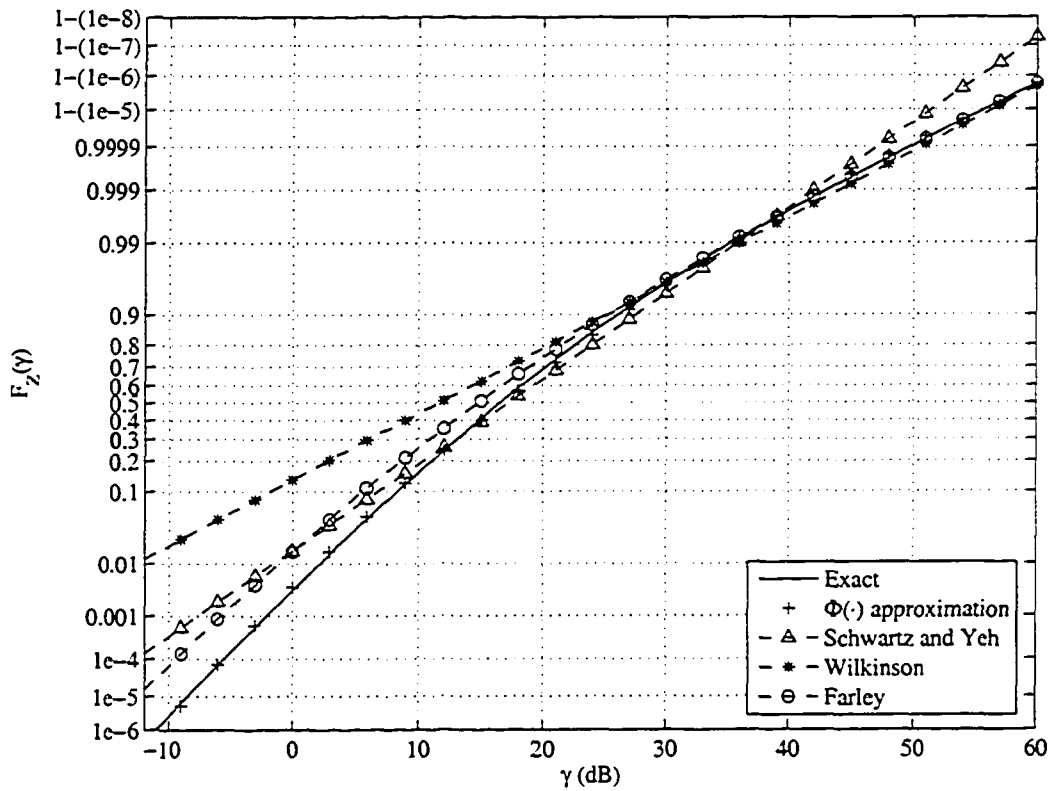
Figure 2.11. The CDF of a sum of $N = 6$ lognormal RVs ($\sigma_X = 12$ dB) and various CDF approximations.

46
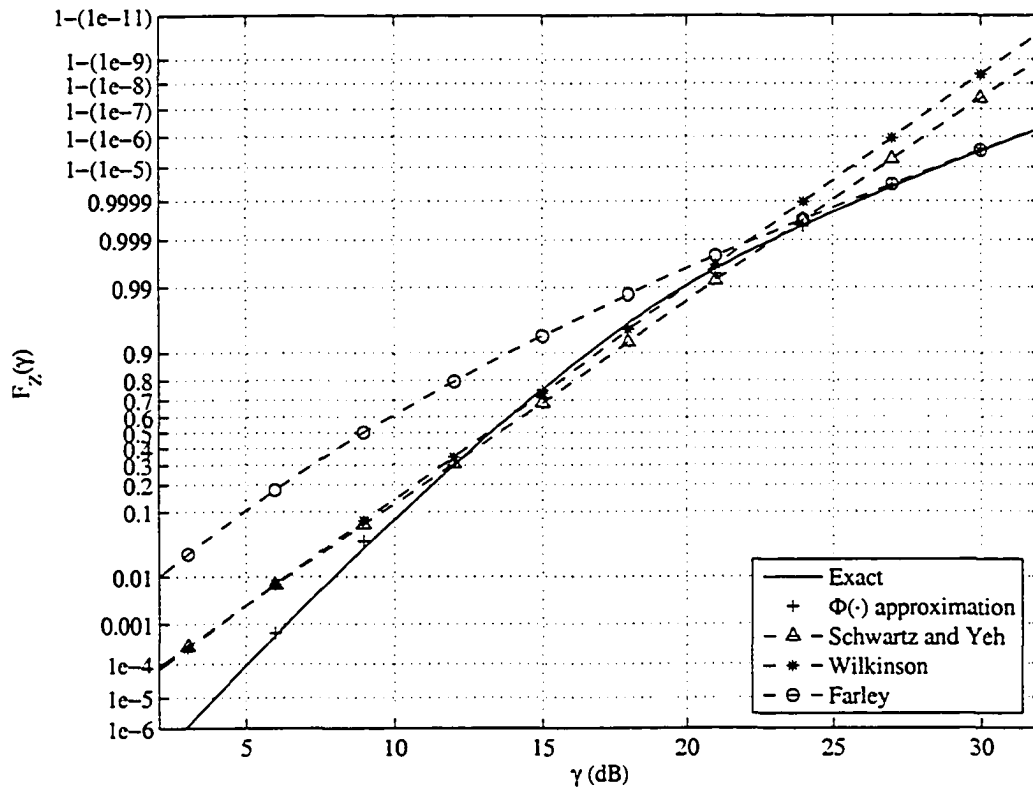
Figure 2.12. The CDF of a sum of $N = 10$ lognormal RVs ($\sigma_X = 6$ dB) and various CDF approximations.

47
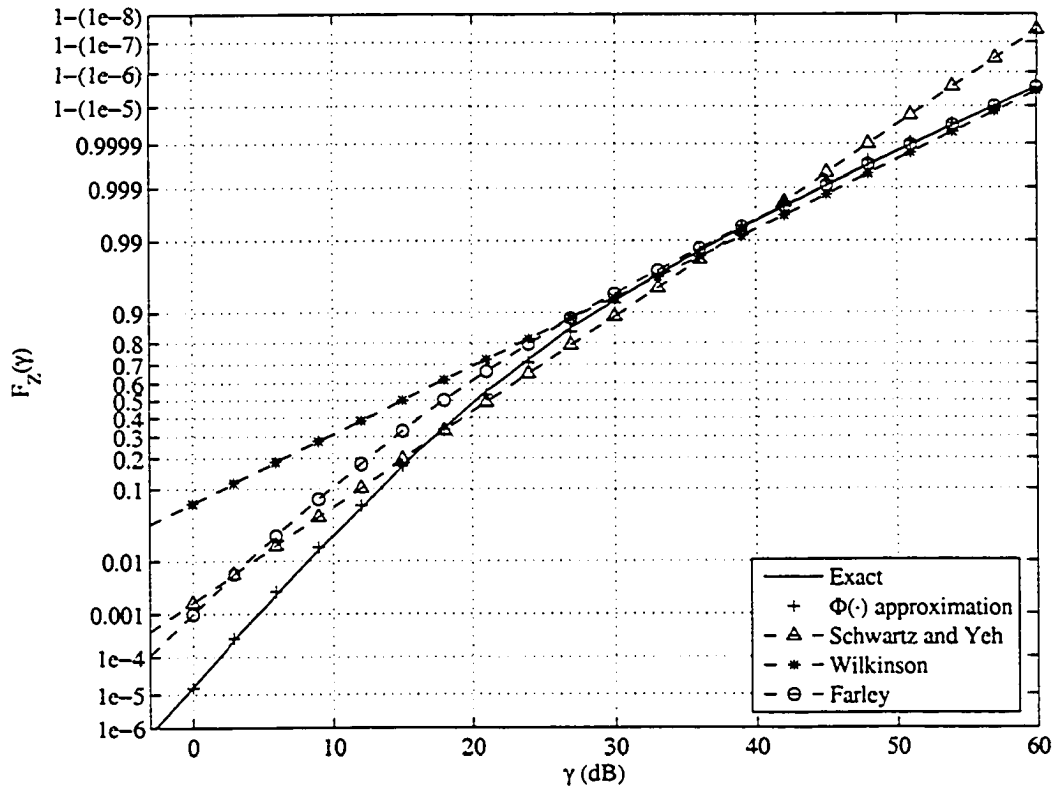
Figure 2.13. The CDF of a sum of $N = 10$ lognormal RVs ($\sigma_X = 12$ dB) and various CDF approximations.

48
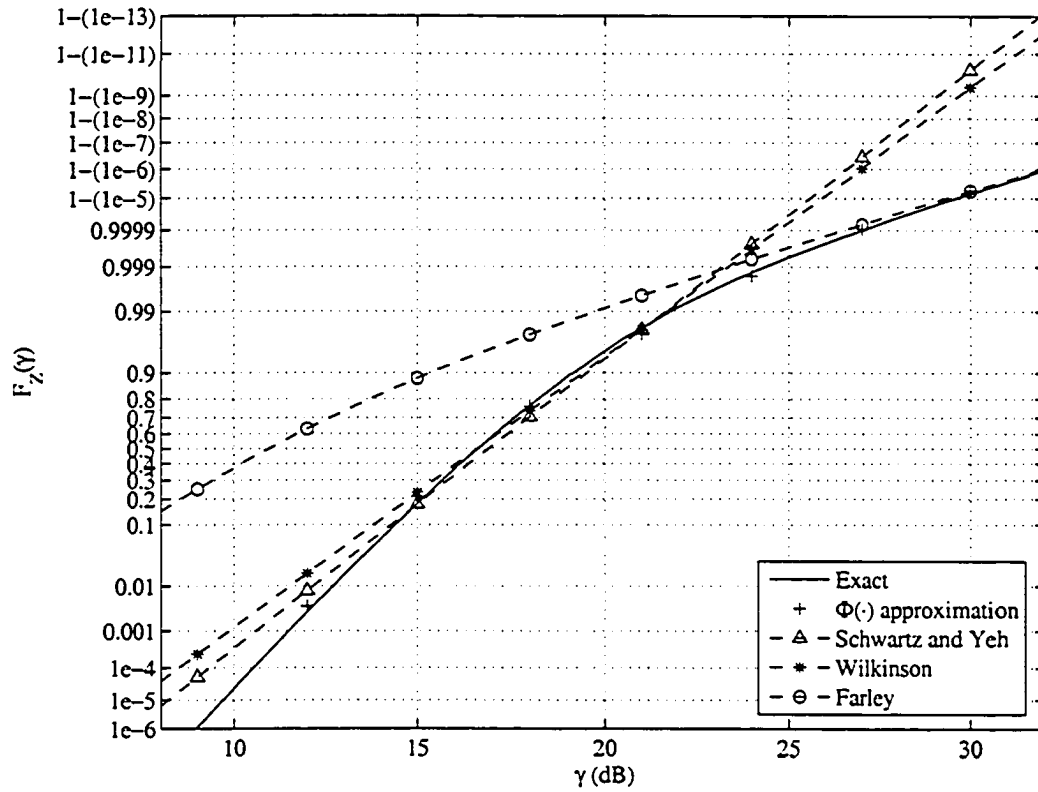
Figure 2.14. The CDF of a sum of $N = 20$ lognormal RVs ($\sigma_X = 6$ dB) and various CDF approximations.

49
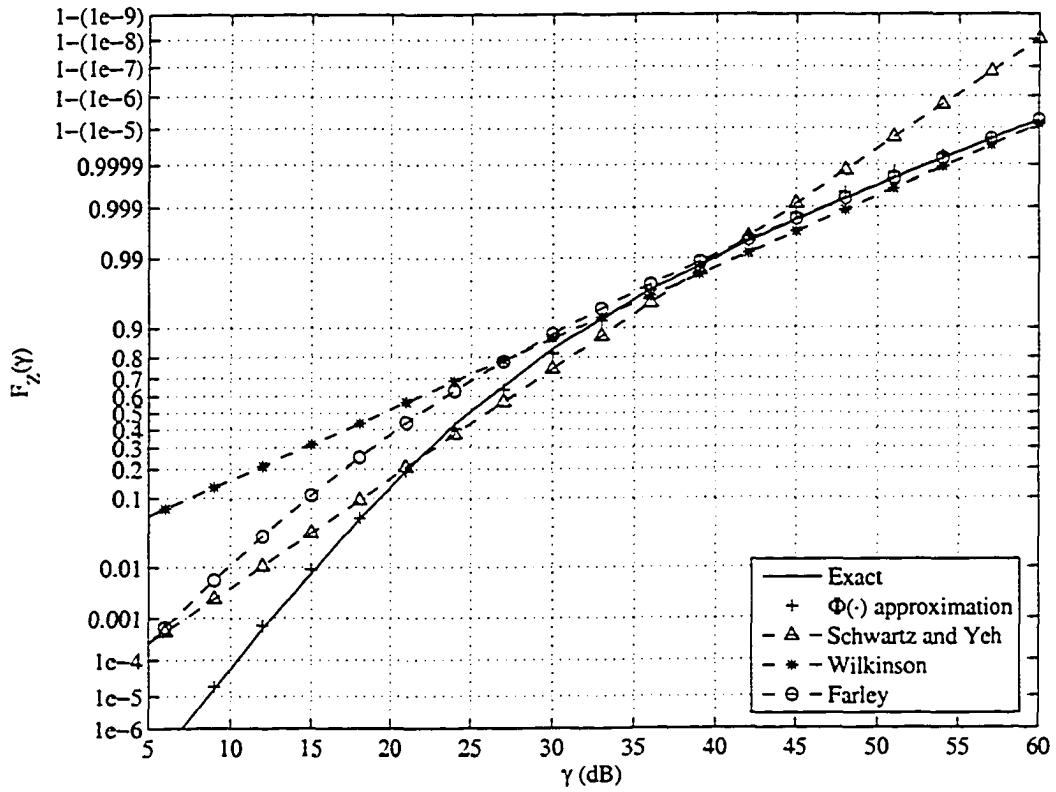
Figure 2.15. The CDF of a sum of $N = 20$ lognormal RVs ($\sigma_X = 12$ dB) and various CDF approximations.

50

PDF of the distribution can be determined by using the relation

$$f_Z(z) \triangleq \frac{dF_Z(z)}{dz}.$$ (2.18)

Note that the derivative of an accurate approximation to a function is not in general, necessarily an accurate approximation to the derivative of the function. Consider, for example, a Fourier approximation to a square wave. The derivative of the square wave is infinite at the transitions, but the derivative of the Fourier approximation is finite at these transitions. As a result, it is necessary to evaluate whether the exponential approximation given by (2.15) will produce an equally accurate approximation to the PDF as the CDF.

Assuming that (2.18) will produce an accurate PDF, (2.17) can be formally differentiated to yield

$$f_Z(z) = \frac{a_1 a_2 z^{-(a_2/\lambda+1)}}{\lambda \sqrt{2\pi}} \exp\left(-\frac{1}{2}(a_0 - a_1 z^{-a_2/\lambda})^2\right)$$ (2.19)

as a potential approximation to the PDF of a sum of lognormal RVs, where the values of a_0, a_1, and a_2 are identical to the values obtained for the CDF. In units of dB, the approximate PDF can be expressed as

$$f_Z(\gamma) = \frac{a_1 a_2}{\sqrt{2\pi}} \exp\left(-\frac{1}{2}(a_0 - a_1 e^{-\gamma a_2})^2 - \gamma(a_2 + \lambda)\right).$$ (2.20)

The PDF approximation is shown in Figures 2.16 - 2.23 for values of $N = 2, 6, 10$ and 20 for dB spreads of 6 and 12. In addition, the PDF obtained using Schwartz and Yeh's, Wilkinson's, and Farley's methods are also plotted on Figures 2.16 - 2.23 to allow for comparisons. The PDF is determined numerically by performing an inverse transform using a modified Clenshaw-Curtis method on the characteristic function that is also obtained using the modified Clenshaw-Curtis method [22]. A number of observations can be made from these plots.

1. The PDF approximation obtained from the exponential CDF approximation is accurate over the entire range.

2. The PDF obtained using Schwartz and Yeh's method is only accurate when the PDF is decreasing. Schwartz and Yeh's approximation deviates by as much as 3 orders of magnitude, but the error decreases as γ increases and as the dB spread is reduced.

51

3. Wilkinson's approximation follows Schwartz and Yeh's approximation very closely for $\sigma_X = 6$ dB, but does not accurately approximate the PDF as N increases. For $\sigma_X = 12$ dB, Wilkinson's approximation is always worse than Schwartz and Yeh's by over 2 orders of magnitude for the increasing section of the PDF. In the decreasing section, Wilkinson's approximation is very close to the numerically determined PDF.

4. Taking the derivative of (1.59) results in an approximation for the PDF based on Farley's approximation to the CDF. It is observed that this PDF is better than both Schwartz and Yeh's, and Wilkinson's approximation for $N = 2$, but as N increases, Farley's approximation is very inaccurate over the entire range of γ. This is consistent over all dB spreads.

5. The exponential PDF approximation is very consistent over γ, N and σ_X, which is in contrast to the other approximations considered.

2.4 Summary

A new method for approximating the distributions and densities of a sum of lognormal RVs was introduced in this chapter. It can easily be seen when using lognormal probability paper that a lognormal sum distribution is not lognormal and as a consequence should not be approximated as one. This leads to new methods of approximating the distribution and densities based on lognormal probability paper. In this chapter, a highly accurate, closed-form approximation for the lognormal sum distribution was introduced based on the use of lognormal probability paper that linearizes the distribution. It was seen that this new approximation was very accurate for a large number of parameters, such as the number of summands and dB spread. The approximation was also compared to other well known approximations by Schwartz and Yeh, Wilkinson, and Farley. It was determined that the new approximation performed many orders of magnitude better than the other approximations, and only slightly deviated from the exact distribution.
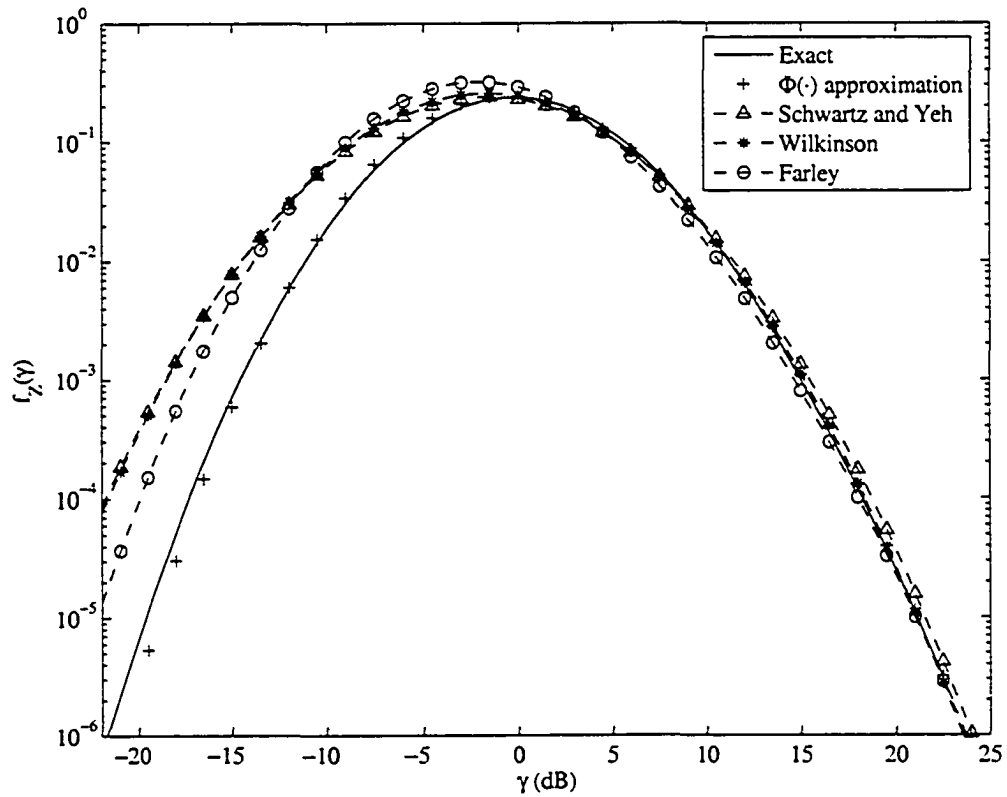
Figure 2.16. The PDF of a sum of $N = 2$ lognormal RVs ($\sigma_X = 6$ dB) and various PDF approximations.

53
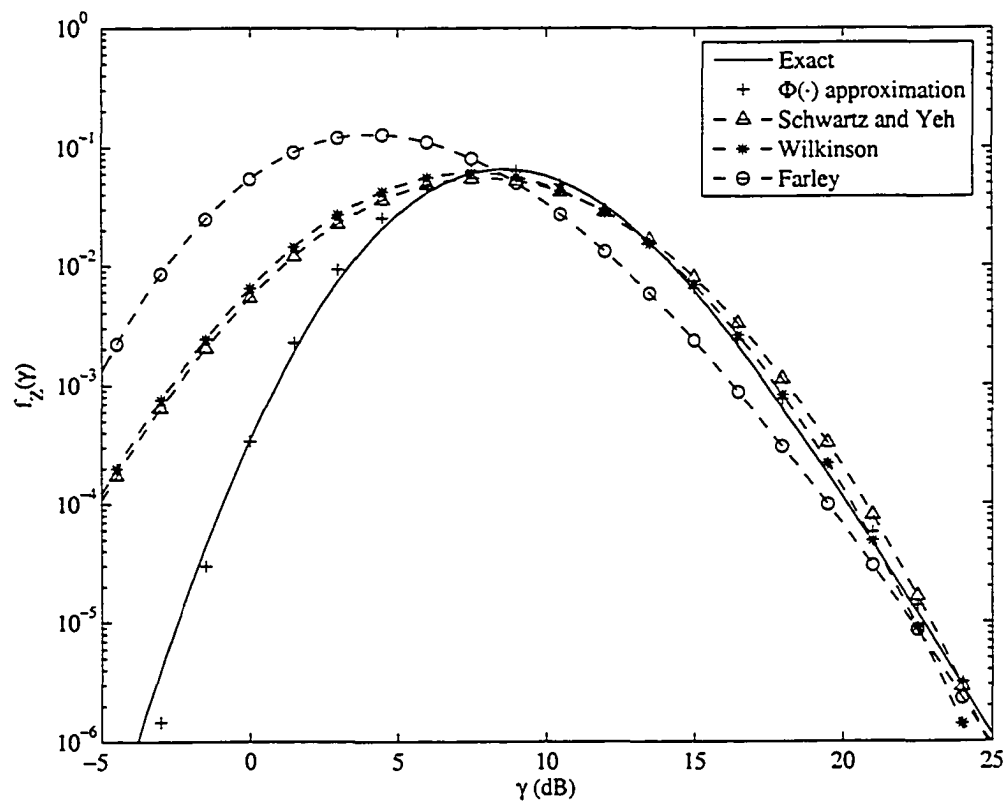
Figure 2.17. The PDF of a sum of $N = 6$ lognormal RVs ($\sigma_X = 6$ dB) and various PDF approximations.

54
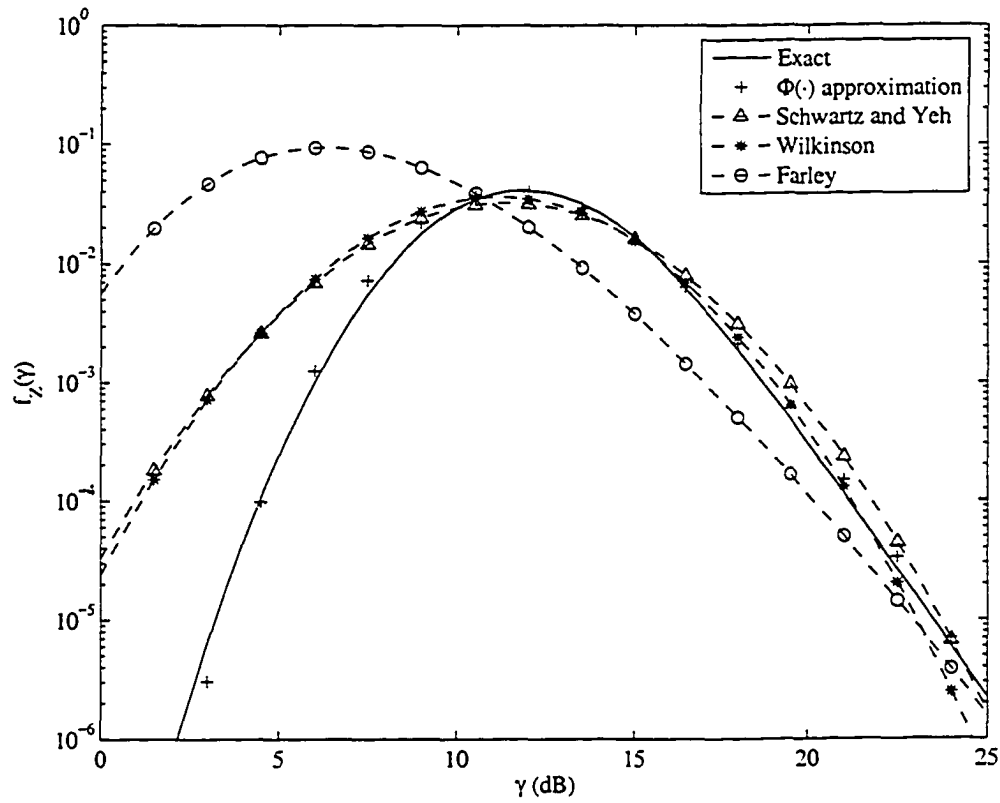
Figure 2.18. The PDF of a sum of $N = 10$ lognormal RVs ($\sigma_\chi = 6$ dB) and various PDF approximations.

55
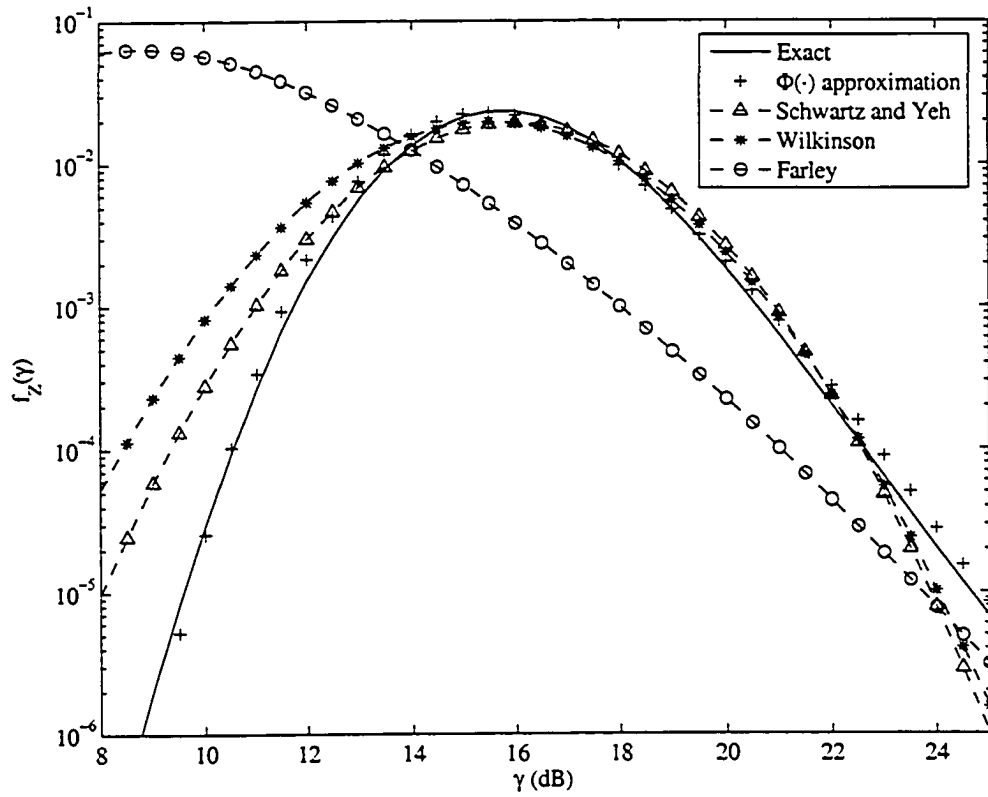
Figure 2.19. The PDF of a sum of $N = 20$ lognormal RVs ($\sigma_X = 6$ dB) and various PDF approximations.

56
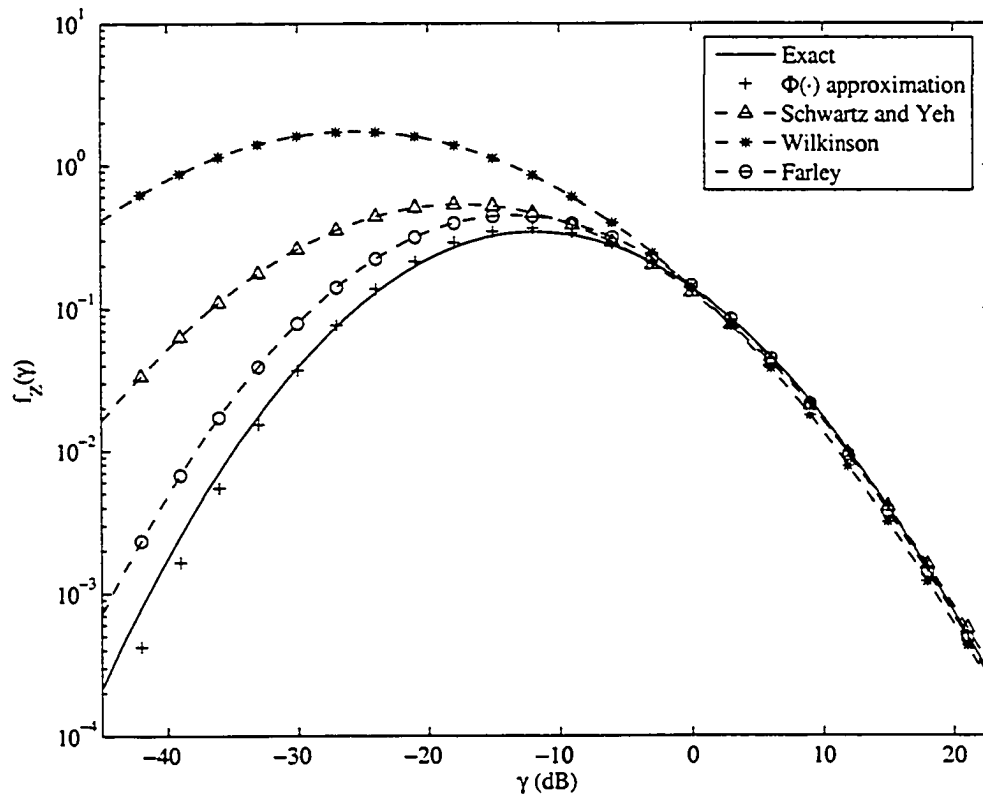
Figure 2.20. The PDF of a sum of $N = 2$ lognormal RVs ($\sigma_\chi = 12$ dB) and various PDF approximations.

57
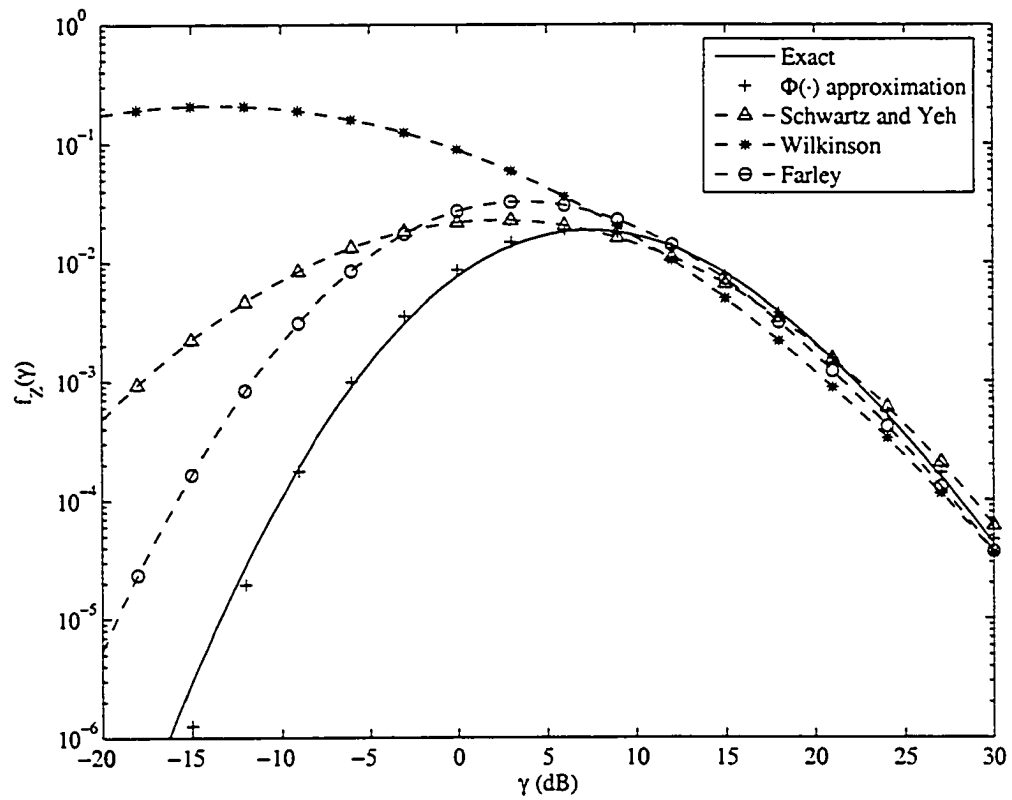
Figure 2.21. The PDF of a sum of $N = 6$ lognormal RVs ($\sigma_\chi = 12$ dB) and various PDF approximations.

58
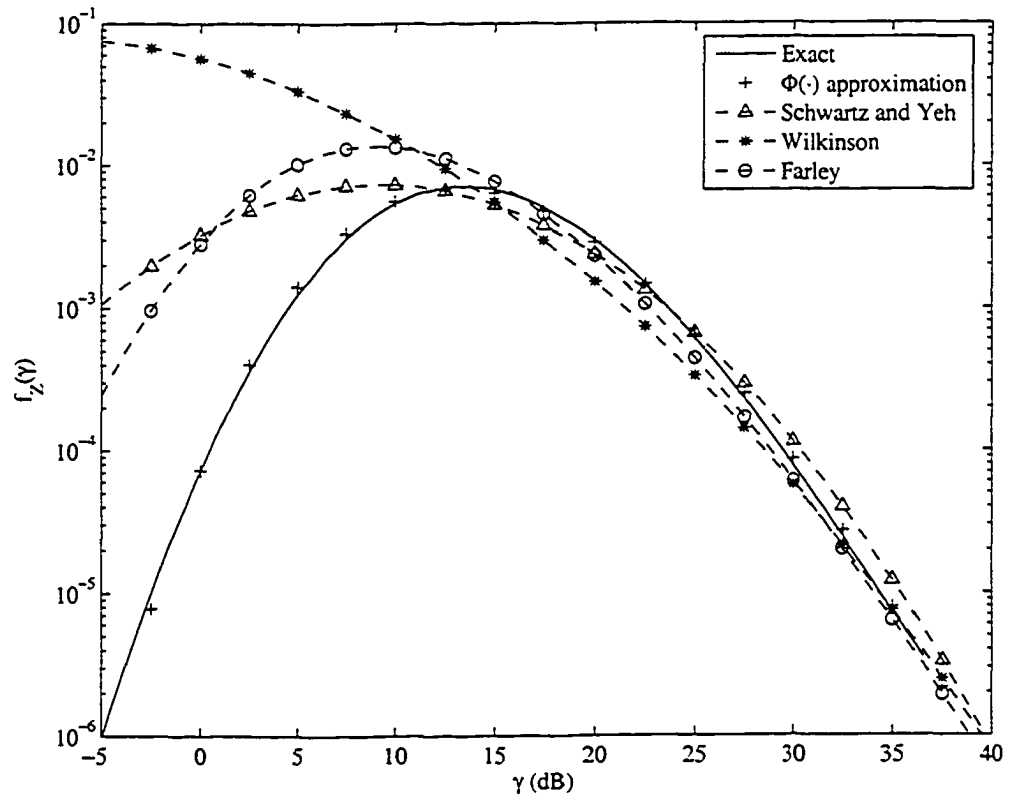
Figure 2.22. The PDF of a sum of $N = 10$ lognormal RVs ($\sigma_X = 12$ dB) and various PDF approximations.

59
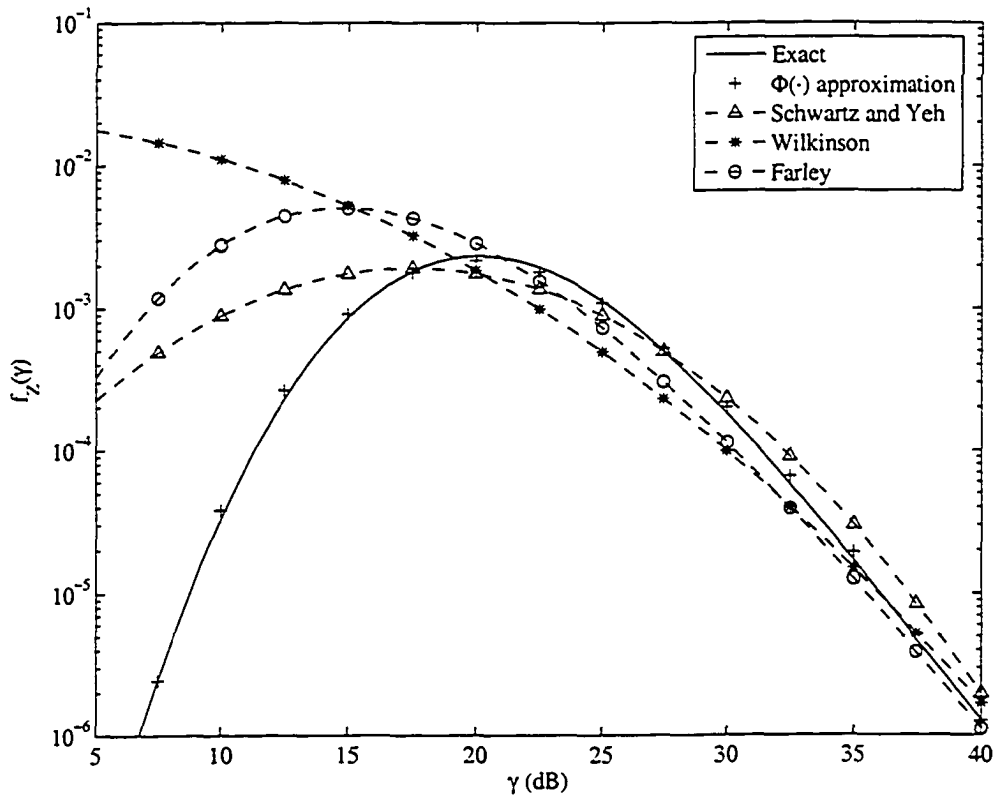
Figure 2.23. The PDF of a sum of $N = 20$ lognormal RVs ($\sigma_\chi = 12$ dB) and various PDF approximations.

60

From the CDF approximation it was possible to obtain a PDF approximation that was also accurate over the same large range of parameters. The PDF approximation was also compared to Schwartz and Yeh's, Wilkinson's, and Farley's approximations. The new PDF approximation was considerably more accurate than the existing approximations over the entire range of the PDF. Schwartz and Yeh's, and Wilkinson's methods were only accurate over the decreasing part of the PDF while the PDF obtained using Farley's CDF approximation was found to be highly inaccurate for more than 2 summands and not a suitable PDF approximation. The approximation will be extended to correlated RVs in Chapter 3.

61

Chapter 3

Approximation to the Sum Distribution of Non-Independent, Identically Distributed Lognormal Random Variables

In a shadowing environment it is possible that the received signal on each diversity branch is the result of the same obstacles near the receiver. Hence, the signals can be correlated. As a result, it is necessary to determine the distribution and density of a sum of correlated lognormal RVs. This problem has not been as extensively studied as the iid case that was considered in Chapter 2. The few approximations that exist in the literature are based on extensions of methods used for a sum of iid lognormal RVs [18],[19],[27]. In this chapter, we will extend the exponential approximation to the CDF and PDF of a sum of iid lognormal RVs determined in Chapter 2 to a sum of correlated lognormal RVs. We will also compare the exponential approximation to extensions of Schwartz and Yeh's, and Wilkinson's approximations.

62

3.1 CDF of the Sum of Correlated Lognormal RVs

In practical systems, there is a statistical correlation between the shadowed received signals. This is a result of the received signals being shadowed by the same obstacles and obstructions in the area of the receiver. Accordingly, the correlation coefficient is defined as

$$\rho_{ij} = \frac{E[(Y_i - m_{Y_i})(Y_j - m_{Y_j})]}{\sigma_{Y_i}\sigma_{Y_j}} = \frac{E[(X_i - m_{X_i})(X_j - m_{X_j})]}{\sigma_{X_i}\sigma_{X_j}}. \tag{3.1}$$

In this thesis, when a sum of correlated lognormal RVs is considered, it will be assumed that $\rho_{ii} = 1$ and $\rho_{ij} = \rho$ for $i \neq j$. This means that we will be considering a sum of non-independent, identically distributed (niid) lognormal RVs which is also know as a sum of correlated lognormal RVs. Note that the analysis is still valid for a sum of non-independent, non-identically distributed lognormal RVs.

As in the case of a sum of iid lognormal RVs, an approximation to correlated sum distribution can be determined using a moment matching method. Abu-Dayya and Beaulieu [18] derived expressions for the approximate moments $m_{\hat{Y}}$ and $\sigma_{\hat{Y}}^2$ by applying the technique offered by Wilkinson [14]. The approximate moments are given by

$$m_{\hat{Y}} = 2\ln u_1 - \frac{1}{2}\ln u_2 \tag{3.2}$$

$$\sigma_{\hat{Y}}^2 = \ln u_2 - 2\ln u_1 \tag{3.3}$$

where

$$u_1 = \sum_{i=1}^{N} e^{m_{Y_i} + \frac{1}{2}\sigma_{Y_i}^2}, \tag{3.4}$$

$$u_2 = \sum_{i=1}^{N} e^{2m_{Y_i} + 2\sigma_{Y_i}^2} + 2\sum_{i=1}^{N-1}\sum_{j=i+1}^{N} e^{m_{Y_i} + m_{Y_j} + \frac{1}{2}\left(\sigma_{Y_i}^2 + \sigma_{Y_j}^2 + 2\rho_{ij}\sigma_{Y_i}\sigma_{Y_j}\right)}. \tag{3.5}$$

Using these moments, the CDF still takes on the same form as the iid case, as given by (1.40).

Another method used in the iid case to determine the distribution of a sum of lognormal RVs was a recursive method determined by Schwartz and Yeh [14]. This technique was

63

extended to a sum of correlated RVs by Safak [19]. Using an extension of Schwartz and Yeh's method, the mean and variance of $\hat{Y}$ are given by

$$m_{\hat{Y}} = m_{Y_1} + G_1 \tag{3.6}$$

$$\sigma_{\hat{Y}}^2 = \sigma_{Y_1}^2 - G_1^2 + \frac{2(\rho_{12}\sigma_{Y_2} - \sigma_{Y_1})\sigma_{Y_1}}{\sigma_{Y_d}^2} G_3 + G_2 \tag{3.7}$$

where G_1, G_2 and G_2 are given by (1.45), (1.49) and (1.50) respectively,

$$\sigma_{Y_d}^2 = \sigma_{Y_1}^2 + \sigma_{Y_2}^2 - 2\rho_{12}\sigma_{Y_1}\sigma_{Y_2} \tag{3.8}$$

replaces (1.43), and ρ_{ij} is defined by (3.1). For more than two lognormal RVs, the moments are determined using the same recursive approach introduced by Schwartz and Yeh as outlined in [19] but with ρ_{12} replaced by

$$\rho_{Z_{k-1}Y_k} = \frac{E[(Z_{k-1} - m_{Z_{k-1}})(Y_k - m_{Y_k})]}{\sigma_{Z_{k-1}}\sigma_{Y_k}}$$

$$= \sigma_{Z_{k-2}} \frac{\rho_{Z_{k-2}Y_k}}{\sigma_{Z_{k-1}}} + \frac{\rho_{(k-1)k}\sigma_{Y_{k-1}} - \rho_{Z_{k-2}Y_k}\sigma_{Z_{k-2}}}{\sigma_{Z_{k-1}}\sigma_{Y_{d_{k-1}}}^2} G_3(\sigma_{Y_{d_{k-1}}}, m_{Y_{d_{k-1}}}) \tag{3.9}$$

where

$$Z_k = \ln(Y_1 + Y_2 + \cdots + Y_k), \tag{3.10}$$

$$Y_{d_k} = Y_k - Z_{k-1}. \tag{3.11}$$

Another method for determining an approximation to the distribution of a lognormal sum is based on plotting the distribution on probability paper. Given the shape of the curves in this plot, new techniques can be used to determine an approximation. For example, Beaulieu and Xie [17],[22] derived a minimax approximation that fit a lognormal RV to the sum distribution that would minimize the maximum error. Another technique was discussed in Chapter 2, that fit an exponential curve to the sum distribution on lognormal probability paper. It was easy to find these new approximations because the exact CDF could be easily calculated using a modified Curtis-Clenshaw integration. In this integration, the product of the CFs of the lognormal distribution can be calculated numerically, which

64

can then be used to obtain the CDF for the sum RV. This type of analysis is only valid for a sum of independent RVs because a sum of correlated RVs cannot be expressed as a product of CFs [20]. Accordingly, it is necessary to use simulation to obtain the CDF of a sum of correlated lognormal RVs. Since simulations can take a long time, determining an accurate approximation is very important because it can be used to obtain solutions to problems that might otherwise be difficult to obtain through simulation.

Before a simulation of a sum distribution can be obtained it is necessary to simulate the summands and generate the sum. The summands, which are correlated RVs, can be generated using two different methods. The first one requires that the joint distribution be available for the set of RVs to be simulated [28]. For example, if a set of correlated Gaussian RVs are required, it would be possible to use the joint Gaussian distribution to obtain the simulation points. The drawback of such a method is that as the number of RVs increases, the joint distribution becomes complex and cumbersome to use. Another method that uses the marginal distribution of the RVs and defines the correlation between the variables will yield similar results [28]. In the case of the lognormal distribution, using marginal distributions is easier to implement as N become larger.

In order to simulate the distribution of a sum of correlated lognormal RVs it is first necessary to generate correlated lognormal RVs, which can then be used to determine the sum distribution. As a result, we define the vector of correlated lognormal RVs as

$$\bar{L} = [\ L_1 \quad L_2 \quad \dots \quad L_N\ ]^T \tag{3.12}$$

where the marginal PDF of L_i is given by (1.24). The related Gaussian vector is then defined as

$$\bar{X} = [\ X_1 \quad X_2 \quad \dots \quad X_N\ ]^T \tag{3.13}$$

where $X_i = 10 \log_{10} L_i$. We will also define a covariance matrix C_X where the entries are are given by

$$
\begin{aligned}
C_{X_{ij}} &= E[X_i X_j] - \mu_{X_i} \mu_{X_j} \\
&= \rho_{ij} \sigma_{X_i} \sigma_{X_j}.
\end{aligned}
\tag{3.14}
$$

65

By simple algebraic manipulation [28] the covariance of L_i and L_j in terms of the moments of X is expressed as

$$C_{L_{ij}} = e^{\lambda \mu_{X_i} + \lambda \mu_{X_j} + \frac{\lambda^2}{2}\left(\sigma_{X_i}^2 + \sigma_{X_j}^2\right)} \left(e^{\lambda^2 \rho_{ij}\sigma_{X_i}\sigma_{X_j}} - 1\right). \tag{3.15}$$

This implies that that the correlation between L_i and L_j is related to ρ_{ij} by

$$\rho_{L_{ij}} = \frac{e^{\lambda^2 \rho_{ij}\sigma_{X_i}\sigma_{X_j}}}{\sqrt{(e^{\lambda^2 \sigma_{X_i}^2} - 1)(e^{\lambda^2 \sigma_{X_j}^2} - 1)}}. \tag{3.16}$$

Given this relation it is possible to define the correlation in terms of the lognormal RVs or the Gaussian RVs. In this thesis we will define the correlation in terms of the Gaussian RVs.

In order to generate the correlated lognormal RVs, we first generate $\bar{W}$, a normal random vector with zero-mean, unit-variance and zero correlation. The correlated normal vector is then expressed

$$\bar{X} = B^T \bar{W} \tag{3.17}$$

where B is the Cholesky decomposition of C. The Cholesky decomposition is defined as the decomposition given by

$$C = B^T B \tag{3.18}$$

and is possible because C is a positive definite matrix [29]. Finally, the correlated lognormal random vector is given by

$$\bar{L} = \exp(\lambda \bar{X}). \tag{3.19}$$

Taking the sum of the components of the random vector results in a sum of correlated lognormal RVs. Simulating this process will result in a sum of correlated RVs that is then used to determine the PDF and CDF. More details about the method used to simulate the RVs can be found in Appendix A. The simulated CDF is plotted in Figures 3.1 - 3.6 on lognormal probability paper.

Just as in the iid case, the sum of correlated lognormal RVs have a desirable shaped when plotted on lognormal probability paper. As a result, it is possible to use the same

66
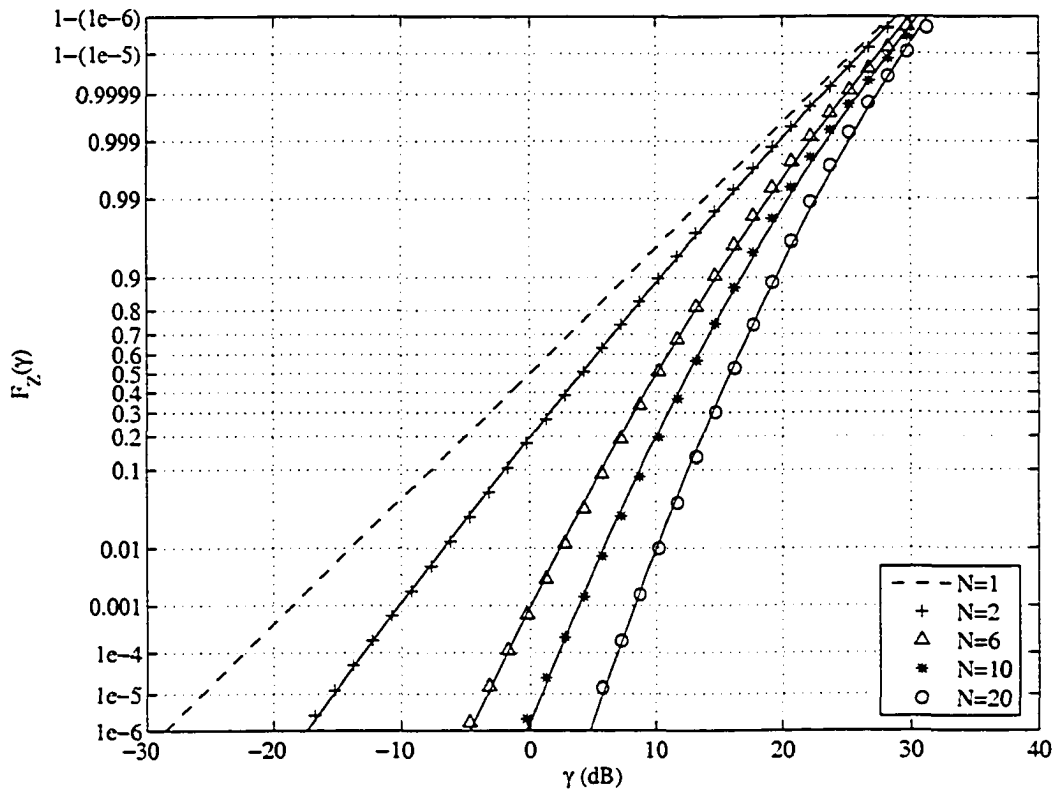
Figure 3.1. The CDF of a sum of N correlated lognormal RVs ($\sigma_X = 6$ dB, $\rho = 0.1$) and the exponential approximating function for $N = 2$, 6, 10 and 20 (line is simulation and marker is approximate).

67
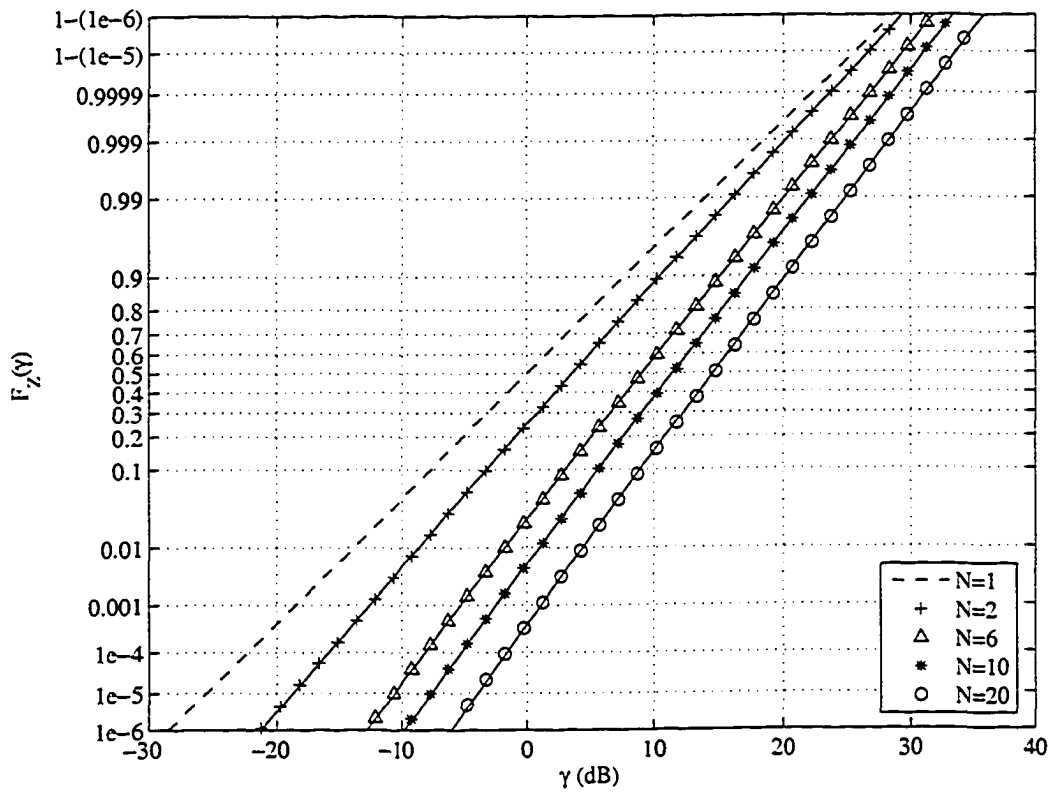
Figure 3.2. The CDF of a sum of N correlated lognormal RVs ($\sigma_X = 6$ dB, $\rho = 0.5$) and the exponential approximating function for $N = 2$, 6, 10 and 20 (line is simulation and marker is approximate).

68
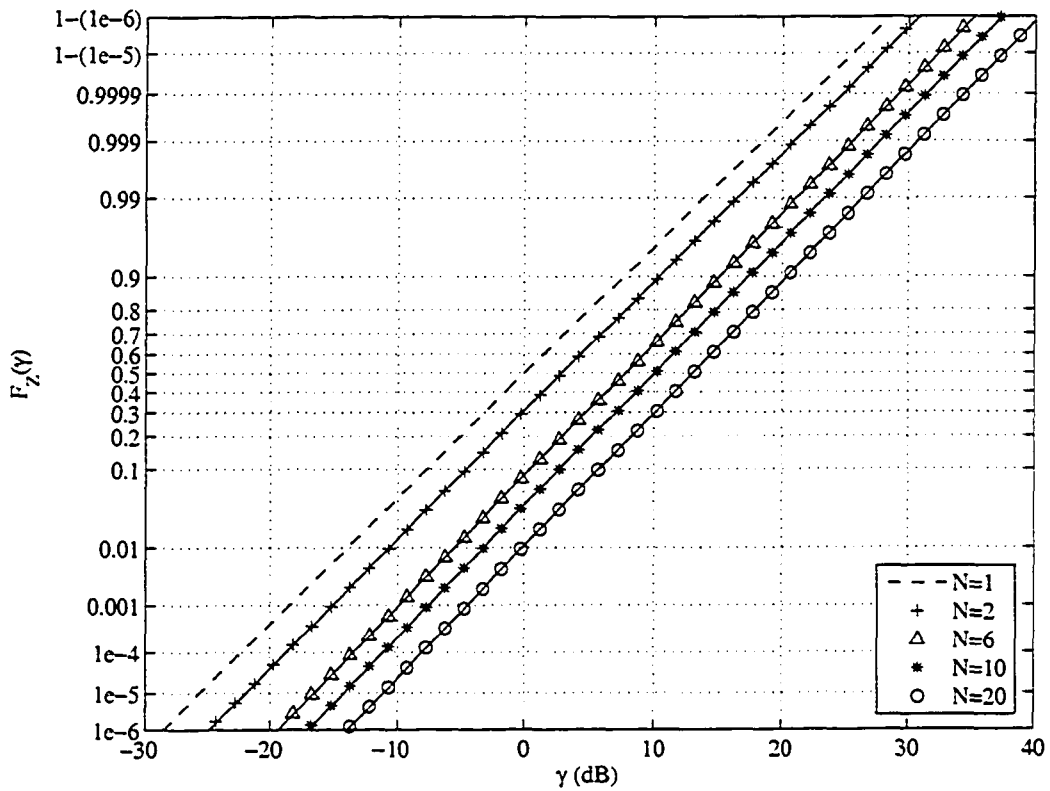
Figure 3.3. The CDF of a sum of N correlated lognormal RVs ($\sigma_X = 6$ dB, $\rho = 0.9$) and the exponential approximating function for $N = 2, 6, 10$ and 20 (line is simulation and marker is approximate).

69
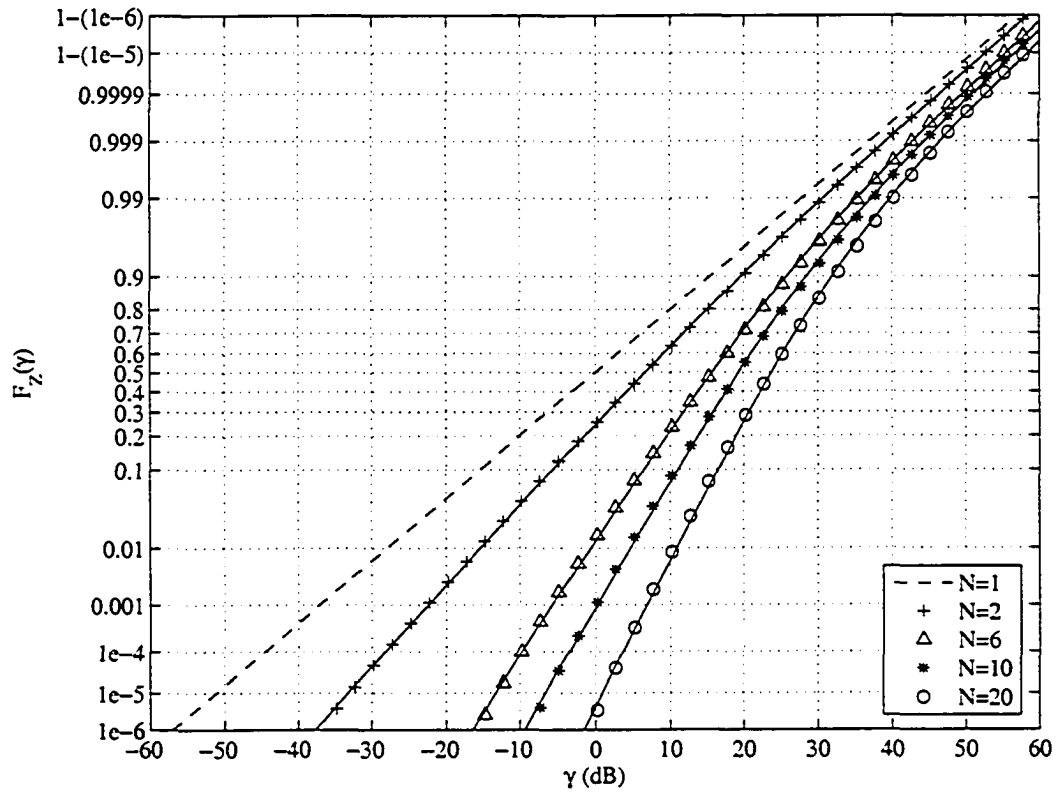
Figure 3.4. The CDF of a sum of N correlated lognormal RVs ($\sigma_X = 12$ dB, $\rho = 0.1$) and the exponential approximating function for $N = 2$, 6, 10 and 20 (line is simulation and marker is approximate).

70
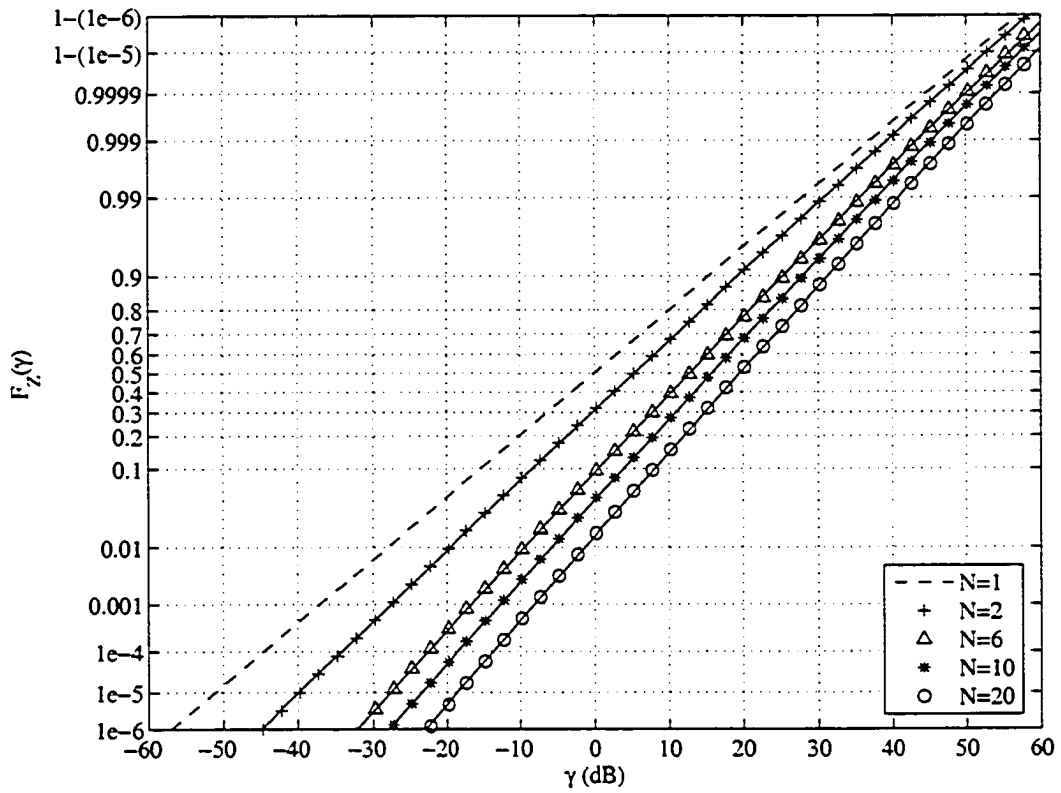
Figure 3.5. The CDF of a sum of N correlated lognormal RVs ($\sigma_\chi = 12$ dB, $\rho = 0.5$) and the exponential approximating function for $N = 2$, 6, 10 and 20 (line is simulation and marker is approximate).

71
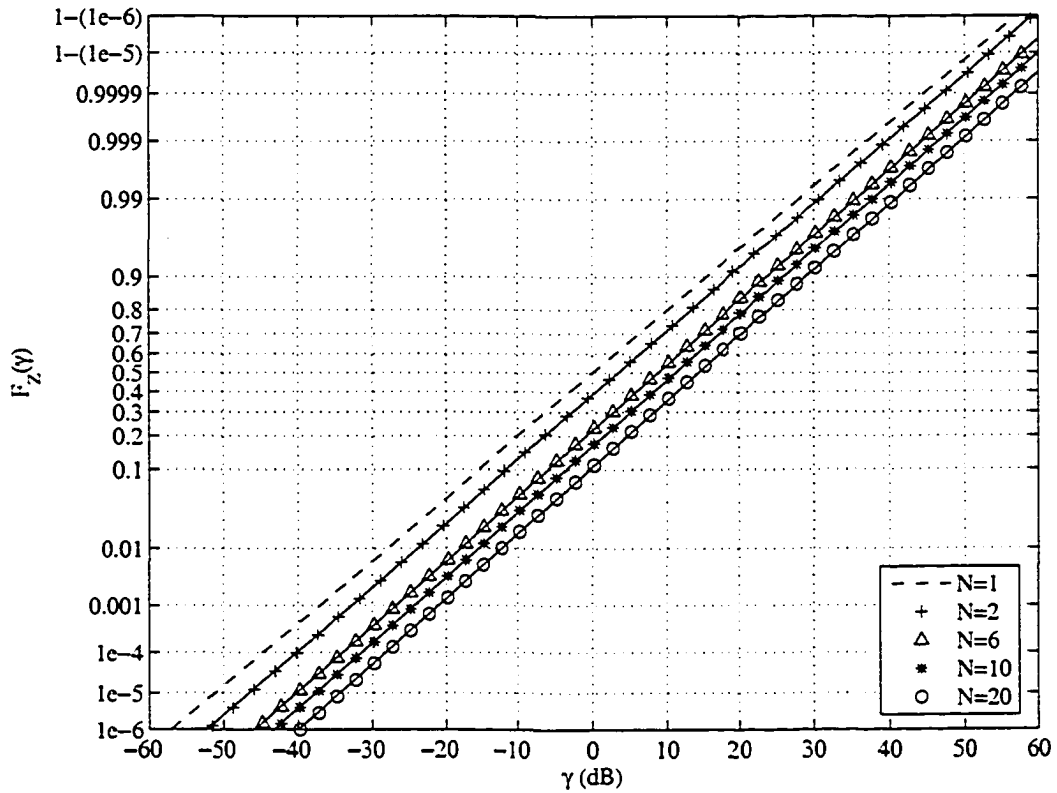
Figure 3.6. The CDF of a sum of N correlated lognormal RVs ($\sigma_X = 12$ dB, $\rho = 0.9$) and the exponential approximating function for $N = 2$, 6, 10 and 20 (line is simulation and marker is approximate).

72

TABLE 3.1

The coefficients for the approximation $\Phi(a_0 - a_1 e^{-a_2 \gamma})$ for $\sigma_\chi = 6$ dB.

N	$\rho = 0.1$			$\rho = 0.5$			$\rho = 0.9$		
	a_0	a_1	$a_2 10^3$	a_0	a_1	$a_2 10^5$	a_0	a_1	$a_2 10^6$
2	32.160	33.015	6.43	138.16	138.84	1.358	490.25	490.75	3.484
3	23.424	24.973	9.93	137.93	139.07	1.436	490.09	490.91	3.516
4	19.584	21.713	12.89	137.77	139.24	1.486	489.98	491.02	3.534
5	17.803	20.440	15.07	137.64	139.37	1.520	489.89	491.11	3.545
6	16.598	19.703	16.98	137.54	139.48	1.546	489.82	491.18	3.552
7	15.655	19.188	18.73	137.45	139.57	1.566	489.76	491.24	3.557
8	15.336	19.258	19.76	137.37	139.65	1.581	489.71	491.30	3.561
9	14.858	19.151	20.98	137.30	139.72	1.594	489.66	491.34	3.564
10	14.617	19.260	21.87	137.24	139.79	1.605	489.62	491.38	3.567
11	14.577	19.538	22.41	137.19	139.84	1.614	489.58	491.42	3.569
12	14.700	19.952	22.63	137.14	139.89	1.622	489.55	491.46	3.571
13	14.560	20.123	23.31	137.09	139.94	1.630	489.52	491.49	3.571
14	14.637	20.469	23.56	137.05	139.99	1.635	489.49	491.52	3.574
15	14.498	20.596	24.12	137.01	140.03	1.641	489.46	491.54	3.575
16	14.506	20.857	24.44	136.97	140.06	1.646	489.44	491.57	3.577
17	14.518	21.116	24.74	136.94	140.10	1.650	489.41	491.59	3.577
18	14.830	21.619	24.45	136.90	140.13	1.654	489.39	491.61	3.578
19	14.926	21.936	24.57	136.87	140.16	1.657	489.37	491.63	3.579
20	15.011	22.239	24.70	136.84	140.20	1.661	489.35	491.65	3.580

73

TABLE 3.2

The coefficients for the approximation $\Phi(a_0 - a_1 e^{-a_2 \gamma})$ for $\sigma_\chi = 12$ dB.

N	$\rho = 0.1$			$\rho = 0.5$			$\rho = 0.9$		
	a_0	a_1	$a_2 10^3$	a_0	a_1	$a_2 10^3$	a_0	a_1	$a_2 10^4$
2	29.211	29.893	3.434	83.237	83.731	1.108	399.87	400.15	2.132
3	21.589	22.778	5.124	83.087	83.899	1.161	399.78	400.25	2.155
4	16.524	18.095	7.166	82.982	84.013	1.194	399.72	400.31	2.164
5	14.986	16.888	8.288	82.902	84.101	1.219	399.67	400.36	2.170
6	13.857	16.050	9.316	82.838	84.170	1.237	399.64	400.40	2.174
7	13.064	15.515	10.19	82.784	84.228	1.251	399.61	400.43	2.177
8	12.582	15.266	10.85	82.738	84.278	1.263	399.58	400.45	2.180
9	12.091	14.992	11.55	82.697	84.321	1.273	399.55	400.48	2.183
10	11.833	14.928	12.02	82.661	84.359	1.282	399.53	400.50	2.184
11	11.524	14.809	12.57	82.629	84.394	1.290	399.51	400.52	2.186
12	11.349	14.805	12.95	82.599	84.425	1.296	399.50	400.54	2.187
13	11.167	14.788	13.34	82.573	84.453	1.303	399.48	400.55	2.188
14	11.091	14.859	13.59	82.548	84.479	1.307	399.47	400.57	2.189
15	10.929	14.846	13.95	82.525	84.504	1.313	399.45	400.58	2.191
16	10.855	14.906	14.18	82.504	84.526	1.317	399.44	400.60	2.193
17	10.680	14.872	14.57	82.484	84.547	1.321	399.44	400.62	2.193
18	10.628	14.944	14.76	82.465	84.567	1.325	399.43	400.63	2.193
19	10.577	15.013	14.95	82.447	84.586	1.328	399.42	400.64	2.194
20	10.529	15.079	15.13	82.431	84.603	1.332	399.41	400.65	2.195

74

approximation as in the iid case to approximate the correlated sum CDF. For the correlated sum case, the coefficients a_0, a_1 and a_2 will have to be recomputed for the cases being considered using the same technique as Chapter 2. The value of the coefficients for $\rho = 0.1$, 0.5 and 0.9 can be found in Tables 3.1 and 3.2, for $\sigma_X = 6$ and 12 dB respectively. From Figures 3.1 - 3.6 it is observed that the exponential approximation is accurate over a large range of probabilities, N, σ_X and ρ. Also, as ρ increases, the CDF becomes closer to a straight line, closely resembling the distribution of a single lognormal RV. For $\rho = 0.9$, the CDF is almost a straight line for any value of N. This means that for values of $N > 2$, the distribution is almost that of a single lognormal RV but with a shifted mean as represented by the distribution moving to the right and the slope staying constant as N increases.

To determine the usefulness of the exponential approximation, it is necessary to compare it with the extensions of Wilkinson's, and Schwartz and Yeh's methods for computing the distribution. In Figures 3.7 - 3.12, the exponential approximation is plotted along with Schwartz and Yeh's, and Wilkinson's approximations for $N = 2$, 6, 10 and 20, and $\rho = 0.1$, 0.5 and 0.9 for $\sigma_X = 6$ dB. From these figures, the following observations can be made.

1. For low correlation, Schwartz and Yeh's, and Wilkinson's approximation are not very accurate. Also, as N increases, the accuracy of the moment matching methods decrease. This is similar to the observations made in Chapter 2 for a sum of iid lognormal RVs.

2. Wilkinson's approximation deviates from the exact value by up to 4 orders of magnitude in the tail of the complementary CDF and by up to 2 orders of magnitude in the tail of the CDF. Schwartz and Yeh's accuracy is very similar to that of Wilkinson's.

3. As the correlation increases, the accuracy of Wilkinson's, and Schwartz and Yeh's method approach that of the exponential approximation. This is a result of the highly correlated sum CDF exhibiting similar statistics to that of a single lognormal RV. Also, the moment matching methods assume that the sum distribution is given by another lognormal RV, which more closely matches the behavior of the sum of highly correlated lognormal RVs than a sum of iid lognormal RVs.

75

Similar observations are made for $\sigma_X = 12$ dB in Figures 3.13 - 3.18.

3.2   PDF Approximation

An equally important test of the exponential approximation is to determine if the PDF is as accurate for the correlated sum as it was for the iid sum. Also, it is important to see how much an improvement the exponential approximation can provide over the moment matching techniques.

Just as in the iid case, the approximate PDF for a correlated sum is given by (2.19). Using the values of a_0, a_1 and a_2 in Tables 3.1 and 3.2, the PDF has been plotted in Figures 3.19 - 3.22 for a few select cases. From these plots it is possible to see that the PDF approximation is accurate over the entire range of interest. The accuracy is not affected by the number of RVs, dB spread, or correlation coefficient. For low correlation values, Schwartz and Yeh's, and Wilkinson's approximations are not very accurate and the accuracy increases as the correlation coefficient is increased. For large correlation coefficients, there is little advantage to use either Schwartz and Yeh's approximation or the exponential approximation. Wilkinson's approximation is very accurate in these cases and easier to calculate than the other approximations. Overall the exponential approximation is an excellent approximation for low to medium correlation, where it is dramatically better than Schwartz and Yeh's, and Wilkinson's approximations.

3.3   Summary

The exponential approximation introduced in Chapter 2 was extended to a sum of correlated lognormal RVs. Using simulation, it was seen that the new approximation is accurate over a large range of parameters, just as in the iid case. The exponential approximation was also compared to Schwartz and Yeh's, and Wilkinson's approximations. It was found that for low values of correlation, the exponential approximation outperformed the moment matching techniques. For high correlation, all the approximations performed almost iden-

76

tically. It was shown that the exponential approximation is accurate not only for a sum of iid lognormal RVs but also for a sum of correlated RVs.

77
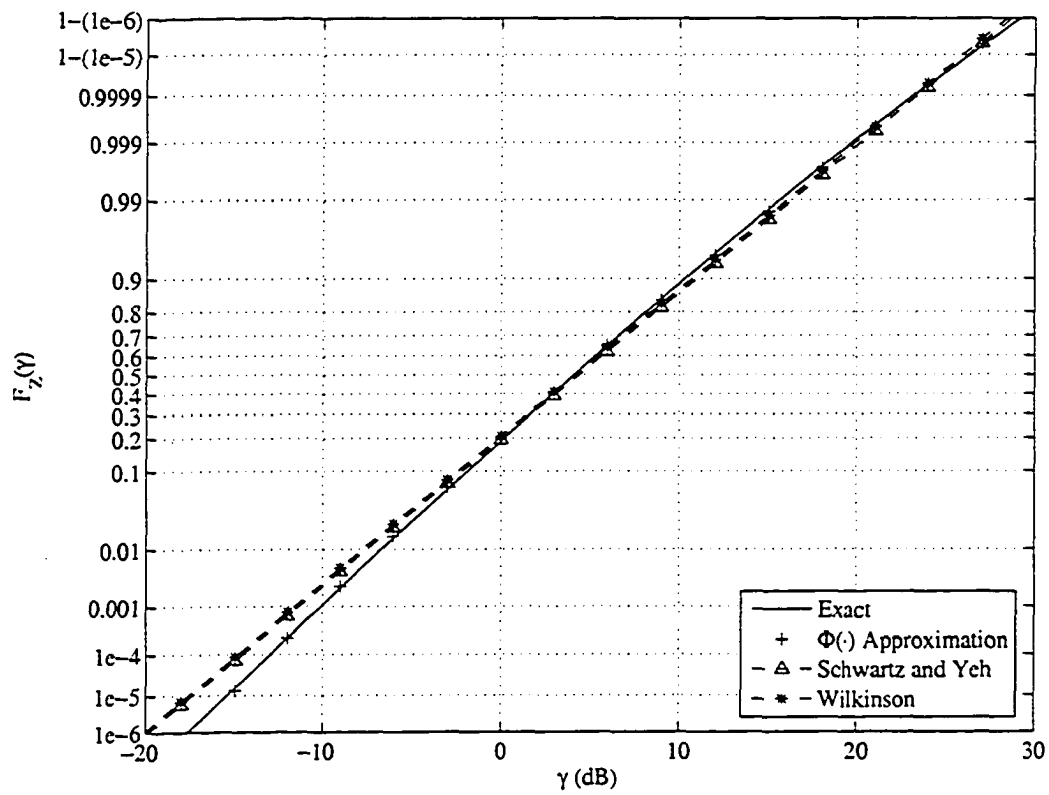
Figure 3.7. The CDF of a sum of $N = 2$ correlated lognormal RVs ($\sigma_\chi = 6$ dB, $\rho = 0.1$) and various approximations.

78
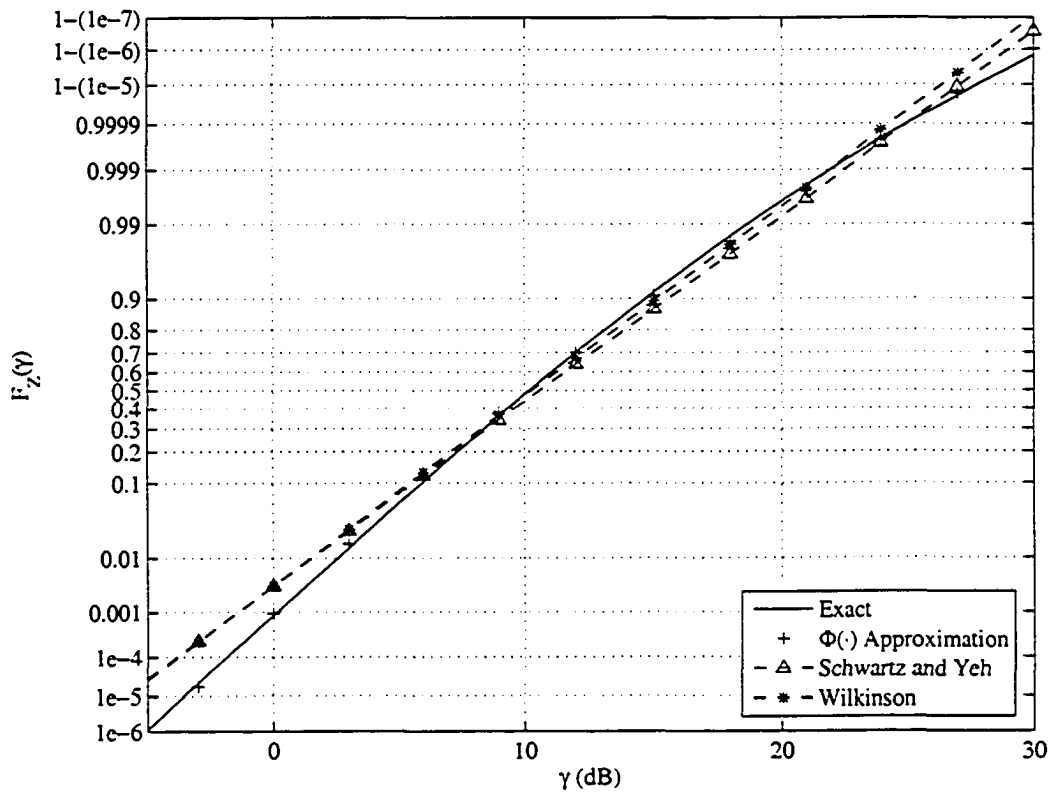
Figure 3.8. The CDF of a sum of $N = 6$ correlated lognormal RVs ($\sigma_\chi = 6$ dB, $\rho = 0.1$) and various approximations.

79
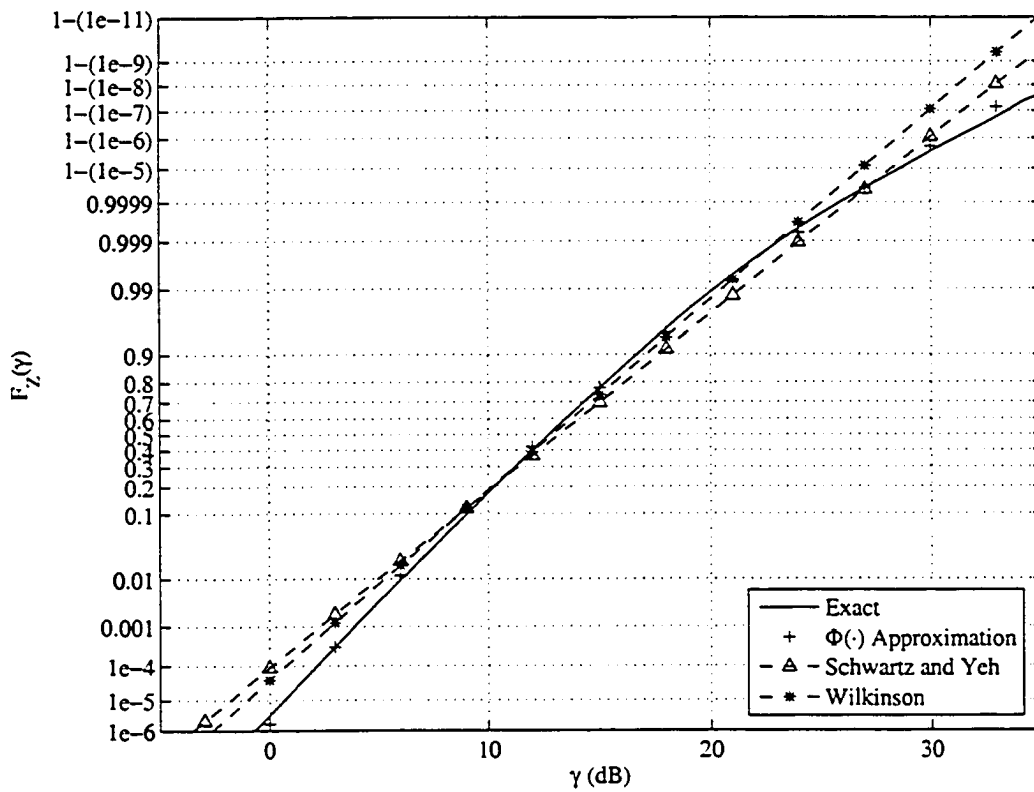
Figure 3.9. The CDF of a sum of $N = 10$ correlated lognormal RVs ($\sigma_X = 6$ dB, $\rho = 0.1$) and various approximations.

80
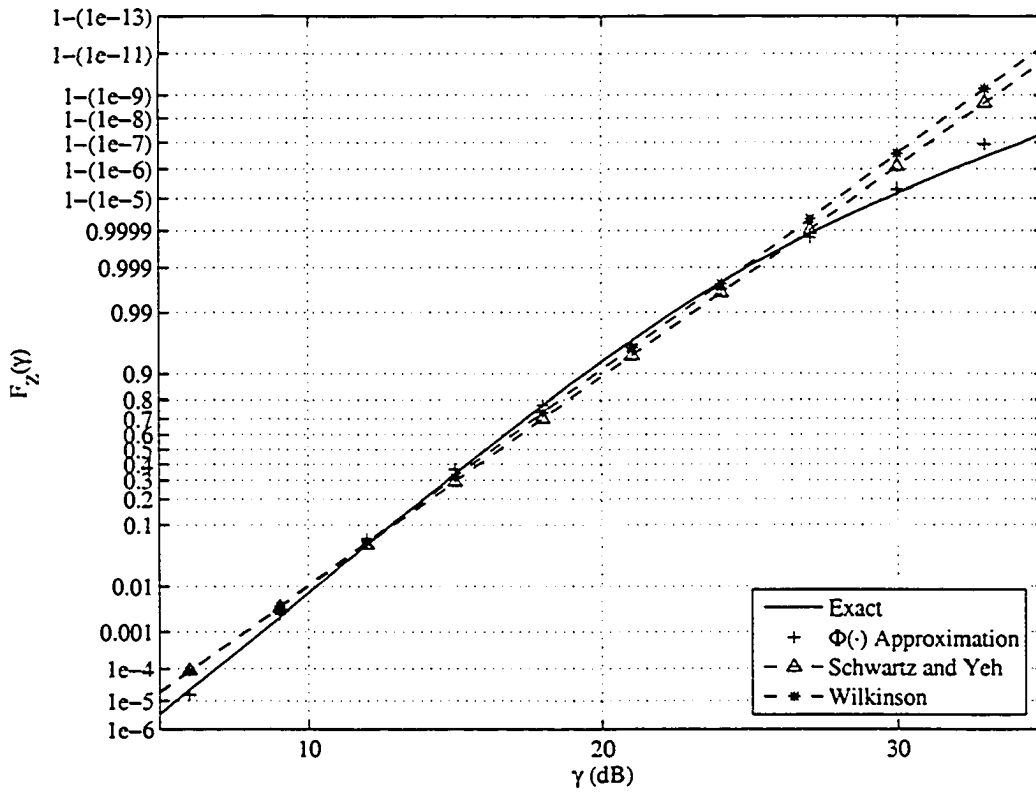
Figure 3.10. The CDF of a sum of $N = 20$ correlated lognormal RVs ($\sigma_X = 6$ dB, $\rho = 0.1$)

and various approximations.

81
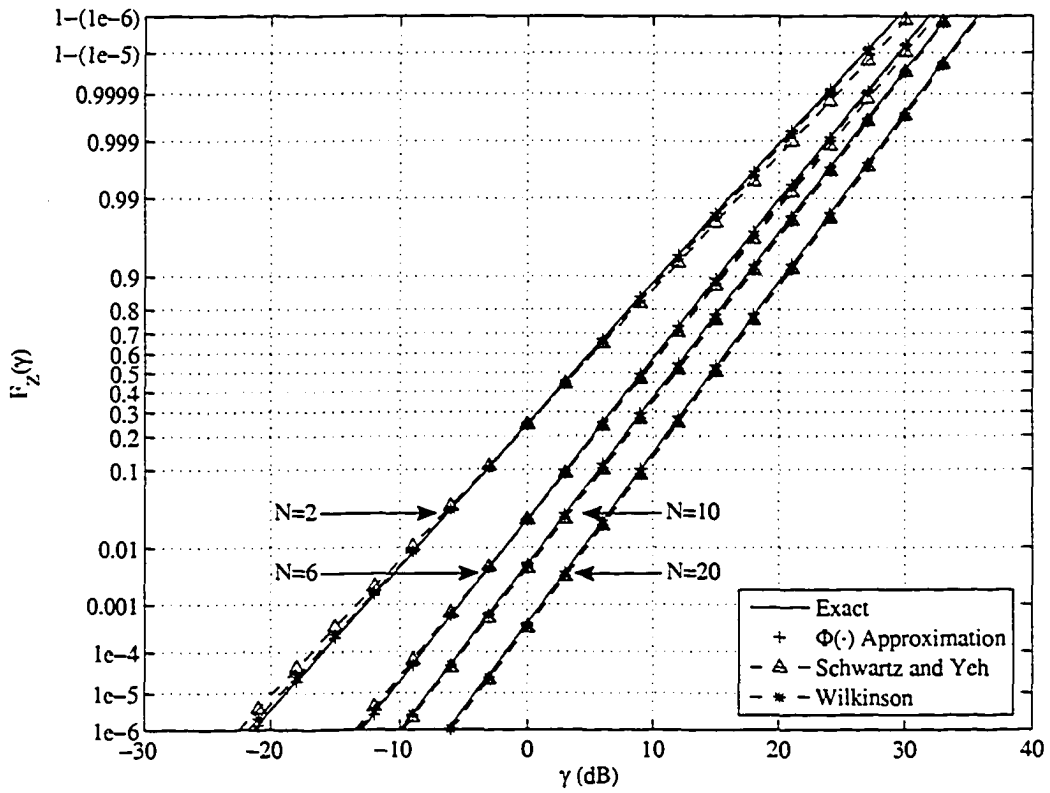
Figure 3.11. The CDF of a sum of $N = 2, 6, 10$ and 20 correlated lognormal RVs ($\sigma_\chi = 6$ dB, $\rho = 0.5$) and various approximations.
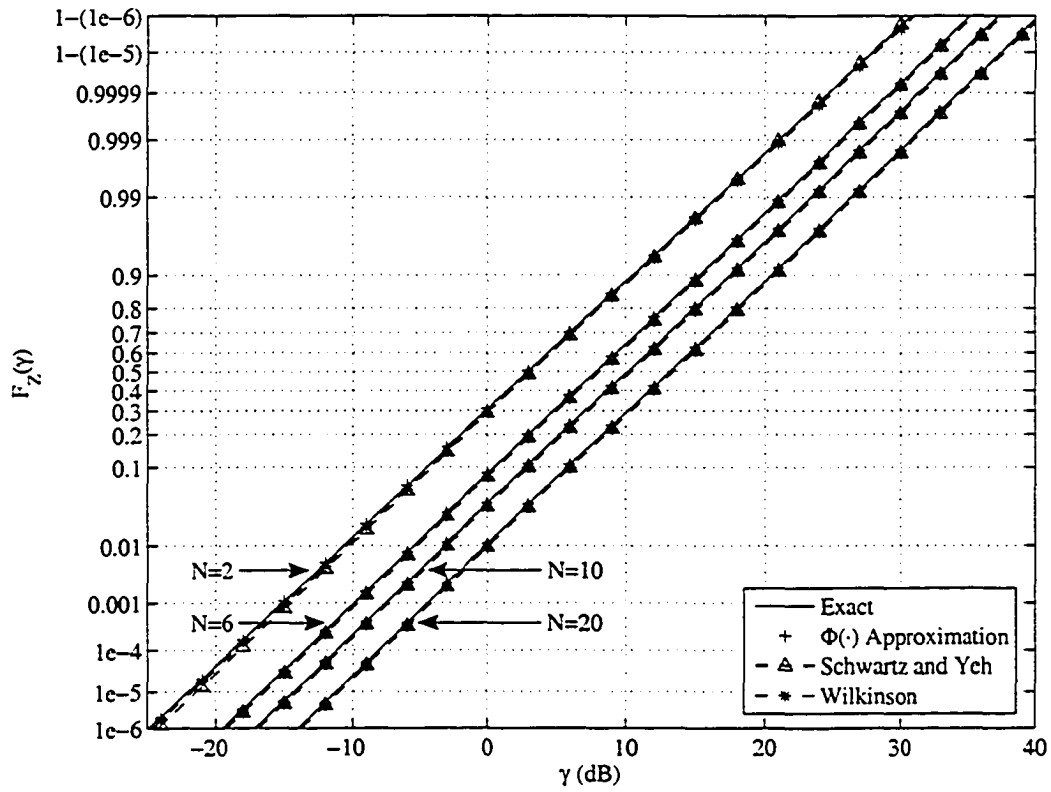
Figure 3.12. The CDF of a sum of $N = 2, 6, 10$ and 20 correlated lognormal RVs ($\sigma_X = 6$ dB, $\rho = 0.9$) and various approximations.
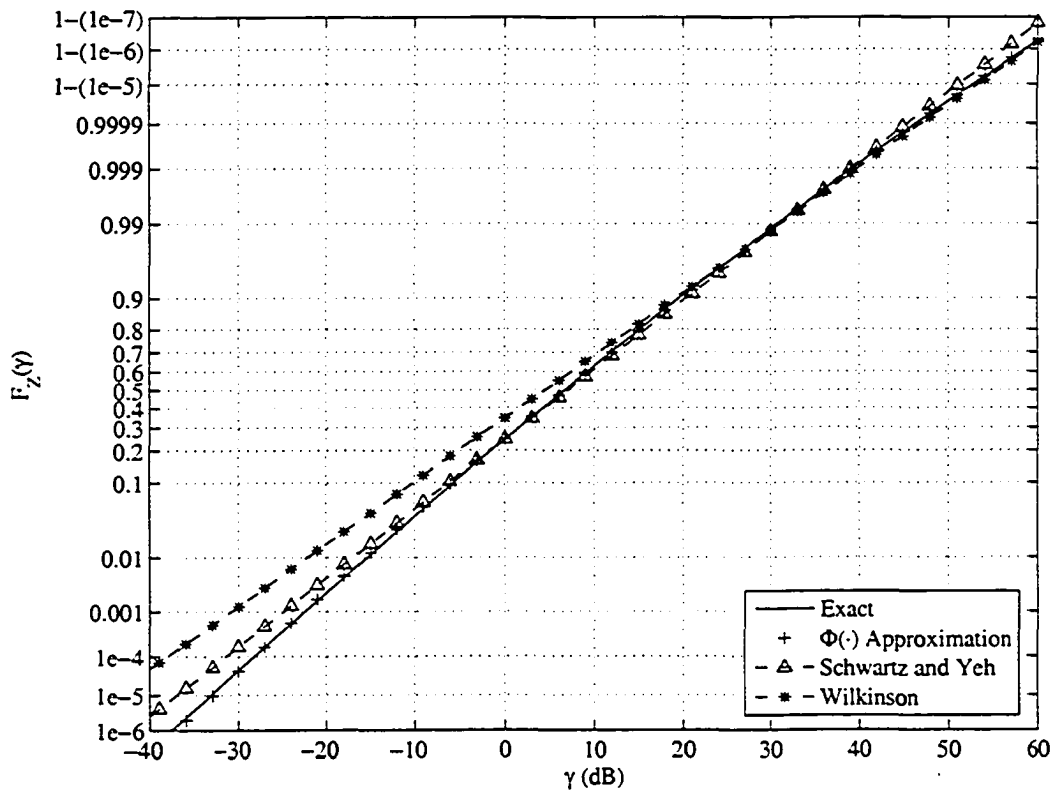
Figure 3.13. The CDF of a sum of $N = 2$ correlated lognormal RVs ($\sigma_X = 12$ dB, $\rho = 0.1$) and various approximations.

84
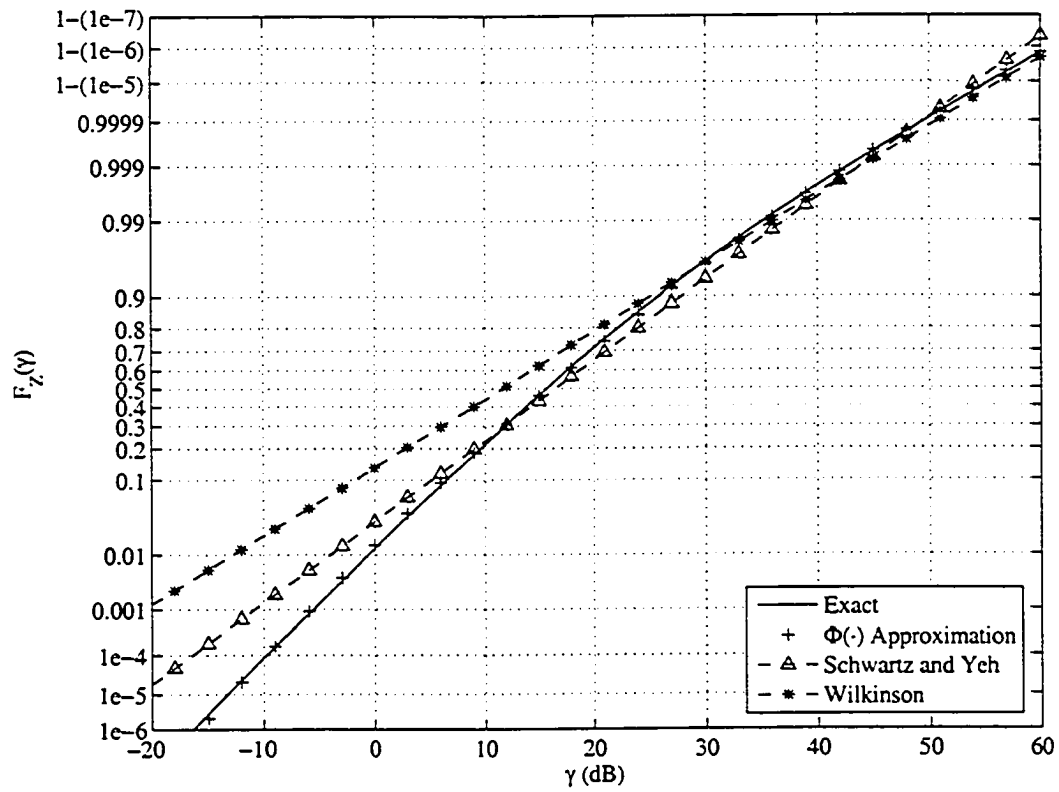
Figure 3.14. The CDF of a sum of $N = 6$ correlated lognormal RVs ($\sigma_X = 12$ dB, $\rho = 0.1$) and various approximations.

85
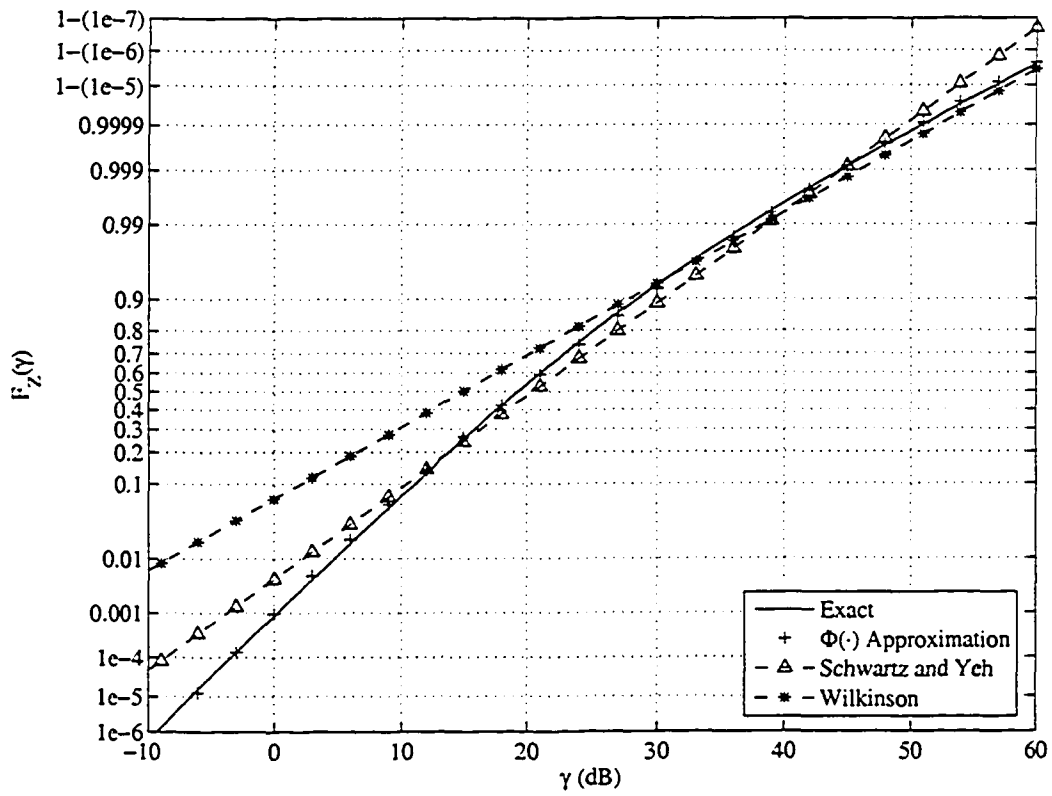
Figure 3.15. The CDF of a sum of $N = 10$ correlated lognormal RVs ($\sigma_X = 12 \, \text{dB}, \rho = 0.1$) and various approximations.

86
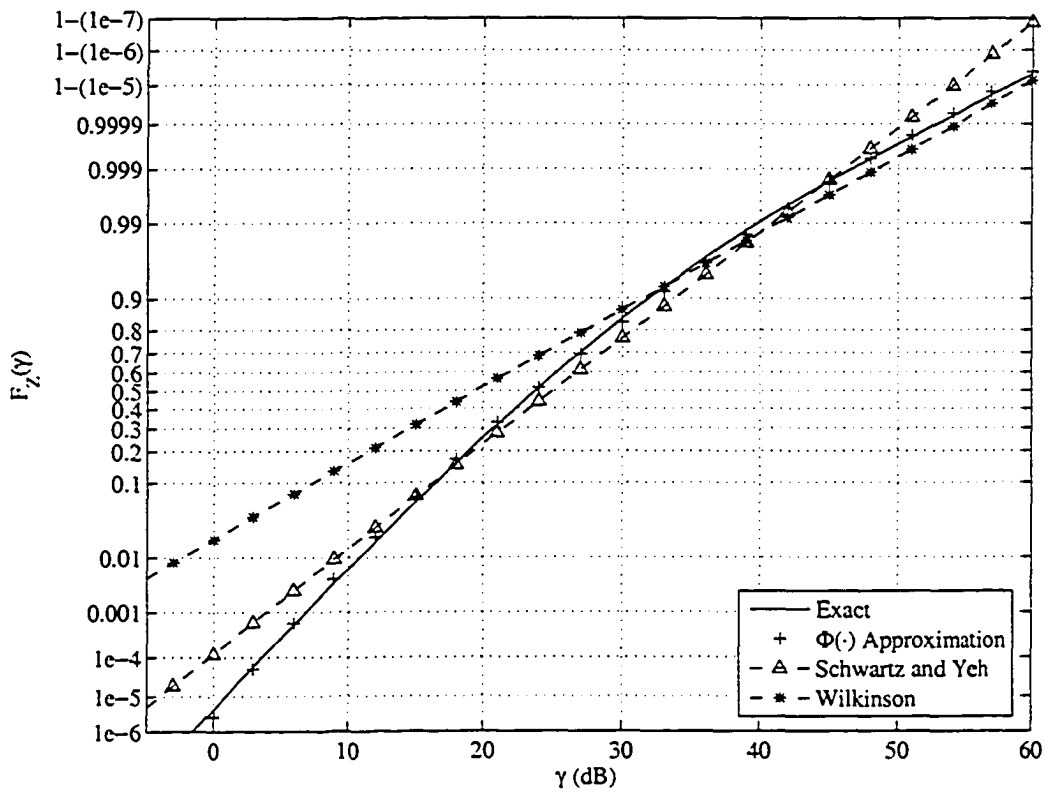
Figure 3.16. The CDF of a sum of $N = 20$ correlated lognormal RVs ($\sigma_X = 12\,\mathrm{dB}, \rho = 0.1$) and various approximations.

87
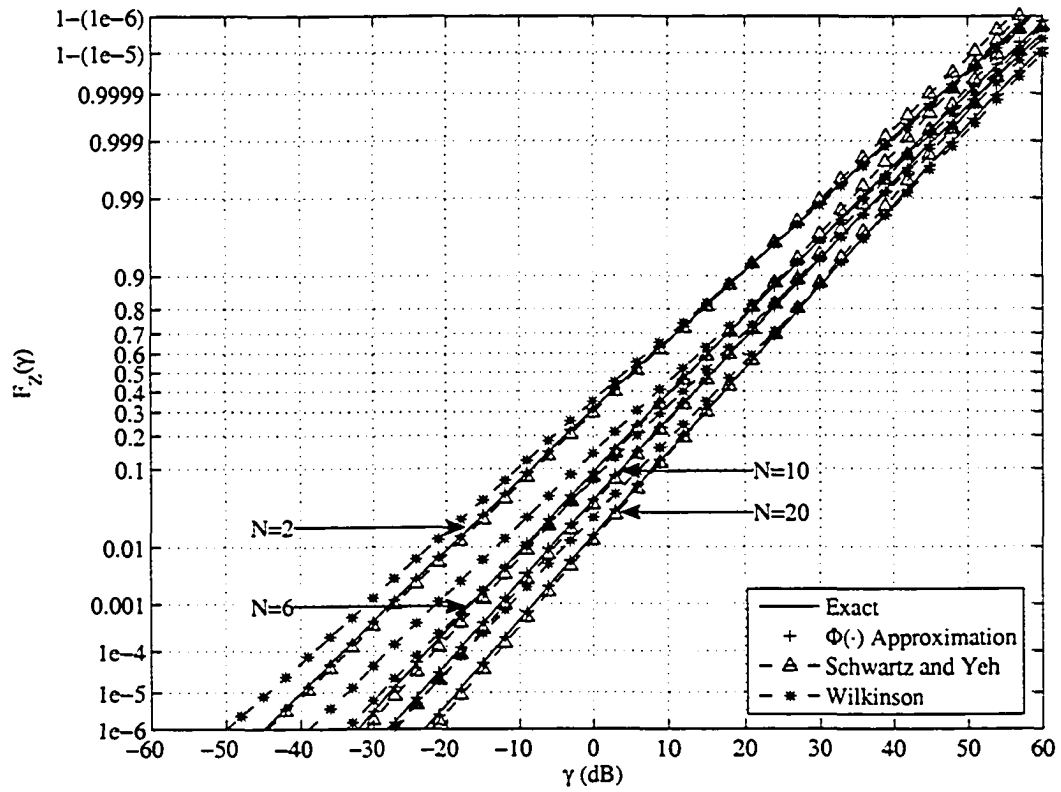
Figure 3.17. The CDF of a sum of $N = 2, 6, 10$ and 20 correlated lognormal RVs ($\sigma_X = 12$ dB, $\rho = 0.5$) and various approximations.

88
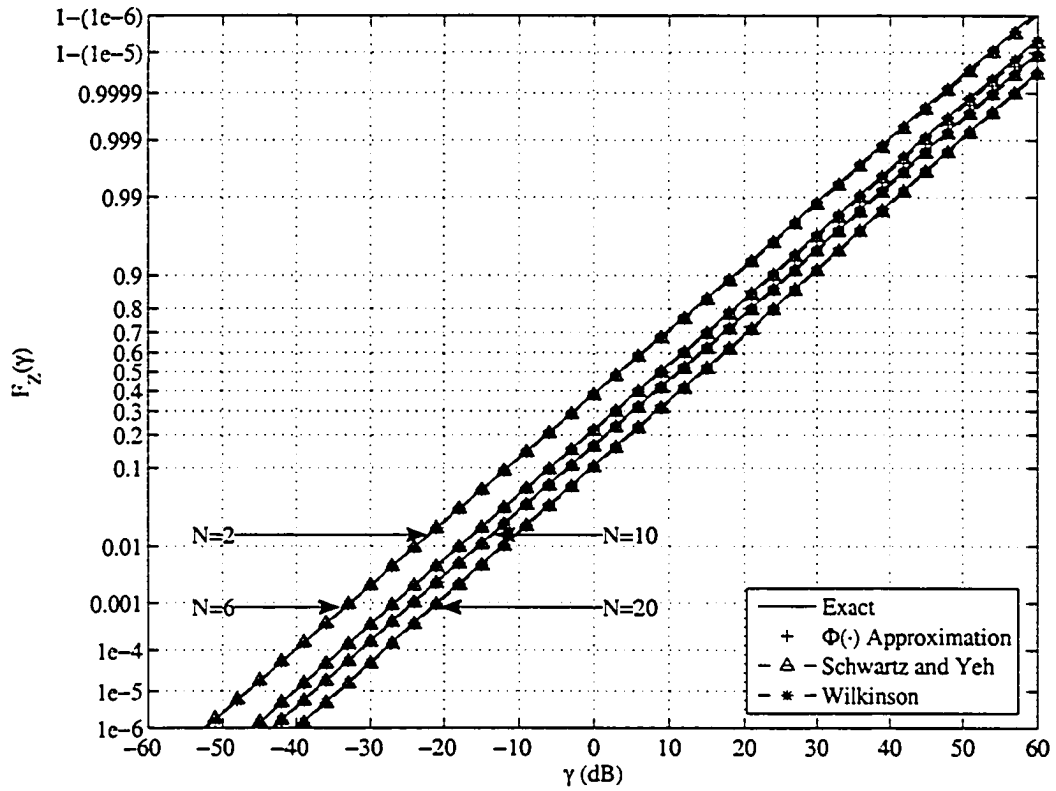
Figure 3.18. The CDF of a sum of $N = 2, 6, 10$ and 20 correlated lognormal RVs ($\sigma_X = 12$ dB, $\rho = 0.9$) and various approximations.

89
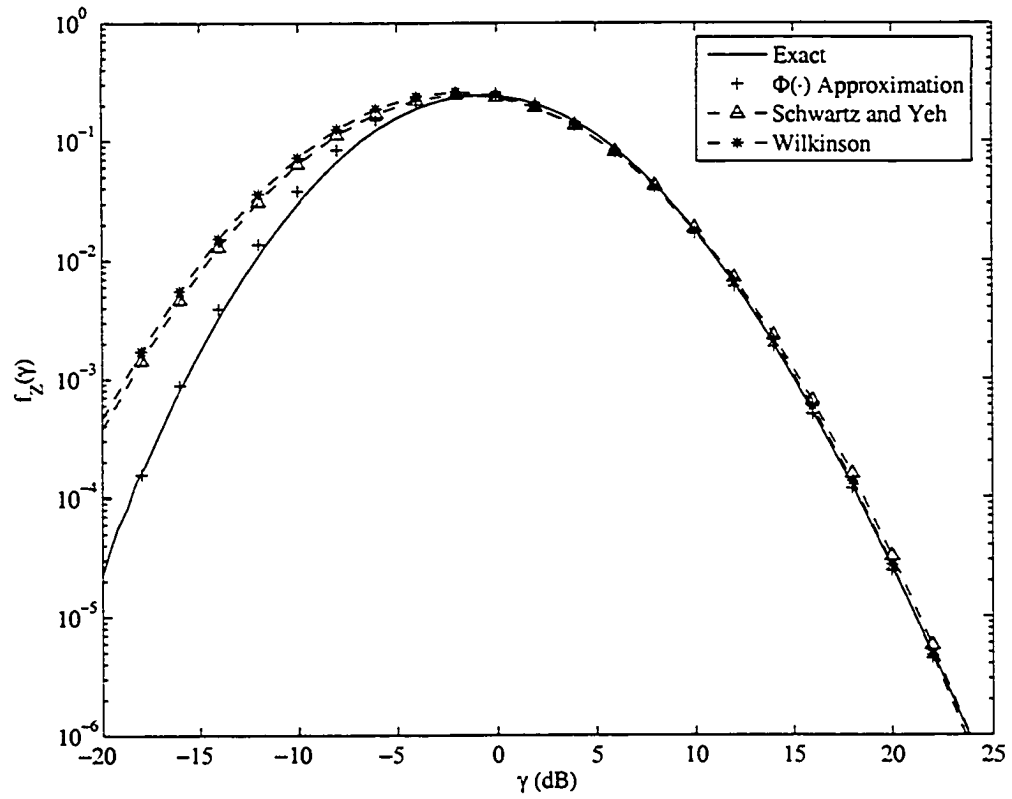
Figure 3.19. The PDF of a sum of $N = 2$ correlated lognormal RVs ($\sigma_X = 6$ dB, $\rho = 0.1$) and various approximations.
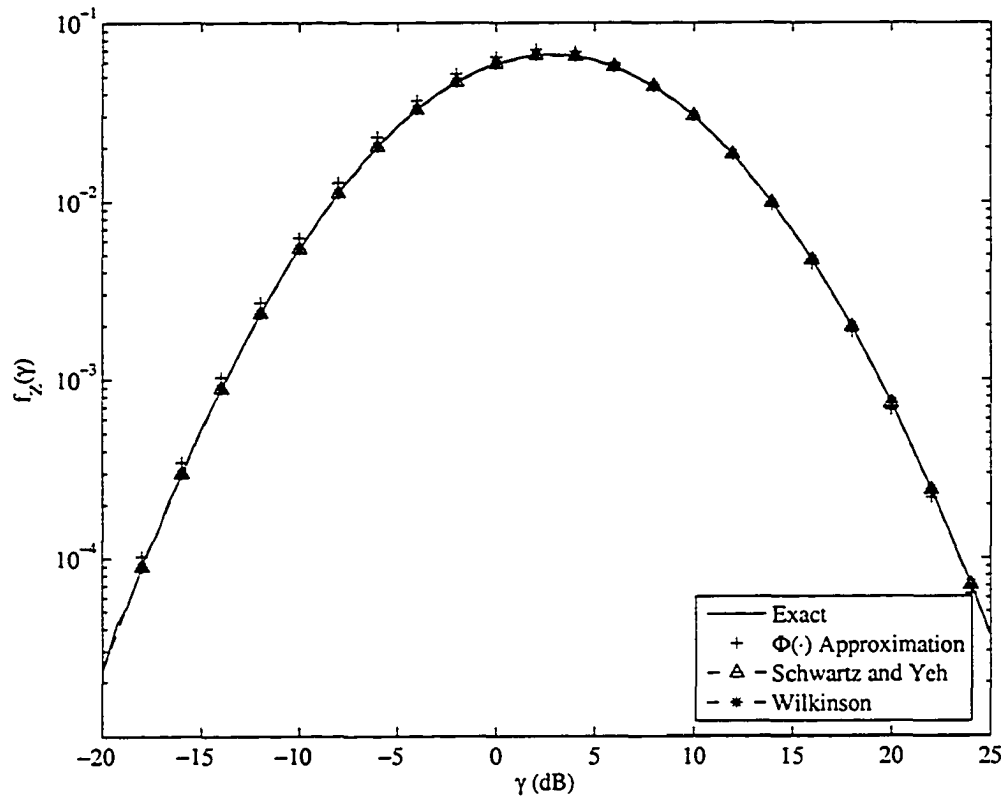
Figure 3.20. The PDF of a sum of $N = 10$ correlated lognormal RVs ($\sigma_X = 6$ dB, $\rho = 0.9$) and various approximations.

91
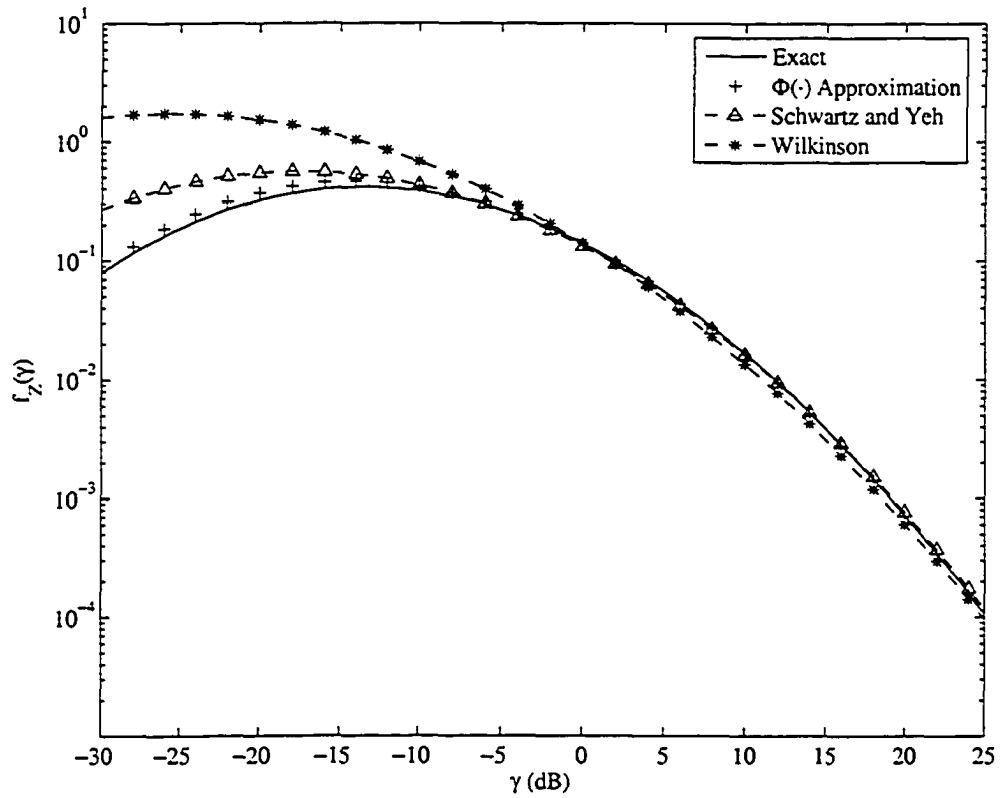
Figure 3.21. The PDF of a sum of $N = 2$ correlated lognormal RVs ($\sigma_X = 12$ dB, $\rho = 0.1$) and various approximations.

92
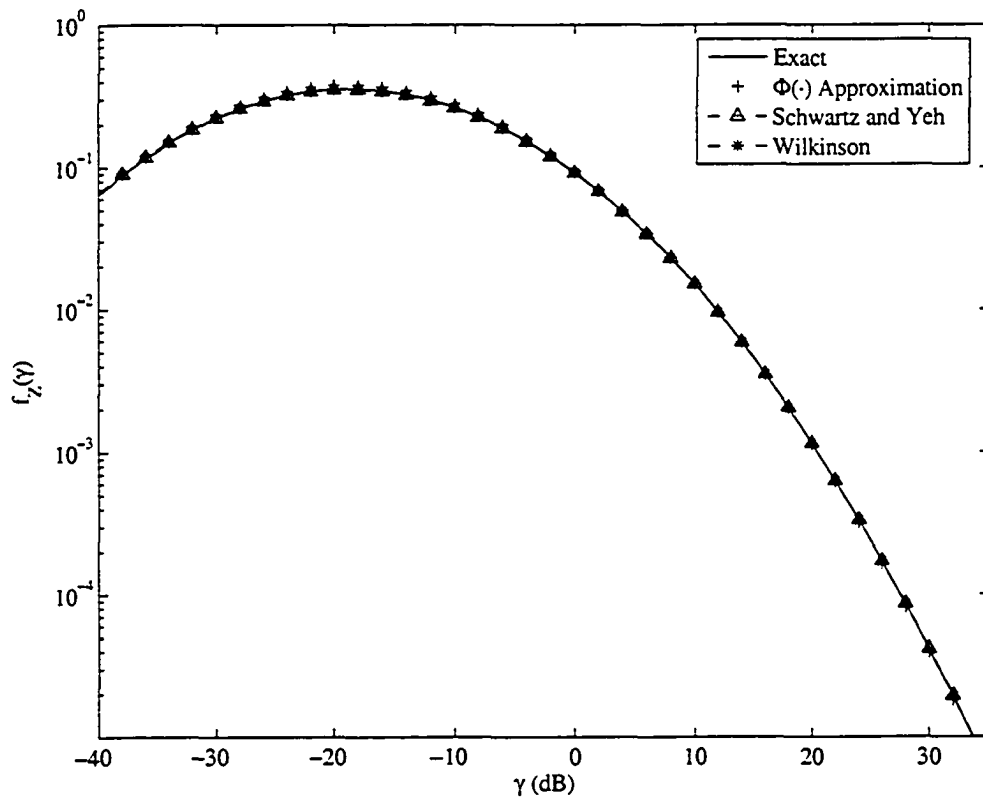
Figure 3.22. The PDF of a sum of $N = 10$ correlated lognormal RVs ($\sigma_X = 12$ dB, $\rho = 0.9$) and various approximations.

Chapter 4

Performance of a Pulse Amplitude and Position Modulation Ultra-Wide Bandwidth Wireless System over Lognormal Fading Channels

UWB is a rapidly emerging and viable technology for short distance, indoor wireless communication systems [30]. It also has other attractive uses in radar, imaging, and positioning systems [5]. A typical UWB system is carrier-less and can overlay existing wireless systems using low power, ultra-short pulses to transmit information. The interference between systems is mitigated by using signals with flat power spectral densities. One possible modulation scheme is PAPM which does not have any spectral lines [31], making PAPM suitable for UWB signals.

The performance of PAPM UWB using a MRC receiver in a lognormal fading channel was evaluated by Liu [32]. A single integral approximation to the error rate was determined based on Wilkinson's approximation [14] to the lognormal sum distribution. It was seen in Chapter 2 that Wilkinson's approximation to the CDF is not very accurate and the accuracy is dependent on the dB spread and number of summands. The exponential ap-

94

proximation based on lognormal probability paper was shown to be more accurate than any other approximation and not dependent on dB spread or number of summands. Using the exponential approximation it is possible to determine a more accurate BER expression for PAPM UWB using MRC in lognormal fading channels. Furthermore, it is possible to extend the method to obtain accurate single integral expressions for EGC, which have not previously been presented. Using the single integral expressions it will be possible to compare PAPM UWB with MRC and EGC diversity in a lognormal fading environment.

4.1 System Model

A typical PAPM UWB signal has the form [32]

$$s(t) = \sum_{n=-\infty}^{\infty} \sqrt{E_s} b_n^0 p(t - nT_f - \frac{1 - b_n^1}{2}\delta) \tag{4.1}$$

where T_f is the time duration of a frame (pulse repetition time), $p(t)$ is the pulse shape and E_s is the symbol energy. The energy of the pulse is normalized so that $\int_{-\infty}^{\infty} p^2(t)dt = 1$. The two bits b_n^0 and b_n^1, determine the n-th transmitted symbol. A non-return to zero format is utilized, such that $\{b_n^0 b_n^1\} \in \{11, 1 - 1, -11, -1 - 1\}$. Furthermore, the symbols are precoded by interchanging $\{-11\}$ and $\{-1 - 1\}$, to reduce the complexity of the receiver.

The impulse response of the channel is given by [6]

$$h(t) = \sum_{l=0}^{N-1} \alpha_l \delta_D(t - lT_p) \tag{4.2}$$

where N is the number of resolvable paths, $\delta_D(\cdot)$ is the Dirac delta function, T_p is the minimum path resolution and pulse width, and α_l is the fading coefficient for the l-th path. More complex models exist for modeling the impulse response of a UWB channel [6], but (4.2) was chosen because it is simple and will yield simple expressions for the performance of the system. In this model, it is necessary to account for random pulse inversions [6] because UWB is a carrierless system. This is accomplished by making $\alpha_l = \theta_l \beta_l$ where the parameter β_l is the fading amplitude and $\theta_l \in \{\pm 1\}$ with equal probability.

95

The fading amplitude can be considered to be a lognormal random variable with a variance of 3-5 dB [6],[7],[33]. Also it can be considered to be constant during a symbol interval. Thus, the received signal present in a RAKE receiver is

$$r(t) = \sum_{l=0}^{N-1} \alpha_l p(t - lT_p) + n(t) \tag{4.3}$$

where $n(t)$ is the additive white Gaussian noise (AWGN) with two-sided power spectral density $N_0/2$. The receiver for PAPM UWB uses two template waveforms [32]

$$\phi_1(t) = p(t) + p(t - \delta), \tag{4.4a}$$

$$\phi_2(t) = p(t) - p(t - \delta). \tag{4.4b}$$

The correlation of a time shifted pulse $p(t)$ and the template waveforms are

$$\tilde{R}_1(x) = R(x) + R(x - \delta), \tag{4.5a}$$

$$\tilde{R}_2(x) = R(x) - R(x - \delta) \tag{4.5b}$$

where

$$R(x) = \int_{-\infty}^{\infty} p(t)p(t - x)dt \tag{4.6}$$

is the autocorrelation of the pulse shape. The correlator output is determined for the N resolvable paths and then combined using MRC or EGC. The structure of a PAPM UWB receiver using MRC is shown in Figure 4.1.

4.2 Maximal Ratio Combining

A single integral expression for the BER of an MRC receiver was derived by Liu [32] using an orthogonal signaling scheme [33]. The performance of the receiver is dependent on the value of δ that is chosen. In an orthogonal signaling scheme, δ is chosen to be the minimum value such that $R(\delta) = 0$. Since δ is a fraction of the pulse width of $p(t)$, it is assumed that $R(T_p - \delta) \approx 0$. It is also assumed that perfect estimates of the fading coefficient are available for each resolvable path of the receiver.

96
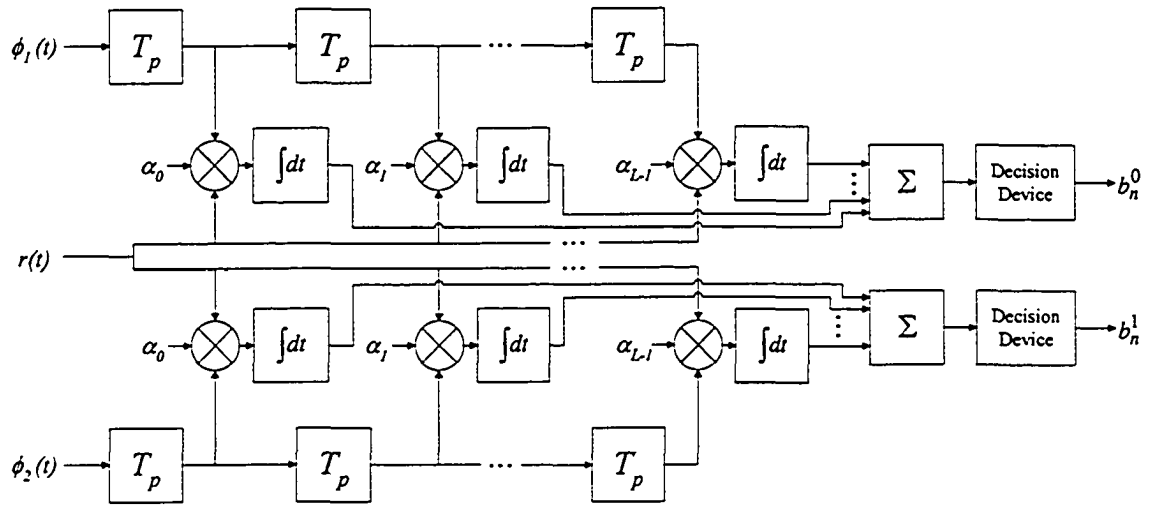
Figure 4.1. The UWB PAPM receiver block diagram.

Given these assumptions and assuming detection of the first symbol, it is possible to write the decision variable, without loss of generality, as

$$\lambda_i = \sum_{l=0}^{N-1} \alpha_l^2 \sqrt{E_s} b_0^0 \tilde{R}_i \left(\frac{1 - b_0^1}{2} \delta \right) + n_i \qquad (4.7)$$

where

$$n_i = \sum_{l=0}^{N-1} \alpha_l \int_0^{T_f} n(t) \phi_i(t - lT_p) dt. \qquad (4.8)$$

Furthermore, since $T_p \ll T_f$ [30] no ISI occurs due to multipath because it can be assumed that all the multipath components are contained within a frame. The bit decision is made by independently passing λ_i through a decision device with a threshold of zero. The noise

97

is uncorrelated for λ_1 and λ_2, which is shown by

$$E[n_1 n_2] = E\left[\sum_{k=0}^{N-1} \alpha_k \int_0^{T_f} n(t)\phi_1(t - kT_p)dt \sum_{l=0}^{N-1} \alpha_l \int_0^{T_f} n(\tau)\phi_2(\tau - lT_p)d\tau\right]$$

$$= \sum_{k=0}^{N-1}\sum_{l=0}^{N-1} E[\alpha_k \alpha_l] \int_0^{T_f}\int_0^{T_f} E[n(t)n(\tau)]\phi_1(t - kT_p)\phi_2(t - lT_p)dtd\tau$$

$$= \sum_{k=0}^{N-1}\sum_{l=0}^{N-1} E[\alpha_k \alpha_l]\frac{N_0}{2}[\tilde{R}_1((l-k)T_p - \tilde{R}_1((l-k)T_p + \delta)]$$

$$= \sum_{k=0}^{N-1} E[\alpha_k^2]\frac{N_0}{2}[\tilde{R}_1(0) - \tilde{R}_1(\delta)]$$

$$= 0. \tag{4.9}$$

As a result, the decisions for b_n^0 and b_n^1 can be made independently. Due to the independence of the statistics λ_1 and λ_2, either statistic can be analyzed to determine the BER.

For a fixed $\{\beta_l\}$, λ_i is a Gaussian RV, and, thus the conditional BER for λ_1 can be written as

$$P_{e1|\beta} = \Pr(\lambda_1 < 0|b_0 = \{1,1\})\Pr(b_0 = \{1,1\})$$

$$+ \Pr(\lambda_1 < 0|b_0 = \{1,-1\})\Pr(b_0 = \{1,-1\})$$

$$+ \Pr(\lambda_1 > 0|b_0 = \{-1,1\})\Pr(b_0 = \{-1,1\})$$

$$+ \Pr(\lambda_1 > 0|b_0 = \{-1,-1\})\Pr(b_0 = \{-1,-1\})$$

$$= \Pr\left(n_1 > \sum_{l=0}^{N-1} \beta_l^2\sqrt{E_s}\right). \tag{4.10}$$

When $\{\beta_l\}$ is fixed, the noise variance can be shown to be

$$\sigma_{n_i}^2 = N_0 \sum_{l=0}^{N-1} \beta_l^2. \tag{4.11}$$

Using the result of (4.11), (4.10) is written as

$$P_{e1|\beta}(\beta_{MRC}) = Q\left(\sqrt{\frac{E_s}{N_0}}\beta_{MRC}\right) \tag{4.12}$$

98

where $\beta_{MRC} = \sum_{l=0}^{N-1} \beta_l^2$. The unconditional BER is then given by

$$P_{e1} = \int_0^\infty P_{e1|\beta}(z) f_\beta(z) dz \qquad (4.13)$$

where $f_\beta(z)$ is a lognormal sum PDF. A closed-form expression does not exist for this PDF and an approximation must be used. An approximation to the BER is derived in [32] based on Wilkinson's method [14], but as seen in Chapter 2 Wilkinson's method is not the best approximation to the lognormal sum distribution [13],[17],. Using the exponential approximation to the PDF given by (2.19) the BER is approximated as

$$P_{e1} = \int_0^\infty Q\left(\sqrt{\frac{E_s}{N_0}} z\right) \frac{a_1 a_2 z^{-(a_2/\lambda+1)}}{\lambda \sqrt{2\pi}} \exp\left(-\frac{1}{2}(a_0 - a_1 z^{-a_2/\lambda})^2\right) dz. \qquad (4.14)$$

The values of a_0, a_1 and a_2 are chosen depending on the model that is used to represent the lognormal fading channel.

4.3 Equal Gain Combining

For MRC, the channel fading gains are required and they can be difficult to estimate accurately. Another possible combining technique is EGC, which only requires the phase of the fading channels. In a carrier-less UWB system, determining the phase is even simpler because the phase is either 0 or π, to account for pulse inversion [33]. In a practical system, performing EGC will be simpler than MRC but there will be a performance trade-off.

Just as with MRC, a single integral expression can be determined for the BER of PAPM UWB with EGC diversity. Using an EGC combining scheme the decision variable is given by

$$\lambda_i = \sum_{l=0}^{N-1} \beta_l \sqrt{E_s} b_0^0 \bar{R}_i \left(\frac{1-b_0^1}{2}\delta\right) + n_i. \qquad (4.15)$$

Again, without loss of generality, we can just look at the first branch of the receiver. The

99

BER for this branch can be written as

$$P_{e1|\beta} = \Pr\left(n_1 > \sum_{l=0}^{N-1} \beta_l \sqrt{E_s}\right)$$

$$= Q\left(\sqrt{\frac{E_s}{N_0 N}} \beta_{EGC}\right) \tag{4.16}$$

where $\sigma_{n_i}^2 = N_0 N$ and $\beta_{EGC} = \sum_{l=0}^{N-1} \beta_l$. The unconditional BER can then be written using the exponential approximation as

$$P_{e1} = \int_0^\infty Q\left(\sqrt{\frac{E_s}{N_0 N}} z\right) \frac{a_1 a_2 z^{-(a_2/\lambda + 1)}}{\lambda \sqrt{2\pi}} \exp\left(-\frac{1}{2}(a_0 - a_1 z^{-a_2/\lambda})^2\right) dz. \tag{4.17}$$

The constants a_0, a_1 and a_2 are not the same for EGC and MRC because the sum distributions are different in these two combining schemes. Also, the parameters will change depending on the severity of the fading and the number of branches in the receiver.

4.4 Numerical Results

A reasonable model for an indoor UWB channel is an exponentially decaying multipath intensity profile [33], as represented by

$$E[\alpha_l^2] = e^{-\psi l}. \tag{4.18}$$

Given a fixed dB spread for all N paths, it can be seen that β_{MRC} and β_{EGC} are sums of independent, non-identically distributed lognormal RVs. The exponential approximation provided in Chapter 2 is for a sum of iid lognormal RVs. Accordingly, it will be necessary to verify that this approximation is accurate in the non-iid case.

The exact distributions of β_{MRC} and β_{EGC} are determined by numerically integrating the CFs using the modified Clenshaw-Curtis method [22]. The parameters a_0, a_1 and a_2 are determined for $\psi = 0.046$ and a variance of 4 dB [32] using a non-linear least squares algorithm as in Chapter 2. The values of the parameters for the approximation to the distribution of β_{MRC} and β_{EGC} can be found in Tables 4.1 and 4.2 respectively. The exact PDFs

100

TABLE 4.1

The coefficients for the exponential approximation to β_{MRC}.

N	a_0	a_1	a_2
2	26.521	26.199	0.005882
3	16.956	16.196	0.01048
4	13.322	13.794	0.01472
5	11.698	12.495	0.01802
6	10.714	11.808	0.02086
7	9.993	11.366	0.02086
8	9.315	10.960	0.02353
9	8.949	10.846	0.02867
10	8.635	10.777	0.03074

TABLE 4.2

The coefficients for the exponential approximation to β_{EGC}.

| N	a_0	a_1	a_2
2	36.886	36.894	0.008809
3	24.752	25.539	0.01542
4	20.536	22.042	0.02087
5	17.929	20.124	0.02624
6	16.894	19.761	0.03003
7	15.810	19.348	0.03430
8	15.431	19.651	0.03742
9	14.954	19.843	0.04067
10	15.237	20.796	0.04202
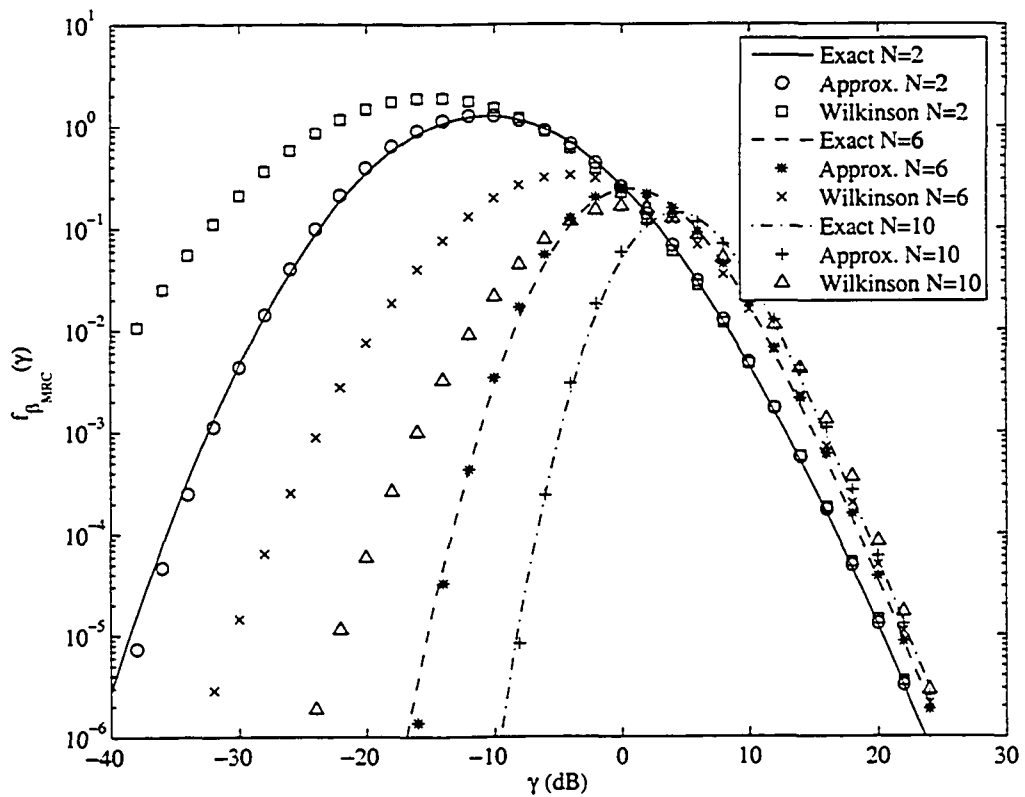
Figure 4.2. The PDF of β_{MRC}, the $\Phi(a_0 - a_1 e^{-a_2 \gamma})$ approximation, and Wilkinson's approximation for $N = 2$, 6 and 10.

102
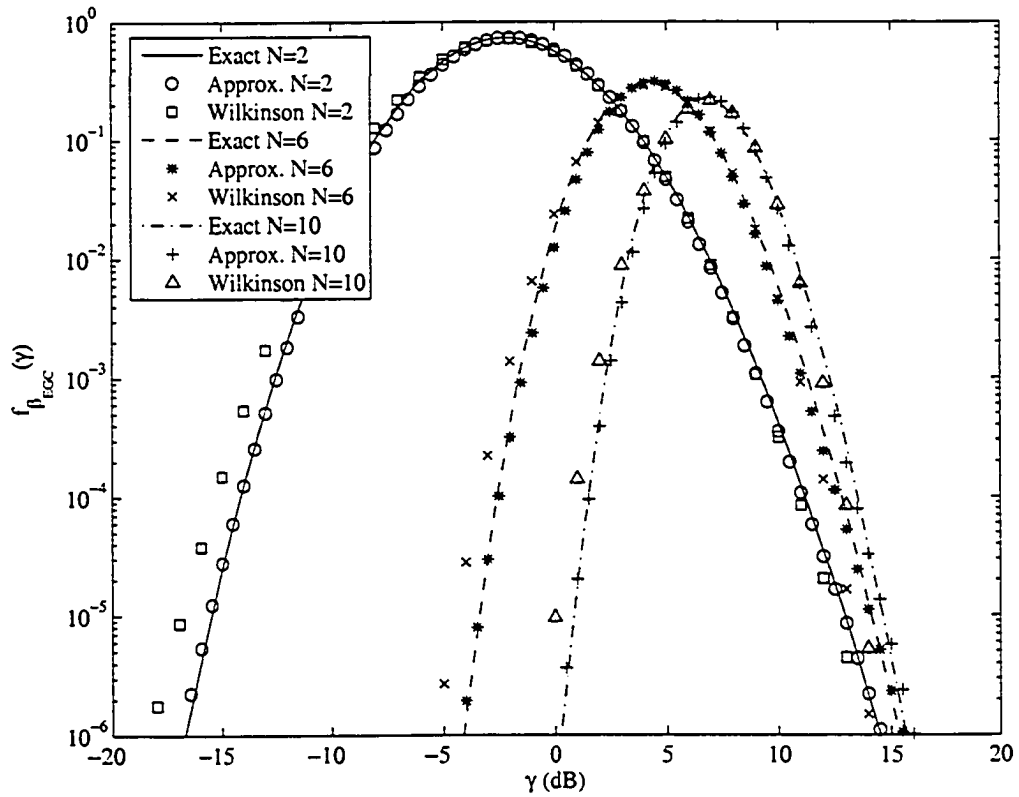
Figure 4.3. The PDF of β_{EGC}, the $\Phi(a_0 - a_1 e^{-a_2 \gamma})$ approximation, and Wilkinson's approximation for $N = 2$, 6 and 10.

103

of β_{MRC} and β_{EGC}, along with the new approximation and Wilkinson's approximation for $N = 2$, 6 and 10 can be found in Figures 4.2 and 4.3 respectively. It can be observed that the new approximation is many orders of magnitude better than Wilkinson's approximation in the given non-iid channel. For example, for the β_{MRC} distribution, Wilkinson's approximation is 4 orders of magnitude worse than the exact distribution. As a result, this new approximation should give a better approximation to the average error rate performance of PAPM UWB in the same channel.

Evaluating (4.14) and (4.16) using the previously obtained coefficients we obtain the approximate BER. The simulated BER and Wilkinson's approximation are compared to the new approximation in Figures 4.4 and 4.5. It can be observed that the new approximation is more accurate than Wilkinson's approximation for the given values of N. For example, in the case of MRC, Wilkinson's approximation overestimates the BER by a factor of 3.7 when $N = 2$ and $P_e = 10^{-3}$, and by a factor of 280 when $N = 10$ and $P_e = 10^{-6}$. We see that Wilkinson's approximation is less accurate for MRC than for EGC by comparing Figures 4.4 and 4.5. This is a result of the variance of the individual summands in EGC being less than the variance of the summands in MRC. As the variance decreases, the accuracy of the PDF obtained using Wilkinson's approximation increases and accordingly the accuracy of the approximate BER using Wilkinson's method increases. Comparing Figures 4.4 and 4.5, it can also be seen that for $P_e = 10^{-6}$, MRC performs better than EGC by 0.2, 0.8 and 1.2 dB for $N = 2$, 6 and 10 respectively. This is as expected, because MRC is a maximum-likelihood receiver in Gaussian noise. The gain in performance is small for small values of N and might be vitiated by implementation losses. If Wilkinson's approximation was used to predict the difference in performance for $P_e = 10^{-6}$, MRC would outperform EGC by 4.0, 6.5 and 6.1 dB for $N = 2$, 6 and 10 respectively. It is obvious that Wilkinson's approximation is neither a good choice to predict the performance of a MRC or EGC system, nor to predict the difference in performance between the two combining schemes. EGC is a more attractive diversity scheme because it is easier to implement than MRC and provides similar performance. A potential reason to use MRC is when a channel is excessively noisy. In such a case, EGC is unable to cut-off the noise.

104
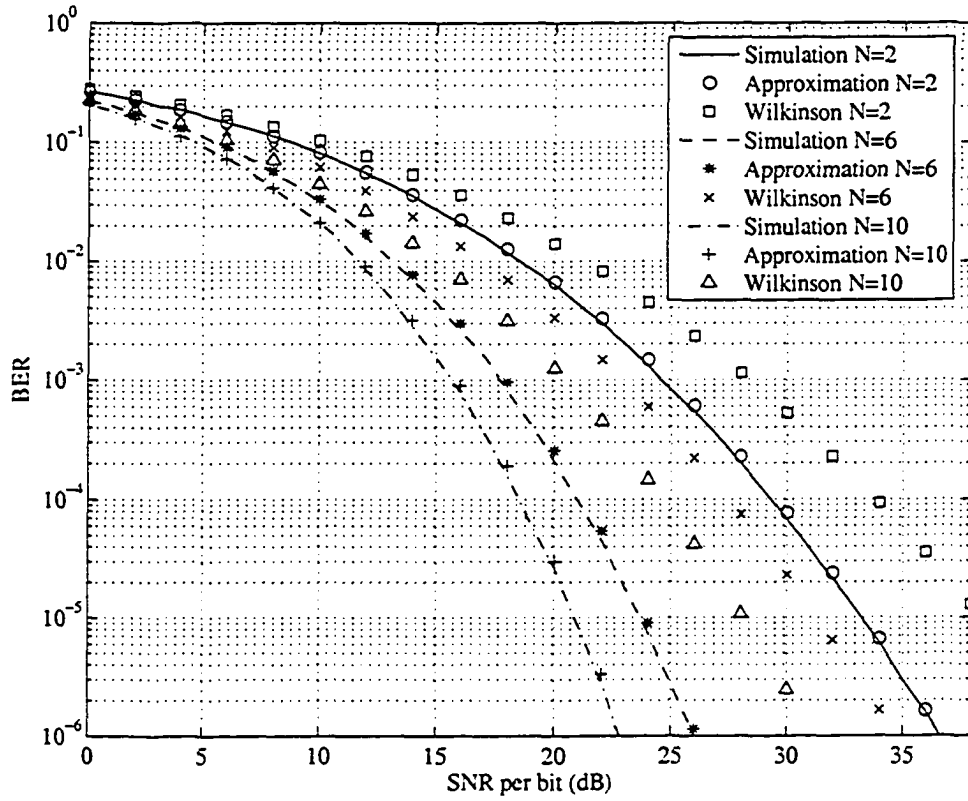
Figure 4.4. The BER of MRC PAPM UWB for $N = 2, 6$ and 10.

105
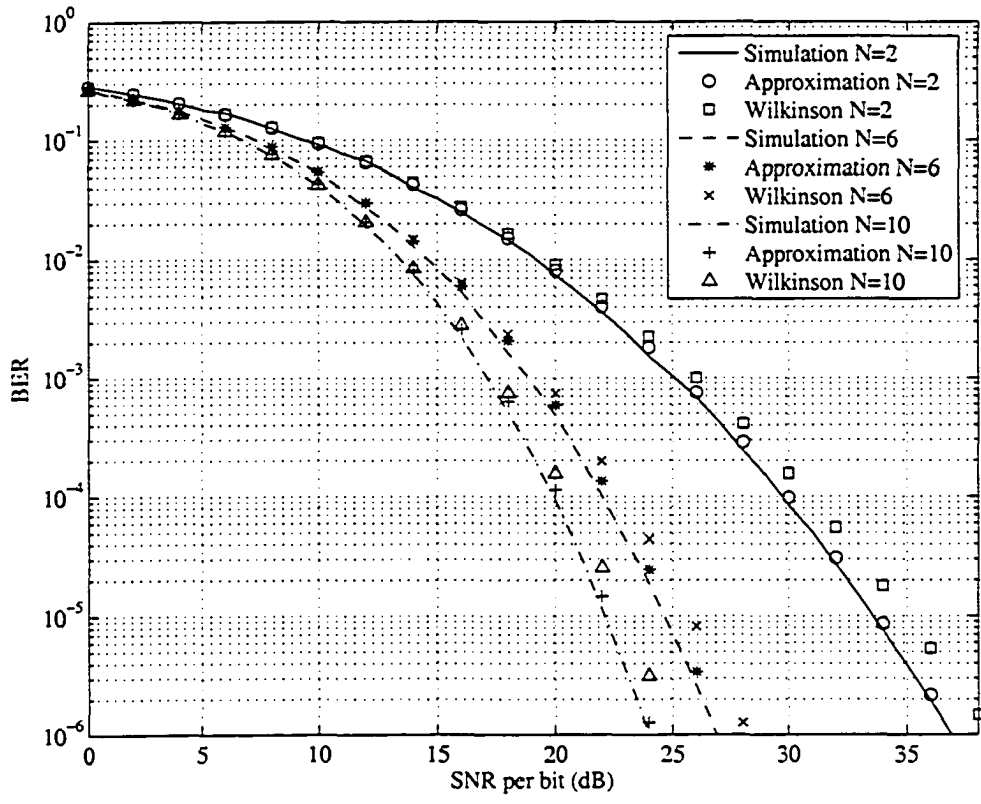
Figure 4.5. The BER of EGC PAPM UWB for $N = 2, 6$ and 10.

106

4.5 Summary

A more accurate approximation for the performance of PAPM UWB with MRC and new results for PAPM UWB with EGC were derived using the exponential approximation to the lognormal sum distribution introduced in Chapter 2. It was shown that the BER approximated by this new approximation is more accurate than using Wilkinson's approximation for all cases of interest. The performances of MRC and EGC diversity used with PAPM UWB were compared. As expected, there is a slight performance advantage for MRC but it is relatively insignificant. Analytical expressions are also derived for MRC and EGC systems with lognormal fading channels.

Chapter 5

Conclusion

A long standing problem in wireless communications is to find a closed-form expression for the distribution of a sum of lognormal RVs. Numerous approximations have been proposed, but none of them are accurate over a large range of parameters. Many of the techniques are based on assuming that a sum of lognormal RVs can be represented by another lognormal RV. It is easily seen on lognormal probability paper that this is not true. The sum distribution is actually a smooth curve that can be easily fit with another curve.

In this thesis, a new approximation to the lognormal sum distribution was proposed based on fitting a curve to the sum distribution on lognormal probability paper. The approximation was found to very accurate over the entire range of the CDF for a large range of dB spreads and number of summands. This is in contrast to many previously published approximations that are only accurate for a small range of values. The CDF approximation was up to 5 orders of magnitude more accurate than an approximation based on moment matching. From the CDF it was possible to determine an approximation to the PDF by taking the derivative. The PDF approximation was also accurate over the same range as the CDF. The PDF approximation was also many orders of magnitude more accurate than Schwartz and Yeh's, and Wilkinson's approximations. This new approximation provided a closed-form expression for the CDF and PDF that would be useful in many applications.

Chapter 2 examined a sum of iid lognormal RVs but another important problem is the

108

distribution of the sum of correlated lognormal RVs. Applying the approximation found in Chapter 2 to the correlated sum distribution results in a very accurate approximation to the correlated sum distribution. For low correlation, the approximation was found to be more accurate than Schwartz and Yeh's, and Wilkinson's approximations. In contrast, for high correlation, the moment matching methods were just as accurate as the new approximation. The same observations were made for the PDF approximation as for the CDF approximation.

Having an expression for the CDF and PDF of a lognormal sum RV allows it to be used in many applications such determining the performance of communication systems. One such application discussed in this thesis was the performance of PAPM UWB using a MRC combining scheme in lognormal fading channels. The new approximation provided a large improvement in the approximation of the performance of the system when compared to the performance approximated by Wilkinson's method. In addition, the new approximation was used to find expressions for the performance of an EGC combining scheme. This allowed for a good comparison to be made between EGC and MRC that would not have been possible using Wilkinson's approximation. In summary, a new approximation to the lognormal sum distribution was proposed that is accurate for a large range of parameters and types of sum distributions, that will prove to be useful in many applications.

References

[1] K. Tachikawa, "A perspective of the evolution of mobile communications," *IEEE Communications Magazine*, vol. 41, pp. 66–73, October 2003.

[2] M. Nakagami, "The m-distribution, a general formula of intensity distribution of rapid fading," in *Statistical Methods in Radio Wave Propagation*, W. Hoffman, Ed. Oxford, England: Pergamon, 1960.

[3] T. S. Rappaport, *Wireless Communications Principles and Practice*, 2nd ed. Upper Saddle River, NJ: Prentice Hall, 2002.

[4] G. L. Stuber, *Principles of Mobile Communication*, 2nd ed. Norwell, MA: Kluwer Academic Publishers, 2001.

[5] L. Yang and G. B. Giannakis, "Ultra-wideband communications: an idea whose time has come," *IEEE Signal Processing Magazine*, vol. 21, pp. 26–54, November 2004.

[6] J. Foerster and Q. Li, "UWB channel modeling contribution from Intel," IEEE P802.15-02/279r0-SG3a, June 2002.

[7] H. Hashemi, "The indoor radio propagation channel," *Proceedings of the IEEE*, vol. 81, no. 7, pp. 943–968, July 1993.

[8] H. Hashemi, "Impulse response modeling of indoor radio propagation channels," *IEEE Journal on Selected Areas in Communications*, vol. 11, no. 7, pp. 967–978, September 1993.

[9] W. C. Lee and S. Y. Yeh, "Polarization diversity system for mobile radio," *IEEE Transactions on Communications*, vol. 20, no. 5, pp. 912–923, October 1972.

[10] D. G. Brennan, "Linear diversity combining techniques," *Proceedings of the IRE*, vol. 47, pp. 1075–1102, June 1959.

[11] M. K. Simon and M.-S. Alouini, *Digital Communication over Fading Channels: A Unified Approach to Performance Analysis*. New York: Wiley, 2000.

[12] T. Eng, N. Kong, and L. B. Milstein, "Comparison of diversity combining techniques for Rayleigh-fading channels," *IEEE Transactions on Communications*, vol. 44, no. 9, pp. 1117–1129, September 1996.

[13] N. C. Beaulieu, A. A. Abu-Dayya, and P. J. McLane, "Estimating the distribution of a sum of independent lognormal random variables," *IEEE Transactions on Communications*, vol. 43, no. 12, pp. 2869–2873, December 1995.

[14] S. C. Schwartz and Y. S. Yeh, "On the distribution function and moments of power sums with lognormal components," *Bell Systems Technical Journal*, vol. 61, no. 7, pp. 1441–1462, September 1982.

[15] N. C. Beaulieu, A. A. Abu-Dayya, and P. J. McLane, "Comparison of methods of computing lognormal sum distributions and outages for digital wireless applications," in *IEEE Internationl Conference on Communications*, New Orleans, LA, May 1994, vol. 3, pp. 1270–1275.

[16] P. Cardieri and T. S. Rappaport, "Statistics of the sum of lognormal variables in wireless communications," in *Proceedings IEEE Vehicular Technology Conference*, Tokyo, Japan, May 2000, vol. 3, pp. 1823–1827.

[17] N. C. Beaulieu and Q. Xie, "An optimal lognormal approximation to lognormal sum distributions," *IEEE Transactions on Vehicular Technology*, vol. 53, no. 2, pp. 479–489, March 2004.

111

[18] A. A. Abu-Dayya and N. C. Beaulieu, "Outage probabilities in the presence of correlated lognormal interferers," *IEEE Transactions on Vehicular Technology*, vol. 43, no. 1, pp. 164–173, February 1994.

[19] A. Safak, "Statistical analysis of the power sum of multiple correlated log-normal components," *IEEE Transactions on Vehicular Technology*, vol. 42, no. 1, pp. 58–61, February 1993.

[20] A. Papoulis and S. U. Pillai, *Probability, Random Variables and Stochastic Processes*, 4th ed. Boston: McGraw Hill, 2002.

[21] J. Gil-Pelaez, "Note on the inversion theorem," *Biometrika*, vol. 3/4, pp. 481–482, December 1951.

[22] Q. Xie, "Minimax approximation to lognormal sum distributions," M.Sc. thesis, University of Alberta, Edmonton, Alberta, Canada, 2002.

[23] R. B. D'Agostino and M. A. Stephens, *Goodness-of-fit techniques*. New York, NY: M. Dekker, 1986.

[24] W. Janos, "Tail of the distributions of the sums of log-normal variates," *IEEE Transactions on Information Theory*, vol. 16, no. 6, pp. 299–302, May 1970.

[25] T. F. Coleman and Y. Li, "An interior, trust region approach for nonlinear minimization subject to bounds," *SIAM Journal on Optimization*, vol. 6, pp. 418–445, 1996.

[26] T. F. Coleman and Y. Li, "On the convergence of reflective Newton methods for large-scale nonlinear minimization subject to bounds," *Mathematical Programming*, vol. 67, no. 2, pp. 189–224, 1994.

[27] M. A. Hamdan, "The logarithm of the sum of two correlated lognormal variates," *Journal of the American Statistical Association*, vol. 66, pp. 105–106, March 1971.

[28] A. M. Law and W. D. Kelton, *Simulation Modeling and Analysis*, 3rd ed. Boston, MA: McGraw-Hill, 2000.

[29] R. A. Horn and C. R. Johnson, *Matrix Analysis*. Cambridge UK: Cambridge Univ. Press, 1990.

[30] M. Z. Win and R. Scholtz, "Impulse radio: how it works," *IEEE Communications Letters*, vol. 2, no. 2, pp. 36–38, February 1998.

[31] Y. Li and X. Huang, "The spectral evaluation and comparison for ultra-wideband signals with different modulation schemes," in *Proceedings World Multiconference on Systemics, Cybernetics and Informatics*, Orlando, FL, July 2000, vol. 6, pp. 277–282.

[32] H. Liu, "Error performance of a pulse amplitude and position modulated ultra-wideband system over lognormal fading channels," *IEEE Communications Letters*, vol. 7, no. 11, pp. 531–533, November 2003.

[33] J. R. Foerster, "The effects of multipath interference on the performance of uwb systems in and indoor wireless channel," in *Proceedings IEEE Vehicular Technology Conference*, Rhodes, Greece, May 2001, vol. 2, pp. 1176–1180.

Appendix A

Generation of Random Variables

In this thesis random numbers are used to generate PDFs and CDFs of a sum of lognormal RVs. There are many random number generators available but they vary in speed and quality. Since random number generators are actually deterministic sequences that appear to be random, it is necessary to carefully choose a random number generator. A good random number generator will have a long period, low correlation, and match the statistical properties of the required distribution. Developing random numbers generators is not a simple task and requires advanced mathematics. Accordingly, software libraries with existing random number generators are used in this thesis.

The GNU Scientific Library (GSL) is a numerical C and C++ library that has implementations of many random number generator. The most robust random number generator in GSL is the MT19937 generator. This generator was chosen for the generation of random variables in this thesis because it has a period of $2^{19937} - 1$ and is comparable in speed to other random number generators. The extremely long period of this generator is more than sufficient for the cases being considered.

The output of the random number generator from GSL is uniformly distributed in the range (0,1). As a result, it is necessary to convert this uniform distribution into the required distribution. GSL contains many subroutines that transform the uniform distribution to the required distributions. For example, the subroutines *gsl_ran_gaussian* and

114

gsl_ran_lognormal generate Gaussian and lognormal random numbers respectively, using the uniform random number generator. With these built in subroutines and random numbers generators it is easy to simulate the lognormal sum distribution. The C code used for the generation of a sum of correlated lognormal RVs can be found in Appendix B.

Appendix B

Code to Generate Correlated Lognormal Random Variables

The following C code in conjunction with GSL is used to generate the PDF of a sum of correlated lognormal RVs.

```c
#include <stdio.h>
#include <stdlib.h>
#include <math.h>
#include <gsl/gsl_rng.h>
#include <gsl/gsl_randist.h>
#include <gsl/gsl_histogram.h>


double **mat_init(double rho, double sigmadB, int N);
void free_matrix(double **a, int N);
double **choldc(double **a, int n);
void print_matrix(double **a, int n);


int main (void)
{
```

116

```c
const gsl_rng_type * T;

const int N = 20;/* number of summands */

char ofpname[]="test.dat";

double rho = 0.9; /* correlation between RVs */

long int num = 2000000000; /* number of random numbers generated */

long int i, j, k;

double zeta = 0.0;  /* mean of RV */

double sigma = 1.38155105579643; /* 6 dB */

double sigmadB = 6;

/*double sigma = 2.76310211159285;*/ /* 12 dB */

double sum;

double **C;

double **LT;

double hmin = -7; /* range of bins in dB/10 */

double hmax = 7;

size_t n=260; /* number of bins in histogram */

double ranges[n+1];

double *y;

double *x;

gsl_rng **r;

double step;

gsl_histogram *h;

FILE *ofp;

double lambda = log(10)/10;

/* create a generator variable */

gsl_rng_env_setup();

T = gsl_rng_default;

//default rng is mt19937

/* initialize r and k vectors */
```

117

```c
r = calloc(N, sizeof(gsl_rng *));

x = calloc(N, sizeof(double));

y = calloc(N, sizeof(double));

/* setup r vector with rng and seed rng */

for(i=0;i<N;i++){

    r[i] = gsl_rng_alloc(T);

    gsl_rng_set(r[i], rand());}

/* printf("matrix initialization\n"); */

C = mat_init(rho, 1.0 , N);

LT=choldc(C, N);

/* printf("LT = \n"); */

print_matrix(LT, N);

/* printf ("generator type: %s\n", gsl_rng_name (r)); */

h = gsl_histogram_alloc(n);

step = (hmax − hmin)/n;

for (i=0; i<=n; i++)

    {ranges[i]=pow(10,hmin + i * step);

        /* ranges[i]=exp(hmin+i*step); */}

gsl_histogram_set_ranges(h, ranges, n+1);

for (i=0; i < num; i++)

    {/* generate N normal RVs */

        for(j=0;j<N;j++){

            y[j] = gsl_ran_gaussian(r[j], sigmadB);}

        /* generate N correlated RVs using LT from Cholesky */

        for(j=0;j<N;j++){

            for(k=0,x[j]=0;k<=j;k++){

                x[j]+= LT[j][k] * y[k];}}

        /* generate sum of N correlated RVs */

        for(j=0,sum=0;j<N;j++)
```

118

```
      sum +=exp(lambda*x[j]);

      gsl_histogram_increment(h, sum);}
```

/* output data to a file */

```
ofp = fopen(ofpname, "w");

for(i=0;i<n;i++)

    {fprintf(ofp, "%10.9f ", h->range[i]);

    fprintf(ofp, "%10.9f ", h->range[i+1]);

    fprintf(ofp, "%10.9f/n", h->bin[i]);}
```

/* clear memory */

```
gsl_histogram_free(h);

fclose(ofp);

for(i=0;i<N;i++) gsl_rng_free(r[i]);

free(r);

free_matrix(C, N);

free(x);

free(y);

return 0;

}


double **mat_init(double rho, double sigmadB, int N)

{

  int i,j;

  double **a;

  a = calloc(N, sizeof(double*));

  for(i=0; i<N;i++)

    {a[i]=calloc(N, sizeof(double));}

  for (i=0; i<N; i++)

    {for (j=0; j<N; j++)

        {if (i==j)
```

119

```c
                a[i][j] = sigmadB * sigmadB;
            else
                a[i][j] = rho * sigmadB * sigmadB;}}
    return a;
}


void free_matrix(double **a, int N)
{
    int i;
    for(i=0; i<N;i++)
        {free(a[i]);}
    free(a);
}


double **choldc(double **a, int n)
{
    int i,j,k;
    double sum;
    double *p;
    p = calloc(n, sizeof(double));
    for(i=0;i<=n-1;i++){
        for(j=i;j<=n-1;j++)
            {for(sum=a[i][j], k=i-1;k>=0;k--)
                {sum -= a[i][k] * a[j][k];}
            if(i==j)
                {if (sum<=0.0)
                    {/* printf("decomposition failed\n");*/
                        exit(1);}
                p[i]=sqrt(sum);}
```

120

```c
            else a[j][i]=sum/p[i];}}
    for(i=0;i<n;i++)
       a[i][i]=p[i];
    for(i=0;i<n;i++)
       for(j=i+1;j<n;j++)
          a[i][j]=0;
    free(p);
    return a;
}


void print_matrix(double **a, int n)
{
    int i,j;
    for(i=0;i<n;i++){
       for(j=0;j<n;j++)
          {printf("%f ", a[i][j]);}
       printf("\n");}
}
```